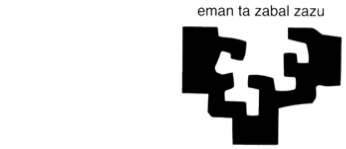

Universidad del País Vasco
Euskal Herriko Unibertsitatea

Magnetoelectric metallic glass/polymer laminated composites: from fabrication to applications

REPORT

presented to aim for the degree of Doctor by UPV/EHU

by

Andoni Lasheras Aransay

under the supervision of

Jon Gutiérrez Etxebarria
Jose Luis Vilas Vilela

Leioa, December 2015

ZTF-FCT
Zientzia eta Teknologia Fakultatea
Facultad de Ciencia y Tecnología

Agradecimientos

Han sido muchísimas las personas que durante estos años me han apoyado directa o indirectamente a realizar esta tesis. Por eso, ahora que este trabajo llega a su fin, me gustaría agradecer a todos el apoyo prestado a lo largo de estos más de cuatro años. Esta tesis está dedicada a todos vosotros.

Lehenik eta behin, esker mila nire tesiaren zuzendariari, Jon Gutiérrez Etxebarria, urte hauetan zehar irakatsi didan guztiagatik, baina batez ere, berarekin lan egiteko emandako aukeragatik. Zure aholku eta ekarpen zientifikoak ezinbestekoak izan dira tesi honetan. Benetan zorte ikaragarria izan da zure gidaritzapean tesi hau burutzea.

Modu berean, nire tesiaren kozuzendariari, Jose Luis Vilas, emandako ekarpena eskertu nahi nioke, batez ere, polimeroen eta piezoelektrikoen arloan.

Eskerrik asko ere Eusko Jaurlaritzari Doktoretza-aurreko Programaren bitartez azken lau urteetan emandako laguntza ekonomikoagatik.

Me gustaría agradecer especialmente a Manu Barandiarán, por darme la oportunidad de trabajar en el Grupo de Magnetismo y Materiales Magnéticos, así como por los conocimientos transmitidos a lo largo de estos años sin los cuales esta tesis no habría sido posible.

Agradecer por supuesto a todos y cada uno de los miembros del Grupo de Magnetismo y Materiales Magnéticos, por acogerme en estos cinco años y facilitarme siempre las cosas. A Maria Luisa Fernández-Gubieda y Alfredo Garcia-Arribas, por ayudarme y apoyarme siempre que lo he necesitado. A Jorge Feuchtwanger, por darme siempre alguna solución a los innumerables problemas que le he planteado. A Valentín, por la amistad ofrecida durante estos años y por ayudarme con algunas de las piezas que me han sido de gran utilidad durante la tesis. A Patricia, eskerrik asko por escucharme siempre que he tenido algún problema, tanto personal como profesional. A Maite, Edu, Javi, Iván, Anabel,

Pablo y Lurdes por hacer que estos más de cuatro años de trabajo hayan sido inmejorables. Así mismo, agradecer a todo el Departamento de Electricidad y Electrónica, y en especial, a Mireia y Inari, por ayudarme a recorrer este camino desde el principio.

Y por supuesto, quiero hacer mención especial a Iñaki Orue, una de las personas más importantes de esta tesis y del cual solo puedo tener buenas palabras. La impagable ayuda ofrecida en el ámbito científico durante estos años sólo es superada por el apoyo personal y los buenos momentos que he pasado contigo. Ha sido realmente una suerte haber podido trabajar contigo. Sin tu ayuda, esto no habría sido posible. Eskerrik asko Iñaki.

Gracias también al centro tecnológico BCMaterials, el cual me ha ayudado a realizar esta tesis y me ha proporcionado todo aquello que he necesitado. En especial, a Dani, Maria y Ariane por ayudarme siempre que lo he requerido y por haber compartido grandes momentos juntos.

A todo el grupo de Química Macromolecular de la Universidad del País Vasco en general, y a Alberto y a Luis León en particular, agradecerles la buena disposición que siempre han mostrado conmigo.

Agradecer ao Grupo de Materiáis Eletroativos Inteligentes e ao Professor Senentxu Lanceros-Méndez a inesquecível estadia de quase 5 meses na Universidade do Minho de Braga. Em especial, gostava de agradecer ao Marco, à Silvinha e ao Pedro Libânio a amizade mostrada nos cinco meses que estive lá. Obrigado por tudo amigos.

Agradecer especialmente a mis aitas, a los que quiero un montón y los cuales son y siempre serán un ejemplo para mí. Por apoyarme siempre en todas las decisiones que he tomado y por haberme formado como persona. Estoy muy orgulloso de vosotros. Esta tesis está especialmente dedicada a vosotros

Eskerrik asko también a Urko y Xabi, porque sois los mejores hermanos que se puede tener. A mi familia en general, porque sin vosotros esto no hubiese sido posible y a mi Amama en particular, porque desde que empecé hace 12 años la

carrera de Física, siempre ha confiado en mí y nunca ha dejado de creer que podía realizar aquello que me propusiese, incluso en los momentos más difíciles.

Finalmente, quero dedicar esta tese à Catarina, não só pela ajuda científica dispensada, sobretudo por estares comigo nos maus momentos. Obrigado por teres aparecido na minha vida.

Resumen

En los últimos años se ha dedicado un gran esfuerzo al estudio de materiales multiferroicos con acoplamiento entre ferroelasticidad y ferromagnetismo. La manifestación más interesante de este acoplamiento se conoce como efecto magnetoeléctrico (efecto ME), que es la tensión eléctrica inducida en un material bajo la aplicación de un campo magnético o viceversa, el cambio de imanación en un material bajo la acción de un campo eléctrico. Este efecto se descubrió en materiales monofásicos hace más de 50 años. Sin embargo, los voltajes inducidos en éstos materiales eran muy bajos y estaban limitados a temperaturas por debajo de ambiente. Debido a estas limitaciones, los materiales ME evolucionaron a sistemas tipo composite. Entre ellos, los composites ME fabricados con combinaciones de elementos magnetostrictivos y piezoeléctricos son los que ofrecen mayores posibilidades a nivel tecnológico, ya que el acoplamiento entre propiedades magnetostrictivas y piezoeléctricas favorecen la inducción de voltajes superiores a los materiales monofásicos tradicionales. Estos composites son bien de tipo granular o de tipo laminado. Además, se ha observado que el acoplamiento ME es superior en este último tipo de composites.

El componente magnetostrictivo en los laminados está normalmente formado por Terfenol-D o por aleaciones ferromagnéticas amorfas. La principal ventaja del Terfenol-D es su alta magnetostricción de saturación, que puede llegar hasta las 2000 ppm. Sin embargo, estas deformaciones se alcanzan a campos magnéticos relativamente altos, por encima de los 1000 Oe, lo que dificulta enormemente su implementación en dispositivos prácticos. Las aleaciones ferromagnéticas amorfas, en cambio, muestran generalmente deformaciones bajas de entre 10-40 ppm, pero a campos magnéticos de apenas unos pocos Oersted, lo que permite el uso de pequeñas fuentes de energía para la generación de dicho campo.

En cuanto a los materiales piezoeléctricos, éstos se diferencian claramente entre los poliméricos y los cerámicos. Aunque los piezoeléctricos cerámicos muestran

una mayor respuesta piezoeléctrica, su fragilidad impide en gran parte su aplicabilidad. Al contrario que los cerámicos, los piezoeléctricos poliméricos tienen un coeficiente piezoeléctrico relativamente bajo, pero muestran excelentes propiedades mecánicas, así como alta resistencia química, lo que los hace atractivos para el uso en laminados ME.

Es por ello que siguiendo estas consideraciones previas, en esta tesis se ha optado por el estudio de laminados ME fabricados con aleaciones ferromagnéticas amorfas como constituyente magnetostrictivo y PVDF como constituyente piezoeléctrico. Al aplicar un campo magnético al constituyente magnetostrictivo, éste se deforma deformando a su vez al constituyente piezoeléctrico, e induciendo así un voltaje de origen magnetoeléctrico.

En este trabajo se han fabricado 32 laminados ME del tipo L-T, con dos cintas magnetostrictivas adheridas a ambas caras de un film de PVDF, formando una estructura tipo sandwich. Para ello, como componente magnetostrictivo se han usado cuatro aleaciones ferromagnéticas de diferente composición basadas en Fe-Co (abreviadas como X=0, X=3, X=6 y X=21). Estas cintas han sido seleccionadas principalmente por su alta susceptibilidad magnética, bajo campo magnético de saturación y valor creciente de la magnetostricción, de 18 ppm (X=0) a 25 ppm (X=21). El estudio se ha realizado para laminados de 3, 2, 1 y 0.5 cm de longitud (en adelante, X=0/PVDF, X=3/PVDF, X=6/PVDF y X=21/PVDF), con las cintas magnetostrictivas en estado as-quenched y tras un tratamiento térmico (cintas ***annealed***). El objetivo del tratamiento térmico es relajar las tensiones producidas en el proceso de fabricación de las cintas y por tanto, inicialmente, mejorar las propiedades magnéticas de las mismas.

Las cintas magnetostrictivas han sido fabricadas mediante la técnica de solidificación ultra-rápida o Melt Spinning. Previamente, las aleaciones madre fueron obtenidas en forma de lingotes mediante un horno de inducción. La caracterización magnética de las cintas magnetostrictivas se ha realizado mediante la obtención de los ciclos de histéresis, la medida de la magnetostricción y la determinación de los principales parámetros magnetoelásticos.

La caracterización del PVDF, adquirido comercialmente, se ha centrado en el comportamiento de la polarización remanente (y determinación de su valor máximo) y su evolución con la temperatura. El epoxy usado para fabricar los laminados ha sido igualmente caracterizado térmicamente mediante TGA y DSC, estudiando así su comportamiento con la temperatura y el tiempo de curado.

Con los componentes ya caracterizados, se ha procedido a la fabricación de los laminados mediante el método de ***Vacuum Bagging***, evitando así la aparición de burbujas durante el proceso de curado y asegurando una presión homogénea, así como una correcta homogeneidad del epoxy.

En la primera fase de la tesis se ha procedido a la caracterización ME de los laminados fabricados, estudiando no sólo el efecto de la longitud en la respuesta ME, si no también analizando la influencia del tratamiento térmico de las cintas magnetostrictivas en dicha respuesta. Los resultados obtenidos muestran para todos los laminados estudiados como el coeficiente ME decrece a medida que se reduce la longitud del laminado. En cuanto al tratamiento térmico se refiere, las respuestas ME varían dependiendo de la composición de la cinta, siendo para algunas de las composiciones mayores las respuestas ME para laminados con cintas en estado ***as-quenched*** que en ***annealed***. El valor más alto obtenido ha sido de 267 V/cm.Oe para el laminado X=3/PVDF de 3 cm de longitud con cintas magnetostrictivas tratadas térmicamente.

Con los coeficientes ME obtenidos se ha procedido a correlacionar el coeficiente ME con los diferentes parámetros implicados en dicha respuesta. Los resultados obtenidos no muestran una correlación directa entre el coeficiente ME y el coeficiente piezomagnético, ni tampoco con el factor de calidad de los laminados, por separado y como predice la teoría. Sin embargo, si se ve una correlación con el producto de ambas magnitudes.

Una vez analizada esta correlación, se ha procedido a calcular el coeficiente de acoplamiento magnetoeléctrico, que no es más que el ratio de la señal ME total medida y la señal ME esperada de forma teórica.

Considerando los resultados obtenidos para el coeficiente ME en función de la longitud de los laminados, se han cuantificación las pérdidas originadas debido a la reducción de dicha longitud. Se han cuantificado las pérdidas derivadas tanto de la reducción de la longitud (influencia del factor desimanador) como del incremento de la frecuencia de trabajo (variación de la tangente de pérdidas en ambos constituyentes, magnetostrictivo y piezoeléctrico). Los resultados obtenidos revelan que las principales pérdidas en la respuesta ME son debidas a la disminución de la longitud del laminado y a los campos de desimanación que esto produce. Los laminados con menos pérdidas corresponden a X=6/PVDF de 3 cm de longitud, ya que la composición de X=6 es la de mayor relación longitud/anchura. Las pérdidas para estos laminados son del 52 y 38 % para laminados con cintas ***as-quenched*** y ***annealed***, respectivamente. Las pérdidas para todos los laminados de 0.5 cm, sin embargo, son considerablemente mayores, oscilando entre el 95 y el 99%. Finalmente, se han corregido los coeficientes ME de los laminados considerando las mencionadas pérdidas. Se ha llegado a la conclusión de que las correcciones funcionan solamente para laminados con cintas en estado ***as-quenched***, y para relaciones longitud/anchura de magnetostrictivo mayores a 6. En dichos casos ha sido posible obtener el coeficiente ME intrínseco de los laminados.

Con la caracterización ME ya realizada, se han analizado algunas potenciales aplicaciones de estos laminados. Para ello, se han empleado los laminados X=3/PVDF y X=6/PVDF de 3 cm de longitud y ambos con cintas magnetostrictivas tratadas térmicamente, ya que los dos presentan un alto coeficiente ME.

La primera de las aplicaciones se ha centrado en el uso de los laminados como almacenadores de energía o ***energy harvesting***. Se han estudiado cuatro tipos de circuitos para la obtención de la señal ME, con el objetivo de determinar cuál era el que mayor potencia de salida ofrecía. Los resultados obtenidos muestran que el circuito multiplicador Cockcroft-Walton de dos etapas es el de mayor potencia de salida. Las potencias de salida máximas medidas han sido de 6.4 μW y 11.7 μW para los laminados de X=6/PVDF y X=3/PVDF, respectivamente.

Considerando el volumen efectivo de los laminados, las densidades de potencia para cada laminado ha sido de 1.2 mW/cm^3 para el laminado de X=6/PVDF y de 0.55 mW/cm^3 para el de X=3/PVDF.

La segunda de las aplicaciones se basa en usar estos laminados como sensores de campo magnético. Para ello, se han realizado medidas de voltaje ME inducido en función del campo magnético aplicado AC y DC. Se ha determinado la histéresis en el caso del campo aplicado DC, repitiendo las medidas con campos crecientes y decrecientes. Se han obtenido sensibilidades a campo magnético DC de 290 y 350 V/T para los laminados de X=3/PVDF y X=6/PVDF, respectivamente. En cuanto al campo AC, los resultados obtenidos muestran un gran aumento de la sensibilidad, llegando a los 12400 y 9328 V/T para los laminados de X=3/PVDF y X=6/PVDF, respectivamente. Con el objetivo de testear la aplicabilidad real de estos dispositivos, se ha realizado una primera medida de nivel de ruido en el laminado de X=6/PVDF. A 10 Hz, se ha obtenido un nivel de ruido magnético de 3 $nT/Hz^{1/2}$, mientras que a la frecuencia de resonancia, dicho valor cae hasta los 67 $pT/Hz^{1/2}$.

Finalmente, se ha estudiado el comportamiento del laminado X=3/PVDF de 3 cm con cintas en estado ***as-quenched*** hasta temperaturas de 90 ºC. Para ello, se ha analizado la influencia de la temperatura en cada componente del laminado. Se ha podido observar como el coeficiente ME decrece de la misma forma que lo hace la polarización remanente del PVDF, ya que tanto el epoxy como las aleaciones ferromagnéticas no sufren cambios significativos a temperaturas hasta 90 ºC. Por último, se han introducido nuevas poli y copoliamidas piezoeléctricas de alta temperatura como alternativa al PVDF. Estos nuevos polímeros piezoeléctricos presentan polarizaciones remanentes que se mantienen constantes hasta temperaturas por encima de 150 ºC. Se han realizado medidas ME en función de la temperatura para el laminado Vitrovac® 4040/poli 2,6, observando un coeficiente ME bastante más modesto que para los laminados fabricados con PVDF, pero que al mismo tiempo presenta la ventaja de mantenerse prácticamente constante hasta temperaturas de 90 ºC.

Table of contents

1. Introduction

This first chapter introduces the multiferroic and magnetoelectric materials, as well as the magnetoelectric (ME) effect. It summarizes the development of the magnetoelectric systems from the single phase materials to the composite ones and analyses the state of the art in the field of ME laminated composites and the improvements achieved in the obtained ME responses. It explains the different configurations when dealing with laminated composites and the advantages and disadvantages of each one. The methods of determination of the ME response magnitude in laminated composites are also commented. The key properties of each type of constituent (magnetostrictive and piezoelectric) involved in these devices are described. Finally, the structure of the report is presented and the objectives of the Thesis are disclosed.

1.1.Multiferroic and magnetoelectric materials

Multiferroic materials are known as materials that combine at least two primary forms of ferroic order, i.e, ferroelectricity, ferroelasticity, ferromagnetism and ferrotoroidicity [1]. However, most of the recent research in this field has been focused on materials exhibiting the combination of some form of the magnetic orders (either ferromagnetism or antiferromagnetism) and ferroelectricity (see Fig. 1.1). So, nowadays the term multiferroic is usually associated to the magnetic ferroelectrics.

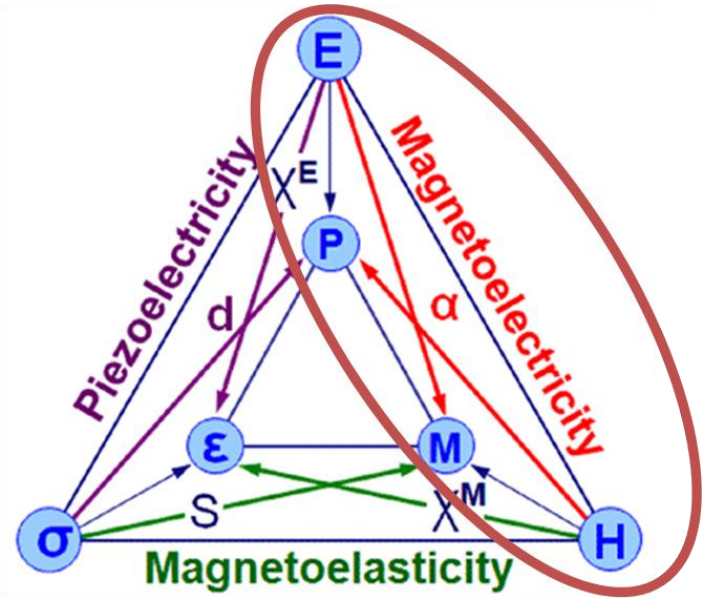

Figure 1.1. Diagram of the magneto-elasto-electric couplings.

Directly related to multiferroic materials is the magnetoelctric (ME) effect, which is defined as the induced electrical polarization (P_i) in a material when an external magnetic field (H_j) is applied (direct ME effect),

$$P_i = \alpha_{ij} H_j \tag{1.1}$$

or vice versa, as the magnetic induction (M_j) arising under the application of an electric field (E_i) (inverse ME effect),

$$M_j = \alpha_{ij}^* E_i \tag{1.2}$$

being α_{ij} the ME coefficient tensor and α_{ij}* the transpose of the tensor.

In the last years multiferroic and magnetoelectric (ME) materials have attracted an increasing interest due to their potential applications in a wide range of fields such as sensors, transducers and data storage, among others [2]. One of the most interesting applications is related with the idea of storing information both in the magnetization, *M,* and polarization, *P*. This type of encoding information in such four-state memory has been already demonstrated [3, 4].

This ME effect was first observed in single-[5] (Cr_2O_3, 20 mV/cm.Oe) and poly-crystals [6] of single-phased materials. Ascher et al. obtained a maximum voltage of 120 mV for the $Ni_3B_7O_{13}I$, being the first reported ME curve in a function of the applied magnetic field [7] (see Fig. 1.2).

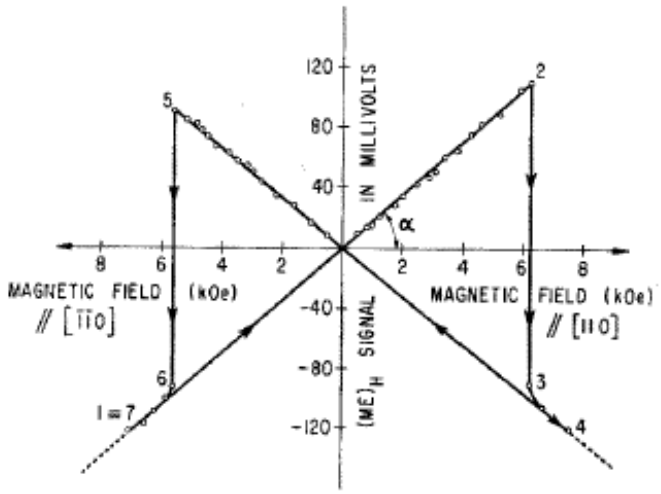

Figure 1.2. First ME curve obtained by Ascher et al. for $Ni_3B_7O_{13}I$ [7].

More recently, Kimura et al. found giant ME effect in $TbMnO_3$ perovskite manganite [8], but at 9 K and applied fields of several Tesla of magnitude.

However, the number of single-phase materials that present ME effect is limited and most of them show low responses. Since those limitations made difficult their applicability, more complex systems started to emerge, being the final

exhibited magnetoelectric property the result of the product between magnetostriction (arising from the ferromagnetic phase) and piezoelectricity (arising from the piezoelectric separated phase). These more complex systems or ***magnetoelectric composites*** are mainly particulated- and laminated-type ones.

Among the particulate composites, several structures fabricated with different magnetostrictive (Co and Ni, mainly) ferrites and PZT ($Pb[Zr_XTi_{1-X}]O_3$, lead and zirconia titanate ceramics) (0.4 V/cm.Oe) [9, 10], as well as with $BaTiO_3$ [11] (0,13 V/cm.Oe) have been studied. However, the high brittleness of the resulting composites was a clear inconvenient for their application in ME devices.

1.1.1. Magnetoelectric laminated composites

Nowadays, it is already well known that laminated ME composites with new constituents such as high permeability soft magnetostrictive materials (as iron-based Metglas alloys) and piezoelectric materials such as PZT or PVDF are those with the highest ME response [12]. Ryu et al. firstly reported a giant ME effect in discs of PZT and Terfenol-D [13] (4,68 V/cm.Oe). Since 2005, the value of the ME coefficient has increased significantly. Fang et al. [14] reached a ME coefficient of 21.46 V/cm.Oe for a Metglas 2605SA1/PVDF laminate achieved at non-resonance frequencies, by taking advantage of a magnetic flux concentrator and is, so far, the highest response obtained at non-resonance frequencies. At the longitudinal Magnetoelastic Resonance (MER), where the energy transference is maximum [15], Jin et al. [16] reported a ME coefficient of 383 V/cm.Oe on cross-linked P(VDF-TrFE)/Metglas 2605 SA1. Recently, ultrahigh ME effect has been found in thin film FeCoSiB/AlN composites deposited on Si cantilever beams, with a maximum ME coefficient of 1800 V/cm.Oe [17].

However, although large ME coefficient could be obtained in this type of thin film composites, the measured voltage, which is a product of the ME coefficient and the thickness of the piezoelectric phase, is still very weak due to the small thickness of the AlN thin film. Zhang et al reported a ME coefficient of 3800 V/cm.Oe on ferromagnetic-elastic- piezoelectric composite based on two PZT

plates and NdFeB magnets, which were elastically coupled by a cantilever beam made of phosphor copper-sheet [18].

In general, most of the ME composites found in the literature can be distributed in two main groups: the ones based on piezoelectric ceramics and the ones based in piezoelectric polymers [19]. Despite the ME voltages obtained for ceramic based ME composites are higher than for the polymer based ones, such composites may become brittle and are limited by reactions at the interface regions, which leads to high dielectric losses and hinder their incorporation into technological applications [12, 20].

Polymer-based ME materials have many advantages over the ceramic based ones. They are easily fabricated by conventional low-temperature processing into a variety of forms, such as thin sheets or molded shapes, and can exhibit improved mechanical properties [12]. Among the piezoelectric polymers, the PVDF and its copolymers are the most used polymers in ME composites since they are the family of polymers with the highest piezoelectric response [21].

Fig. 1.3 shows the four main configurations that have been categorized within the ME laminated composites [22-25]. These are the longitudinally magnetized and longitudinally poled (L-L), the longitudinally magnetized and transversely poled (L-T), the transversely magnetized and longitudinally poled (T-L) and the transversely magnetized and transversely poled (T-T).

Among them, the L-L is the one that shows a better ME response [26]. This is because the longitudinal piezoelectric coefficient d_{11} is, in general, larger than the transversal d_{31} one. However, most of the commercial piezoelectric polymers are polarized along the transversal direction, due to the limited thickness of the polymers and therefore, the difficulty to polarize them longitudinally. In the other two cases, when the magnetic field is applied along the transversal direction, the demagnetizing field plays an important role on the magnetostrictive layers, resulting in a much larger DC magnetic field required to saturate them magnetically. Consequently, the L-T is the most common structure for this type of laminated composites, and it will be also the structure of the laminated composites that will be used in this Thesis.

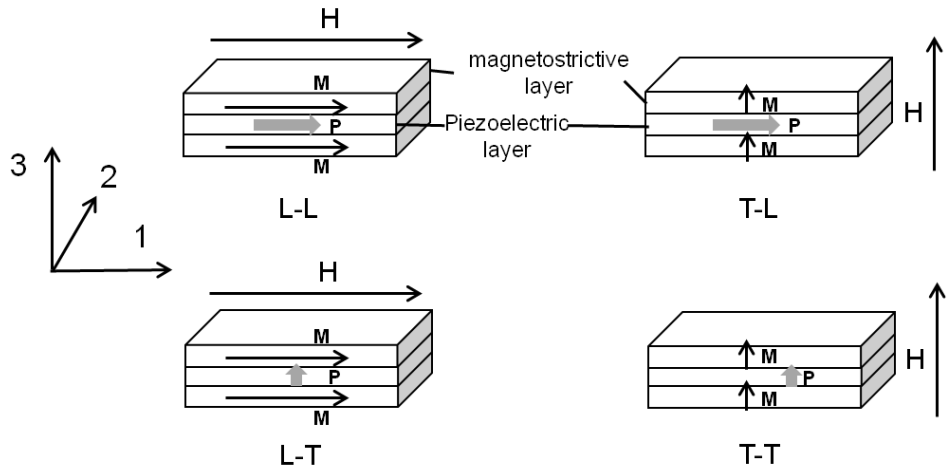

Figure 1.3. Different configurations for the ME laminate composites.

Applications based on the ME effect are as widespread as magnetic field sensors [27, 28], current sensors [29], transformers [30], microwave devices [31] and FMR resonators and filters [32, 33]. Recently, several ME energy harvesters designs have been proposed with Fe-Ni rich alloy and PZT [34], Terfenol-D and PZT [35] or PMNT [36] and Ni-Mn-Ga and PZT [37]. So far, most of them have been fabricated using PZT as the piezoelectric constituent, since it has a higher piezoelectric response. However, due to its fragility, energy harvesting devices fabricated with piezoelectric polymers are been investigated. In Chapter 4 of this Thesis, a specific energy harvesting device, as well as a magnetic field sensor based on ME laminated composites and fabricated with PVDF will be presented.

1.1.2. Determination of the magnetoelectric effect magnitude

The L-T configuration can be explained by an equivalent-circuit approach. This approach is based on the magnetostrictive and piezoelectric constitutive equations, where the magnetostrictive and piezoelectric constituents are coupled through elastic interaction. The piezoelectric constitutive equations are described as follows:

$$S_{1p} = s_{11}^{E} T_{1p} + d_{31,p} E_3 \qquad D_3 = d_{31,p} T_{1p} + \varepsilon_{33}^{S} E_3 \tag{1.3}$$

where D_3 and E_3 are the electric displacement and electric field, ε_{33}^{S} is the dielectric permittivity under constant stress T, s_{11}^{E} is the elastic compliance of the piezoelectric constituent under constant electric field E, $d_{31,p}$ is the transverse piezoelectric constant, and T_{1p} and S_{1p} are the stress and strain of the piezoelectric layer in the longitudinal direction. When the magnetic field is applied along the longitudinal axis, the piezomagnetic constitutive equations can be expressed in the following way:

$$S_{1m} = s_{11}^{H} T_{1m} + d_{11,m} H_1 \qquad B_1 = d_{11,m} T_{1m} + \mu_{11}^{T} H_1 \tag{1.4}$$

where B_1 is the magnetization along the length direction, μ_{11}^{T} is the permeability under constant stress, s_{11}^{H} is the elastic compliance of the magnetostrictive constituent under constant magnetic field, $d_{11,m}$ is the longitudinal piezomagnetic constant, and T_{1m} and S_{1m} are the stress and strain in the longitudinal direction. The appearance of the ME effect alters the previous relations that now show a new ME contribution and will be re-written as:

$$D_3 = d_{31,p} T_{1,p} + \varepsilon_{33}^{S} E_3 + \alpha_{31} H_1 \qquad B_1 = d_{11,m} T_{1m} + \alpha_{31}^{*} E_3 + \mu_{11}^{T} H_1 \tag{1.5}$$

For ME laminated systems the ME coefficient, which is usually defined as the product between the piezomagnetic and piezoelectric effects, can be written as

$$\alpha_{31} = \frac{dE_3}{dH_1} = k_c \left(\frac{\delta\lambda}{\delta H} \right) \left(\frac{\delta E}{\delta\lambda} \right) \propto \left(\frac{\delta\lambda}{\delta H} \right) d_{31} Q \tag{1.6}$$

for laminates with unconstrained longitudinal vibration. In this equation $\delta\lambda/\delta H$ is the piezomagnetic coefficient of the magnetic constituent, $\delta E/\delta\lambda$ is the piezoelectric constant of the dielectric one, k_c is the coupling constant between both constituents and Q is the quality factor.

An exact analytical solution for this coupling coefficient can be obtained by using an equivalent circuit model (see Fig. 1.4).

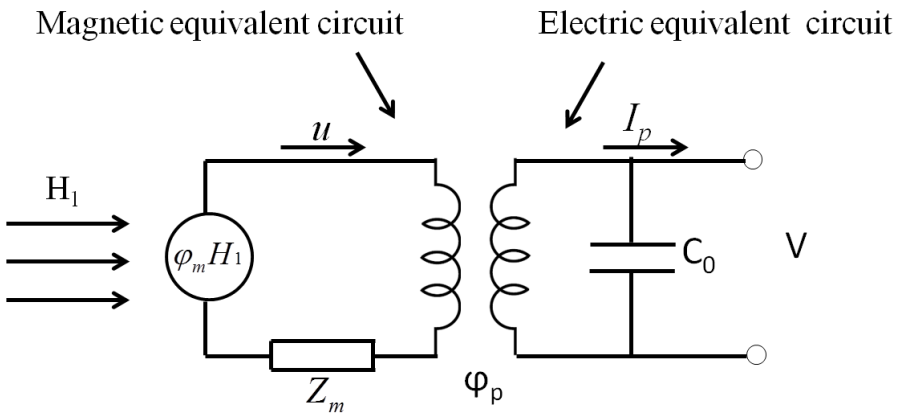

Figure 1.4. Equivalent ME circuit for the L-T configuration at low frequencies.

In this equivalent circuit, the applied *H* magnetic field acts as magnetic induced mechanical voltage ($\varphi_m H_1$), which induces a mechanical current (u) through the magnetoelastic effect with a coupling factor of φ_m. As a consequence of the coupling between magnetostrictive and piezoelectric constituents, $\varphi_m H_1$ results in an electric voltage *V*, with an associated current across the piezoelectric constituent (I_p). A transformer with turn ratio φ_p is used to represent the electromechanical coupling. In the equivalent circuit showed in Fig. 1.4, *Z* is the characteristic mechanical impedance of the laminate and C_0 is the clamped capacitance of the piezoelectric constituent.

Considering open-circuit conditions where I_p=0 and applying the Ohm's law, the ME coefficient at low frequencies for the L-T configuration can be obtained [22]:

$$\alpha_{31}^{LT} = \frac{n d_{11,m} d_{31,p}}{n\varepsilon_{33}^{S} s_{11}^{E} + (1-n) s_{11}^{H} (\varepsilon_{33}^{S} + d_{31,p}^{2} / s_{11}^{E})} \tag{1.7}$$

being $n = t_m / t_{lam}$ the magnetic phase thickness ratio, where t_m is the thickness of the magnetic phase and t_{lam} is the total thickness of the laminate.

At the magnetoelastic resonance (MER) frequency (see Fig. 1.5), the mechanical quality factor of the laminate results in an effective mechanical resistance. Thus, at the MER equation 1.7 can be written as follows [38]:

$$\alpha_{ME}^{Res} = \frac{8Qnd_{11,m}d_{31,p}}{\pi^2\left[n\varepsilon_{33}^{S}s_{11}^{E} + (1-n)s_{11}^{H}(\varepsilon_{33}^{S})\right]} \tag{1.8}$$

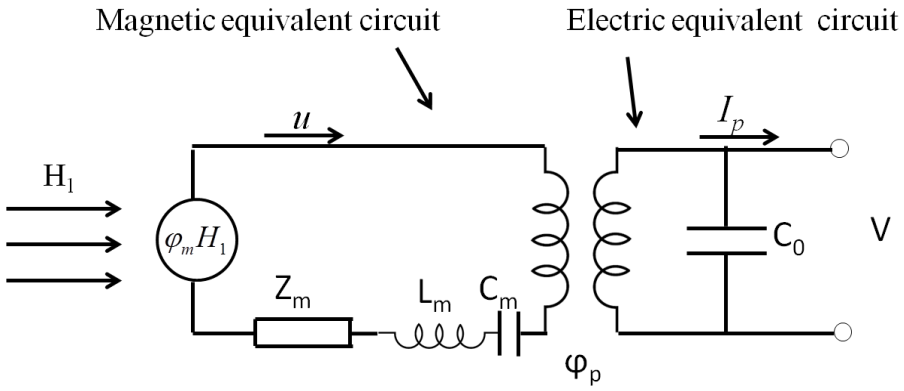

Figure 1.5. Equivalent ME circuit for the L-T configuration at the resonance frequency.

Experimentally, the ME coefficient is easily obtained through the induced ME voltage in the laminate [39]:

$$\alpha_{31} = \frac{dE}{dH} = \frac{dV_{ME}}{t_p \cdot H_{ac}} \tag{1.9}$$

being V_{ME} the induced ME voltage in the piezoelectric element of the laminated composite, t_p the thickness of the piezoelectric layer and H_{ac} the applied AC magnetic field.

1.2. Piezoelectric polymer constituent

The history of piezoelectric materials began with the discovery of piezoelectricity single-crystal materials (Rochelle salt) in 1880. Its subsequent extension into the realm of inorganic material was very successful due to the development of new piezoelectric materials such as Barium titanate ($BaTiO_3$) and perovskite-type ceramics (lead and zirconia titanate ceramics, PZT, $Pb[Zr_XTi_{1-X}]O_3$) [40]. Since then, such materials have been used in sensors, actuators and in acoustic applications due to their high elastic modulus, high dielectric constants and low

dielectric and elastic losses [41]. However, these kinds of materials have some drawbacks, such as their low strains, fragility and high mass density, which are a problem in certain applications in which weight, large area and/or mechanical properties are the key factors. These disadvantages can be overcome by using polymeric materials.

Although piezoelectricity has been found in natural polymers, such as collagen, bones and wood [42], only the synthetic PVDF (poly(vinylidene fluoride) ,$(C_2H_2F_2)_n$) and its copolymers have succeeded commercially. This is due to the fact that PVDF is the polymer with the best piezoelectric, pyroelectric and ferroelectric properties [21].

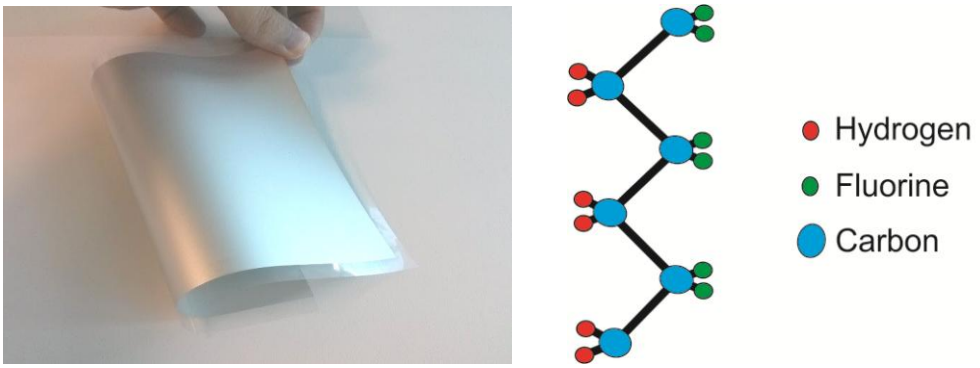

Figure 1.6. Picture of a metallized PVDF film (left) and the structure of the β-phase PVDF (right).

Moreover, PVDF has an excellent chemical resistance and good mechanical properties (see Fig. 1.6, left), which allows to use them in a wide variety of technological applications such as sensors and actuators. This semicrystalline polymer is also known for its polymorphism [43-45], being the β-phase the one with the largest piezoelectric response (see Fig. 1.6, right). Although the PVDF is in general a polymer with great properties, it also has some weaknesses. Actually, the maximum operating temperature is only about 85 °C [46], which limits its use at high temperature. Table 1.1 shows the properties of some piezoelectric materials.

Table 1.1. Properties of some piezoelectric materials

Piezoelectric material	ε (at 1 kHz)	d_{33} (pC/N)	d_{31} (pC/N)	ρ (g/cm^3)	E (GPa)	tan δ (at 1 kHz)
PZT	1200	400	-180	7.8	49	0.06
$BaTiO_3$	1700	191	-78	6.0	67	0.02
PVDF	13	-33	23	1.8	2	0.002
P(VDF/TrFE)	18	-38	12	1.9	1.2	0.016

As can be observed, although the PVDF shows lower piezoelectric response than other materials such as the PZT or $BaTiO_3$, the low dielectric losses as well as the low density make it very attractive for many applications.

Some of the potential applications are more suitable for polymers than for other type of piezoelectric materials. For instance, tactile sensors, which are widely used in industrial automation and robotics, are devices that are sensitive to the contact or touch [47, 48]. In medicine, they are commonly used in laparoscopic surgery and for non-invasive surgery, in which the scalpel and grasper need to be carefully handled inside of the human body.

Other common application where these materials are used is in energy harvesting, where the piezoelectric polymers act as a source for low power devices [49, 50]. In these cases, the mechanical vibrations are transformed into electrical signal. Pressure sensors or hydrophones are also applications where piezoelectric polymers are required [51].

1.3. Properties of the magnetic constituent

1.3.1. Magnetostriction and magnetoelasticity

Magnetostriction is the relative deformation suffered by a ferromagnetic material when subjected to an external applied magnetic field. Due to magnetostriction, each magnetic domain is deformed according to its own magnetization, which in absence of external magnetic field, points along the direction defined by the

magnetic anisotropy. The material will deform in order to minimize its internal energy.

When a magnetic field is applied, all the magnetic moments are oriented along that direction, magnetizing the ferromagnetic material. The local distortions caused by the magnetostriction will turn into a macroscopic deformation, as can be seen in Fig 1.7.

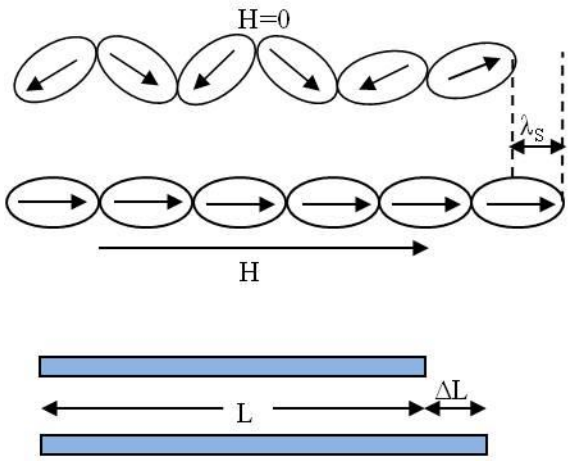

Figure 1.7. Scheme explaining the deformation that a ferromagnetic material suffered under an external magnetic field.

The magnetostriction of a ferromagnetic material is obtained by the following equation:

$$\lambda = \Delta L / L \tag{1.10}$$

where *ΔL/L* is the relative deformation undergone by the ferromagnetic material.

The maximum strain undergone by the ferromagnetic material, λ_s, is called saturation magnetostriction and is characteristic of the material. It is usually small (a few parts per million, except for the Terfenol, which exhibits a strain of 2000 ppm under a magnetic field about 0.2 T), and depending on the sign of the magnetostriction constant, the strain comes out as a elongation (positive sign) or contraction (negative sign).

Since for crystalline samples the deformation is different for each crystallographic direction, magnetostriction is commonly anisotropic. In isotropic materials, the measured deformation in a certain direction can be obtained by this expression:

$$\lambda = \frac{3}{2}\lambda_S\left(\cos^2\theta - \frac{1}{3}\right) \tag{1.11}$$

where θ is the angle between the direction of magnetization and the direction in which the deformation is measured. This expression is also valid for poly-crystals and amorphous materials, where the strain is averaged over different regions.

This coupling between the magnetic and elastic properties of ferromagnetic materials gives rise to a number of physical effects that can be used for sensing purposes. As it was previously commented, the magnetostrictive effect accounts for the change of dimensions produced in a magnetic material upon magnetization. The reverse effect, that is, the change in the magnetic state of a material caused by the application of a mechanical stress, is known as the ***magnetoelastic effect*** (also called inverse magnetostrictive or Villari effect). So, there is an effective interchange of energy from magnetic to elastic and vice versa, in ferromagnetic materials. The parameter that accounts for this energy interchange is known as magnetoelastic coupling coefficient, k ($0<k<1$), and in the case of long rod or ribbon shaped materials is given by the expression:

$$k = \sqrt{\frac{\pi^2}{8}\left[1-\left(\frac{f_r}{f_a}\right)^2\right]} \tag{1.12}$$

where f_r is the resonance frequency and f_a antiresonance frequency.

The clearest manifestation of magnetoelasticity is the dependence of the elastic constants (in particular the Young's modulus, E) of a ferromagnetic magnetostrictive material with the applied magnetic field also known as ***ΔE effect***. In particular, and for those ferromagnetic materials with a main magnetization direction, the ΔE effect is measured as the relative change in the Young modulus:

$$\Delta E(\%) = \frac{E_s - E_{\min}}{E_s} \times 100 \tag{1.13}$$

where E_s is the Young modulus at the saturation and $E_{\min}$ is the minimum value of the Young modulus. The ΔE effect is very small in normal ferromagnetic materials (6 % in nickel and less than 1 % in iron) but is very large in magnetostrictive metallic glasses after proper thermal treatments.

The magnetoelastic effect can be readily used to sense stress or any other related magnitude, and its fundamental advantage over other principles of sensing is its intrinsic non-contact nature, since magnetization changes can be detected inductively.

1.3.2. The magnetoelastic resonance method

An easy experimental set-up to determine the ΔE effect turns out to be the magnetoelastic resonance (MER) method. A stress applied to a material causes its deformation; if we apply a time varying stress we will generate the propagation of elastic waves through the material. Due to the magnetoelastic coupling in ferromagnetic materials, those waves can be magnetostrictively generated using a small amplitude exciting magnetic field, $h.cos(\omega t)$. Those strain waves will provoke magnetoelastically induced alternating changes in the magnetization of the sample that can be inductively detected. Under specific boundary conditions, the propagated waves become stationary, and if their frequency is such that the wavelength of the mechanical oscillation matches the dimension of the sample, a MER will take place. At this resonance frequency, large strain and maximum magnetization oscillation are induced and the apparent susceptibility of the material reaches the maximum.

For a magnetoelastic sample of length L and density ρ, vibrating with free ends, and under simultaneously applied magnetic fields H (static) and $h.cos(\omega t)$ (alternating, $h<<H$) the relationship between Young modulus $E(H)$, and measured resonance frequency is given by:

$$f_r^n = \frac{n}{2L}\sqrt{\frac{E(H)}{\rho}} \tag{1.14}$$

being n the resonance mode number. This resonant frequency is in practice easy to be measured and usually n=1 turns out to be the strongest mode. From this first resonance mode, the Young's modulus can be calculated as:

$$E(H) = \rho(2Lf_r)^2 \tag{1.15}$$

and so the elastic compliance can be derived as:

$$s_{11}^H = \frac{1}{E^H} \tag{1.16}$$

where $E^H = E(H)$ is the Young modulus at that applied magnetic field value.

Another important parameter that can be obtained from the magnetoelastic resonance curve is the mechanical quality factor, Q, which basically quantifies the energy losses of the resonator. Therefore, whereas high Q values turn into a sharper and narrower resonance curve and indicate a low rate of energy losses relative to the stored energy, small Q values give rise to a wider bandwidth and a higher rate of energy losses. Q quality factor can be calculated by the following equation:

$$Q = \frac{f_r}{\Delta f} \tag{1.17}$$

where f_r is the resonance frequency, and Δf is the bandwidth measured at $V_{max}/\sqrt{2}$.

Those three parameters, E(H), k(H) and Q(H), measured as a function of the applied static field or bias, fully characterize the magnetoelastic behaviour of the magnetostrictive/magnetoelastic material.

This magnetoelastic resonance exhibited by magnetostrictive materials has been already successfully implemented in commercial applications. This is the working principle of tags or labels for Electronic Article Surveillance (EAS) systems. If the

label is activated, that is, if it shows a magnetoelastic resonance, it will trigger an alarm when crossing an adequate interrogation and detection system.

1.3.3. Demagnetizing effects

When a ferromagnetic material is placed into a uniform magnetic field, magnetic poles are formed at its opposite ends (see Fig 1.8). These poles cause within the magnetic material a magnetic field opposite in direction to the applied field, H_a, which means that a higher magnetic field is required to saturate magnetically the ferromagnetic materials.

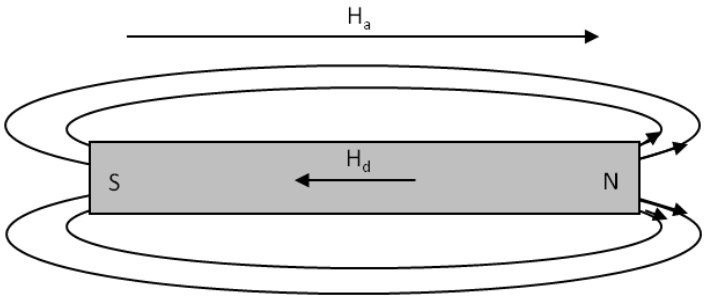

Figure 1.8. Diagram of the demagnetizing field in a ferromagnetic material.

The *demagnetizing field*, H_d, is proportional to the magnetization of the material, H_d=-NM, being N the demagnetization factor and M magnetization. Therefore, the true magnetic field H_t within the ferromagnetic material will be given by $H_t = H_a - NM$.

In the case of ferromagnetic materials with one dimension much higher than the other two (a ribbon shaped sample, for example), N value is very small and can be neglected. However, its value increases as this long dimension becomes shorter, and the true magnetic field value inside the material will be strongly affected. This reduction in the effective magnetic field suffered by the magnetic material will have drastic consequences in the magnetoelectric response of the studied laminates, as it will be deeply analyze in the following Chapters of this report.

1.4. Objectives and structure of the thesis

When this work started in 2012, all previous work in magnetoelectric devices made by the different research groups was fully devoted to achieve the highest possible induced magnetoelectric voltage. In fact, our own experience was focused only in the study of granular ME composites made of magnetostrictive Co-ferrite ($CoFe_2O_4$, $\lambda \approx 100$ ppm) embedded in P(VDF-TrFE) piezoelectric polymer (see Fig. 1.9).

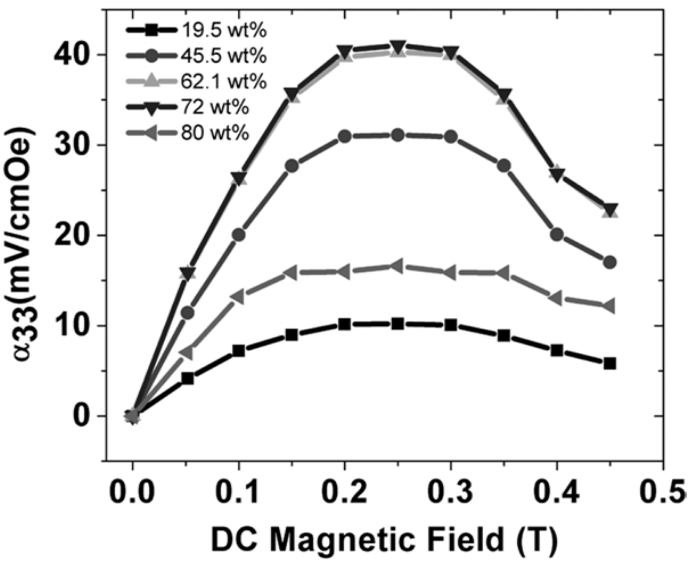

Figure 1.9. Measured ME coefficients as a function of the bias filed and filling fractions of CoFe2O4 nanoparticle (taken from Fig 4 at Ref. [52]).

The maximum ME coupling magnitude measured was of about 40 mV/cm.Oe at an applied bias of 0.25 T, not very suitable results if the purpose is to fabricate an extremely sensitive magnetic field detector, for example.

Besides this fact, at that moment nobody had paid close attention to several remaining more basic questions, such as: can they be experimentally demonstrated the previously theoretically deduced dependences of the ME coupling coefficient with $d\lambda/dH$ and/or Q and/or other parameters? By changing

the size of the magnetoelectric device, is it possible to reach the radio-frequency working range in order to use these devices in near-field communication applications? Is it possible to control and quantify the size effects arising when reducing the size of the devices, for miniaturized applications? If so, what's about temperature effect? How does the magnetoelectric signal change as temperature rises to that of extreme human environments, as the desert, for example?

The aim of this Thesis is to give answer to all these questions:

a) By using magnetostrictive materials with different composition and magnetostriction values, and analyzing the different dependencies of the generated magnetoelectric signal in laminated type composites (subject of study in Chapter 3);

b) By changing the size of the magnetoelectric devices, reaching the radio-frequency working regime and analyzing the effect of the demagnetizing field and subsequently the losses generated in such devices (subject of study also in Chapter 3);

c) By fabricating and studying the applicability of these devices to two different types of sensors: an energy harvesting device and a magnetic field sensor (subject of study of Chapter 4);

d) By showing the first tests performed in order to study the applicability of these magnetoelectric devices at high temperatures (subject of study of Chapter 5);

Finally, the conclusions derived from this work will be presented and new open questions for future work will be pointed out.

References

[1] H. Schmid, "Multi-ferroic magnetoelectrics," *Ferroelectrics,* vol. 162, p. 317, 1994/01/01 1994.

[2] C.-W. Nan, M. I. Bichurin, S. Dong, D. Viehland, and G. Srinivasan, "Multiferroic magnetoelectric composites: Historical perspective, status, and future directions," *Journal of Applied Physics,* vol. 103, p. 031101, 2008.

[3] M. Gajek, M. Bibes, S. Fusil, K. Bouzehouane, J. Fontcuberta, A. Barthelemy*, et al.*, "Tunnel junctions with multiferroic barriers," *Nat Mater,* vol. 6, pp. 296-302, 2007.

[4] Z. Shi, C. Wang, X. Liu, and C. Nan, "A four-state memory cell based on magnetoelectric composite," *Chinese Science Bulletin,* vol. 53, pp. 2135-2138, 2008/07/01 2008.

[5] D. N. Astrov, "Magnetoelectric effect in chromium oxide," *Soviet Physics JETP,* vol. 13, p. 729, 1961.

[6] G. T. Rado and V. J. Folen, "Observation of the magnetically induced magnetoelectric effect and evidence for antiferromagnetic domains," *Physical Review Letters,* vol. 7, pp. 310-311, 1961.

[7] E. Ascher, H. Rieder, H. Schmid, and H. Stössel, "Some properties of ferromagnetoelectric nickel-iodine boracite, Ni 3B7O13I," *Journal of Applied Physics,* vol. 37, pp. 1404-1405, 1966.

[8] T. Kimura, T. Goto, H. Shintani, K. Ishizaka, T. Arima, and Y. Tokura, "Magnetic control of ferroelectric polarization," *Nature,* vol. 426, pp. 55-58, 2003.

[9] J. Van Den Boomgaard, A. M. J. G. Van Run, and J. V. Suchtelen, "Magnetoelectricity in piezoelectric-magnetostrictive composites," *Ferroelectrics,* vol. 10, pp. 295-298, 1976/01/01 1976.

[10] S. Lopatin, I. Lopatina, and I. Lisnevskaya, "Magnetoelectric PZT/ferrite composite material," *Ferroelectrics,* vol. 162, pp. 63-68, 1994/01/01 1994.

[11] J. Ryu, S. Priya, K. Uchino, and H.-E. Kim, "Magnetoelectric Effect in Composites of Magnetostrictive and Piezoelectric Materials," *Journal of Electroceramics,* vol. 8, pp. 107-119, 2002/08/01 2002.

[12] P. Martins and S. Lanceros-Méndez, "Polymer-based magnetoelectric materials," *Advanced Functional Materials,* vol. 23, pp. 3371-3385, 2013.

[13] J. Ryu, A. V. Carazo, K. Uchino, and H. E. Kim, "Magnetoelectric properties in piezoelectric and magnetostrictive laminate composites," *Japanese Journal of Applied Physics, Part 1: Regular Papers and Short Notes and Review Papers,* vol. 40, pp. 4948-4951, 2001.

[14] Z. Fang, S. G. Lu, F. Li, S. Datta, Q. M. Zhang, and M. El Tahchi, "Enhancing the magnetoelectric response of Metglas/polyvinylidene fluoride laminates by exploiting the flux concentration effect," *Applied Physics Letters,* vol. 95, p. 112903, 2009.

[15] G. Srinivasan, "Magnetoelectric composites," in *Annual Review of Materials Research* vol. 40, pp. 153-178, 2010,.

[16] J. Jin, S.-G. Lu, C. Chanthad, Q. Zhang, M. A. Haque, and Q. Wang, "Multiferroic Polymer Composites with Greatly Enhanced Magnetoelectric Effect under a Low Magnetic Bias," *Advanced Materials,* vol. 23, pp. 3853-3858, 2011.

[17] H. Greve, E. Woltermann, R. Jahns, S. Marauska, B. Wagner, R. Knöchel*, et al.*, "Low damping resonant magnetoelectric sensors," *Applied Physics Letters,* vol. 97, p. 152503, 2010.

[18] M. Li, Y. Zhang, G. Liu, H. Shi, W. Xiao, Y. Zhu*, et al.*, "Enhanced magnetoelectric effect in ferromagnetic-elastic-piezoelectric composites," *Journal of Alloys and Compounds,* vol. 613, pp. 93-95, 2014.

[19] P. Martins, R. Gonçalves, S. Lanceros-Mendez, A. Lasheras, J. Gutiérrez, and J. M. Barandiarán, "Effect of filler dispersion and dispersion method on the piezoelectric and magnetoelectric response of CoFe2O4/P(VDF-TrFE) nanocomposites," *Applied Surface Science,* vol. 313, pp. 215-219, 9/15/ 2014.

[20] J. Ma, J. Hu, Z. Li, and C.-W. Nan, "Recent Progress in Multiferroic Magnetoelectric Composites: from Bulk to Thin Films," *Advanced Materials,* vol. 23, pp. 1062-1087, 2011.

[21] P. Martins, A. C. Lopes, and S. Lanceros-Mendez, "Electroactive phases of poly(vinylidene fluoride): Determination, processing and applications," *Progress in Polymer Science,* vol. 39, pp. 683-706, 2014.

[22] S. Dong, J. F. Li, and D. Viehland, "Longitudinal and transverse magnetoelectric voltage coefficients of magnetostrictive/piezoelectric laminate composite: Theory," *IEEE Transactions on Ultrasonics, Ferroelectrics, and Frequency Control,* vol. 50, pp. 1253-1261, 2003.

[23] S. Dong, J. F. Li, and D. Viehland, "Longitudinal and transverse magnetoelectric voltage coefficients of magnetostrictive/piezoelectric laminate composite: Experiments," *IEEE Transactions on Ultrasonics, Ferroelectrics, and Frequency Control,* vol. 51, pp. 794-799, 2004.

[24] S. Dong, J. F. Li, and D. Viehland, "Characterization of magnetoelectric laminate composites operated in longitudinal-transverse and transverse-transverse modes," *Journal of Applied Physics,* vol. 95, pp. 2625-2630, 2004.

[25] S. Dong, J. F. Li, and D. Viehland, "Giant magneto-electric effect in laminate composites," *IEEE Transactions on Ultrasonics, Ferroelectrics, and Frequency Control,* vol. 50, pp. 1236-1239, 2003.

[26] S. Dong, J. F. Li, and D. Viehland, "A longitudinal-longitudinal mode TERFENOL-D/Pb(Mg 1/3Nb 2/3)O 3-PbTiO 3 laminate composite," *Applied Physics Letters,* vol. 85, pp. 5305-5306, 2004.

[27] J. Kiser, P. Finkel, J. Gao, C. Dolabdjian, J. Li, and D. Viehland, "Stress reconfigurable tunable magnetoelectric resonators as magnetic sensors," *Applied Physics Letters,* vol. 102, pp. 042909-042909-4, 2013.

[28] J. Gao, D. Gray, Y. Shen, J. Li, and D. Viehland, "Enhanced dc magnetic field sensitivity by improved flux concentration in magnetoelectric laminates," *Applied Physics Letters,* vol. 99, p. 153502, 2011.

[29] S. Dong, J. G. Bai, J. Zhai, J.-F. Li, G.-Q. Lu, D. Viehland*, et al.*, "Circumferential-mode, quasi-ring-type, magnetoelectric laminate composite—a highly sensitive electric current and/or vortex magnetic field sensor," *Applied Physics Letters,* vol. 86, p. 182506, 2005.

[30] S. Dong, J. Zhai, S. Priya, J. F. Li, and D. Viehland, "Tunable features of magnetoelectric transformers," *IEEE Transactions on Ultrasonics, Ferroelectrics, and Frequency Control,* vol. 56, pp. 1124-1127, 2009.

[31] S. Shastry, G. Srinivasan, M. I. Bichurin, V. M. Petrov, and A. S. Tatarenko, "Microwave magnetoelectric effects in single crystal bilayers of yttrium iron garnet and lead magnesium niobate-lead titanate," *Physical Review B - Condensed Matter and Materials Physics,* vol. 70, pp. 064416-1-064416-6, 2004.

[32] Y. K. Fetisov and G. Srinivasan, "Electric field tuning characteristics of a ferrite-piezoelectric microwave resonator," *Applied Physics Letters,* vol. 88, 2006.

[33] Z. Huang, "Theoretical modeling on the magnetization by electric field through product property," *Journal of Applied Physics,* vol. 100, 2006.

[34] L. Bian, Y. Wen, P. Li, Q. Gao, and M. Zheng, "Magnetoelectric transducer with high quality factor for wireless power receiving," *Sensors and Actuators, A: Physical,* vol. 150, pp. 207-211, 2009.

[35] P. Li, Y. Wen, P. Liu, X. Li, and C. Jia, "A magnetoelectric energy harvester and management circuit for wireless sensor network," *Sensors and Actuators, A: Physical,* vol. 157, pp. 100-106, 2010.

[36] J. Yang, Y. Wen, P. Li, X. Dai, and M. Li, "A new vibration energy harvester using magnetoelectric transducer," *Journal of Magnetics,* vol. 16, pp. 150-156, 2011.

[37] S. Ju, S. H. Chae, Y. Choi, S. Lee, H. W. Lee, and C. H. Ji, "A low frequency vibration energy harvester using magnetoelectric laminate composite," *Smart Materials and Structures,* vol. 22, 2013.

[38] S. Dong, J.-F. Li, and D. Viehland, "Magnetoelectric coupling, efficiency, and voltage gain effect in piezoelectric-piezomagnetic laminate composites," *Journal of Materials Science,* vol. 41, pp. 97-106, 2006/01/01 2006.

[39] R. Jungho, C. Alfredo Vázquez, U. Kenji, and K. Hyoun-Ee, "Magnetoelectric Properties in Piezoelectric and Magnetostrictive Laminate Composites," *Japanese Journal of Applied Physics,* vol. 40, p. 4948, 2001.

[40] G. Busch, "Early history of ferroelectricity," *Ferroelectrics,* vol. 74, pp. 267-284, 1987/08/01 1987.

[41] A. E. Crawford, "Lead zirconate-titanate piezoelectric ceramics," *British Journal of Applied Physics,* vol. 12, pp. 529-534, 1961.

[42] E. Fukada, H. Ueda, and R. Rinaldi, "Piezoelectric and related properties of hydrated collagen," *Biophysical Journal,* vol. 16, pp. 911-918, 1976.

[43] R. Gregorio and R. C. CapitãO, "Morphology and phase transition of high melt temperature crystallized poly(vinylidene fluoride)," *Journal of Materials Science,* vol. 35, pp. 299-306, 2000/01/01 2000.

[44] M. P. Silva, V. Sencadas, G. Botelho, A. V. Machado, A. G. Rolo, J. G. Rocha*, et al.*, "α- and γ-PVDF: Crystallization kinetics, microstructural variations and thermal behaviour," *Materials Chemistry and Physics,* vol. 122, pp. 87-92, 7/1/ 2010.

[45] H. Pan, B. Na, R. Lv, C. Li, J. Zhu, and Z. Yu, "Polar phase formation in poly(vinylidene fluoride) induced by melt annealing," *Journal of Polymer Science Part B: Polymer Physics,* vol. 50, pp. 1433-1437, 2012.

[46] M. P. Silva, C. M. Costa, V. Sencadas, A. J. Paleo, and S. Lanceros-Méndez, "Degradation of the dielectric and piezoelectric response of β-poly(vinylidene fluoride) after temperature annealing," *Journal of Polymer Research,* vol. 18, pp. 1451-1457, 2011/11/01 2011.

[47] L. Seminara, L. Pinna, M. Valle, L. Basirico, A. Loi, P. Cosseddu*, et al.*, "Piezoelectric Polymer Transducer Arrays for Flexible Tactile Sensors," *Sensors Journal, IEEE,* vol. 13, pp. 4022-4029, 2013.

[48] H.-J. Tseng, W.-C. Tian, and W.-J. Wu, "P(VDF-TrFE) Polymer-Based Thin Films Deposited on Stainless Steel Substrates Treated Using Water Dissociation for Flexible Tactile Sensor Development," *Sensors,* vol. 13, p. 14777, 2013.

[49] O. Sharon Rosyln, W. Ting Chong, T. Chin Yaw, Y. Kui, and T. Francis Eng-Hock, "Fabrication of piezoelectric polymer multilayers on flexible substrates for energy harvesting," *Smart Materials and Structures,* vol. 23, p. 015013, 2014.

[50] K. In-Ho, J. SeungSeop, J. Seon-Jun, and J. Hyung-Jo, "A performance-enhanced energy harvester for low frequency vibration utilizing a corrugated cantilevered beam," *Smart Materials and Structures,* vol. 23, p. 037002, 2014.

[51] F. Bauer, "PVF2 polymers: Ferroelectric polarization and piezoelectric properties under dynamic pressure and shock wave action," *Ferroelectrics,* vol. 49, pp. 231-240, 1983/11/01 1983.

[52] P. Martins, A. Lasheras, J. Gutierrez, J. M. Barandiaran, I. Orue, and S. Lanceros-Mendez, "Optimizing piezoelectric and magnetoelectric responses on CoFe 2O4/P(VDF-TrFE) nanocomposites," *Journal of Physics D: Applied Physics,* vol. 44, 2011.

2. Experimental

This Chapter firstly describes the procedure used to fabricate the magnetostrictive ferromagnetic amorphous ribbons by using the melt spinning technique. Afterwards, the home-made system employed to perform the annealing of the magnetostrictive ribbons is presented. The experimental techniques used to characterize the as-quenched and annealed magnetostrictive ribbons are also showed. The piezoelectric properties of the polyvinylidene fluoride (PVDF) are detailed, as well as the thermal characterization of the epoxy used to bond the magnetostrictive and piezoelectric constituents. Finally, the fabrication process of the laminated composites and the experimental set-up to measure the ME response are described. At the end of the Chapter, the results of the magnetic characterization for all the magnetostrictive ribbons, as well as the induced ME voltages in the laminates are summarized.

2.1. Magnetostrictive constituent

Four different ferromagnetic amorphous ribbons were fabricated to be used as magnetostrictive constituents. The compositions fabricated were the following:

- $(Fe_{0.79}Co_{0.21})_{75+x}Si_{15-1.4x}B_{10+0.4x}$ (X=0, X=3 and X=6)
- $Fe_{85-x}Co_xB_{15}$ (X=21)

These magnetostrictive ribbons were chosen due to their expected low anisotropy field, high magnetization value, which implies a high magnetic susceptibility, and also due to their relative high saturation magnetostriction [1-3]. Actually, it has to be noted that according to equations 1.6, 1.7 and 1.8, the ME coefficient is proportional to the magnetostriction per unit applied magnetic field, which makes the metallic glasses more interesting than other high magnetostriction constituents such as Terfenol-D [4].

Aiming to simplify the notation, in the following each composition will be labelled as X=0, X=3, X=6 and X=21.

2.1.1. Fabrication of the magnetostrictive ribbons

The magnetostrictive ribbons were fabricated by the Melt Spinning technique [5]. Before fabricating the ribbons, it is necessary to obtain the mother alloy. An induction furnace (Induret Compact, Reitel) was used for that purpose (see Fig. 2.1) and 16 gr of each composition were prepared, enough to obtain a very long ribbon of several meters.

This furnace consists of a thick helicoidal coil, which is refrigerated with water and surrounds a ceramic crucible. The ceramic crucible has an opening below, which will keep closed with a stopper during the melting process. A thermocouple is introduced into the stopper to control the temperature. In order to favor the melting, the elements are carefully put as compact as possible at the center of the crucible. When all the elements are properly placed, the chamber is closed and vacuum is made inside the chamber, through the Venturi effect.

Previously, the chamber must be purged with argon several times in order to clean its atmosphere as better as possible.

Figure 2.1. Picture of the used Reitel Indurect Compact induction furnace (left). View of the coil and thermocouple of the furnace (right).

The heating happens due to the dissipative Joule effect caused by the induction of "eddy currents" in the metals. These currents arise from a high frequency electric current circulating through the coil. The melting process can be directly visualized through a window located above the crucible. When the alloy is completely melted and homogeneous (approximately at 1300 ºC for these alloys), the crucible is opened by lifting the stopper and an argon pressure of 3-4 bar is introduced, falling down to a suitable copper mold (see Fig. 2.2). In our case, and due to the specific use of our samples, the mold was fabricated to obtain a sample in a form of cylindrical ingot.

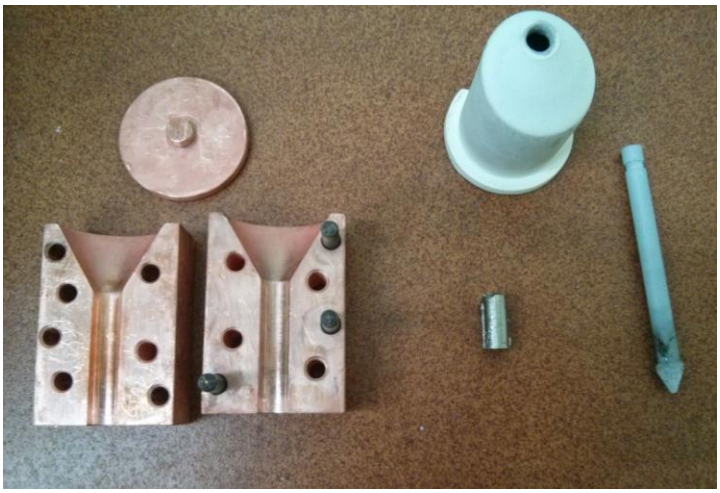

Figure 2.2. Picture of the copper mold, crucible, stopper and the obtained ingot.

Once we have obtained the mother alloys for all compositions, we proceeded to fabricate the ribbons by the Melt Spinning technique (Fig. 2.3, left). The Melt Spinning technique consists in a copper wheel, which is rotating at high speed. The mother alloy is introduced into a quartz tube which is located at a certain distance to the wheel. A high frequency current is passed through the coil by a power supplier, which heats the alloy by the induction of eddy currents, and melts the alloy again (see Fig. 2.3, right). The diameter of the outlet hole of the tube was about 2 mm and the distance between the outlet hole and the wheel was 0.15 mm. All the alloys were ejected at a temperature around 1300 ºC, with an argon overpressure of 200 mbar.

The magnetostrictive ribbons used in this work were fabricated under vacuum conditions, avoiding the oxidation of the metallic glasses. Among the fabricated ribbons, the X=0 one was fabricated in the Department of Chemical Engineering at the University of the Basque Country, under the supervision of the Dr. Angel Rodríguez Pierna. The rest of the compositions were fabricated at the Institute of Metal Physics of the Ural Federal University (Russia), with the help of Denis Shishkin and Anatoly Potapov. Fig 2.3 (left) shows a picture of a Melt Spinner located at the Universitat Politècnica de Catalunya, in Castelldefels, where several tests were performed before fabricating the ribbons.

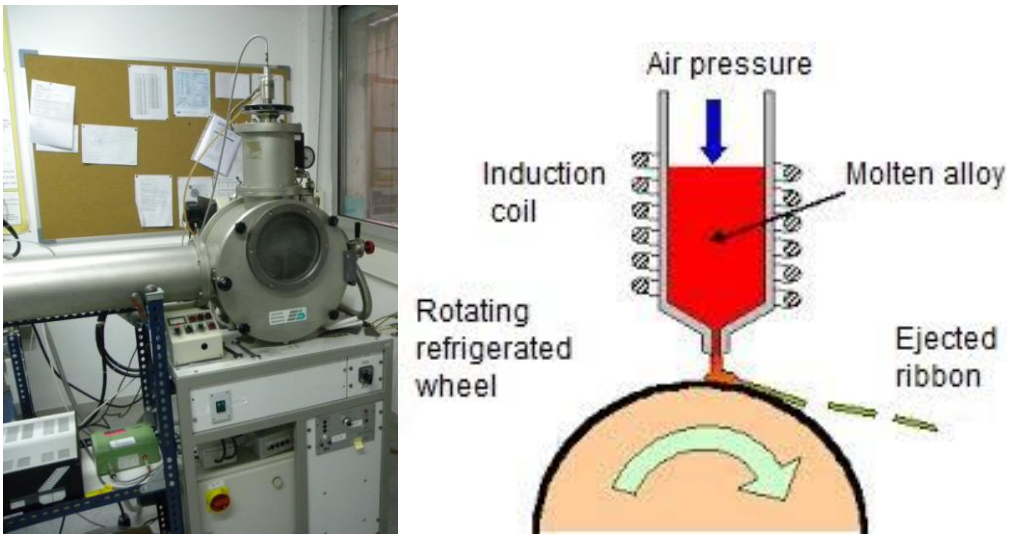

Figure 2.3. Picture of the Melt Spinner located at the Universitat Politècnica de Catalunya (left) were several tested of the optimum parameters were performed. Diagram of the Melt Spinning technique (right).

After their fabrication, ribbons with widths between 1.6 and 5 mm and thicknesses between 10 and 30 μm were obtained. Detailed geometry parameters for all compositions are given in Table 2.1.

Table 2.1. Geometry parameters and density of the obtained magnetostrictive alloys

Magnetostrictive alloys		Width (mm)	Thickness (μm)	ρ (kg/m^3)
$(Fe_{0.79}Co_{0.21})_{75+x}Si_{15-1.4x}B_{10+0.4x}$	X=0	1.8	28	7439
	X=3	5	20	7502
	X=6	1.6	13	7564
$Fe_{85-x}Co_xB_{15}$	X=0	1.8	28	7439

2.1.2. Annealing of the magnetostrictive ribbons

The fabrication process of the magnetostrictive alloys induces some internal stresses during the rapid quenching that determines some of the magnetic parameters of the amorphous ribbons [6, 7]. Therefore, an appropriate heat treatment could help to relieve those stresses and improve the magnetic and

magnetostrictive/magnetoelastic properties[1, 8]. Thus, the fabricated amorphous magnetostrictive ribbons were studied in two different states: in as-quenched (AQ) and annealed (AN) states.

The annealing process was performed by putting carefully amorphous ribbons of 3, 2, 1 and 0.5 cm long of each composition between two aluminium pieces (see Fig 2.4, left). The temperature was measured with a K-thermocouple, located in a small slit at the surface of one of the pieces. Once properly placed, the aluminium pieces were firmly tightened to assure good temperature homogeneity.

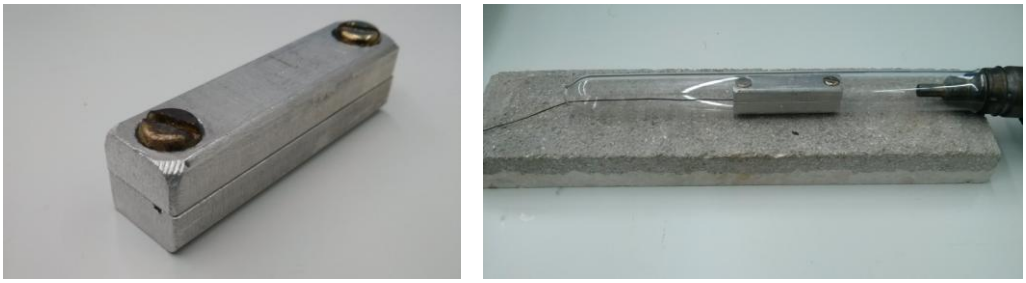

Figure 2.4. Picture of aluminium pieces used for the annealing of the ribbons (left). Picture of the whole system used for the annealing process (right).

In order to minimize heat losses, the aluminium pieces were inserted into a quartz tube resting on a piece of stone for temperature isolation. The quartz tube was fabricated to be opened in both sides, so allowing the hot air to flow across the assembly (Fig 2.4, right). A heat gun was then used to heat the whole system. The system was heated at 300 ºC for 10 minutes. After that, the system was left to cool down to room temperature.

This thermal treatment was chosen after doing several tests with different temperature/time values. It was concluded that temperature was high enough to relieve the stresses produced in the fabrication process and low enough to avoid any crystallization process. A higher temperature led to more brittle ribbons, clearly indicating the onset of crystallization of the amorphous initial structure.

The annealing process was carried out at air atmosphere, which means that some oxide could appear on the surface of the magnetostrictive ribbons. That problem

was overcome by cleaning the sample with phosphoric acid and an ammonia neutralizer.

However, as it will be showed in the section 2.5, not all the compositions show the same behaviour after annealing. In fact, since each composition to be studied was fabricated independently, the induced anisotropy was different for each composition, and consequently, the behaviour of as-quenched and annealed ribbons could also vary from one composition to another.

2.1.3. Magnetic characterization

2.1.3.1. Hysteresis loop and magnetic susceptibility

Hysteresis loops of all ribbons were measured by using a classical inductive hysteresis loop tracer (see Fig. 2.5, right). The magnetic field was generated by a pair of Helmholtz coils driven by a bipolar power supply (KEPCO BOP 20-20M) at a given frequency and calculated from the voltage drop across a standard resistor, assuming a conversion factor of 30.4 Oe/A. The sample was placed in the central region between the coils and surrounded by a small pick-up coil of 2000 turns (see Fig. 2.5, left).

In order to compensate the magnetic flux produced by the Helmholtz coils on the pick-up coil, a compensation coil was placed in series-opposition to the pick-up coil. Therefore, the measured signal was just the one arisen only from the sample magnetization.

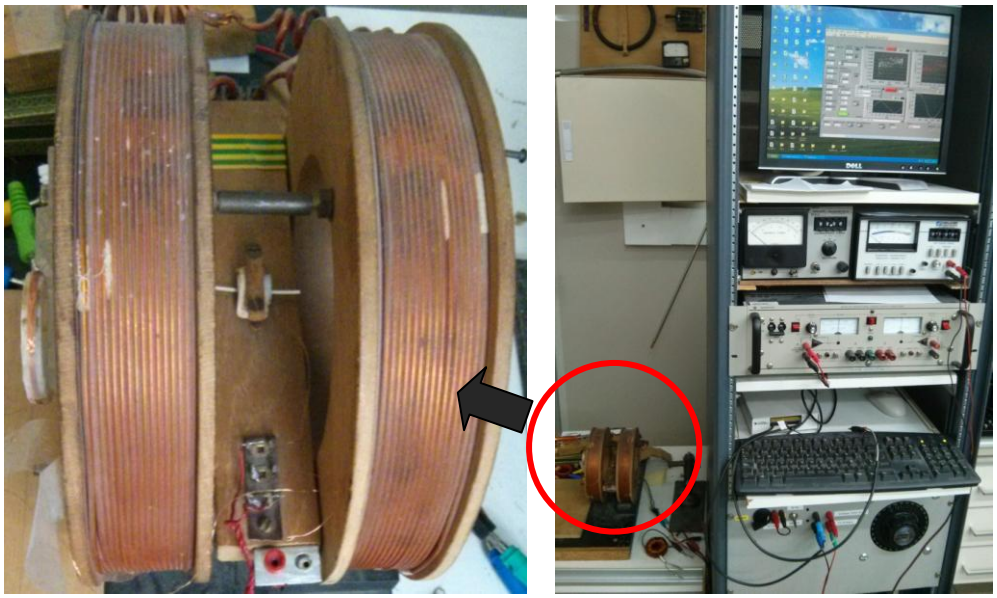

Figure 2.5. Picture of Helmholtz coils, with the sample within pick up (left). General view of the inductive hysteresis loop tracer (right).

The applied time-varying magnetic field changes the magnetization state of the sample, as well as the flux density across the pick-up coil. The voltage induced according to the Faraday's Law is then integrated by a fluxmeter, which calculates the magnetic flux (in Wb/m^2) as $\phi = V_{\text{int}} RC$, where V_{int} is the integrated voltage and RC is a time constant which depends on the selected parameters in the fluxmeter.

The magnetic polarization, $\mu_0 M$ (in Tesla), is then easily obtained from $\phi = (\mu_0 M) NS$, being N the number of turns of the secondary coil (2000) and S, the cross section of the ribbon.

The obtained $\mu_0 M$ values are then displayed as a function of the applied magnetic field. Fig. 2.6 shows the hysteresis loops for the X=6 alloy for a very long ribbon, and 3, 2, 1 and 0.5 cm long pieces.

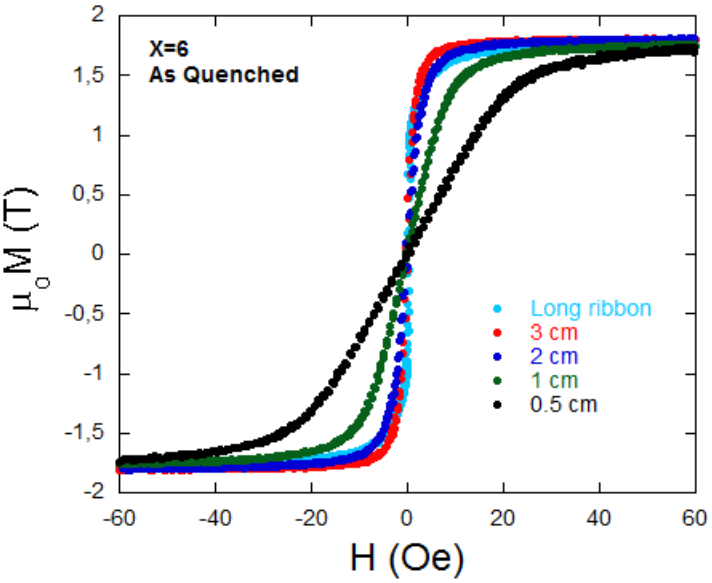

Figure 2.6. Hysteresis loops for different lengths of the X=6 as-quenched composition.

As expected, the smaller the length of the ribbon, more sloping are the measured hysteresis loops due to the demagnetizing effect and so higher external fields are needed to reach magnetic saturation. The magnetic field at which the ferromagnetic ribbons are magnetically saturated is known as the anisotropy field, H_k. A deep study of this demagnetizing field and its influence in the ME response will be shown in Chapter 3.

The intrinsic magnetic susceptibilities of the magnetostrictive ribbons were extracted from the measurements of very long ribbons, by determining the initial slope of the hysteresis loop:

$$\chi_m = \frac{M}{H} \tag{2.1}$$

In the case of the annealed ribbons, the required demagnetizing correction has been exactly extrapolated from that deduced for the as-quenched ribbons of exactly the same length.

2.1.3.2. Measurement of the magnetostriction

The magnetostriction of all samples (as-quenched and annealed state and with lengths ranging from 0.5 cm to 3 cm) was measured by strain gauges, using a Wheatstone bridge working in half bridge configuration and including a passive gauge (see Fig. 2.7, right). The strain gauges (Kiowa Electronic Instruments Co., Ltd.) were chosen to have sufficiently small dimensions to be correctly stuck to the ribbon surface by using a M-Bond 600 adhesive (Micro-Measurements). Squared shaped strain gauges of 0.2 mm side, with a gauge factor of 1.99 and a resistance of 120 Ω have been used for magnetostriction measurements.

The measuring mechanism is simply based on the changes of the ohmic resistance of the strain gauge conductor due to the elongation or piezoresistive effect (see Fig. 2.7, left). This strain is calculated from the following expression:

$$\varepsilon = \frac{\Delta L}{L} = \frac{\Delta R/R}{GF} \tag{2.2}$$

Being $\Delta R/R$ the ratio of fractional change in electrical resistance and GF, the Gauge Factor of the strain gauge.

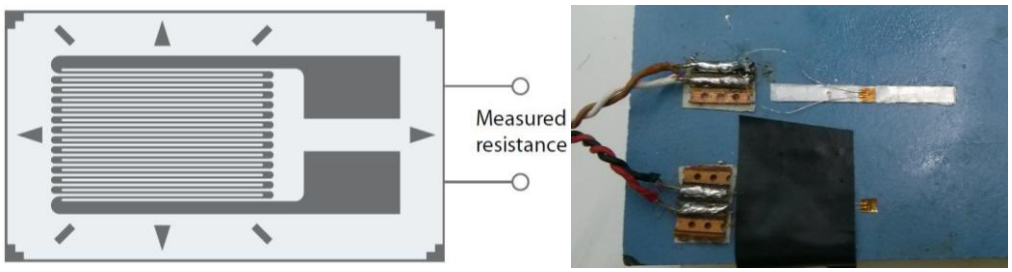

Figure 2.7. Diagram of a strain gauge (left). Picture of the half bridge configuration used to measure the magnetostriction of the ribbons (right).

The external magnetic field was generated with the same coil system that was described in the previous section. The change of the electrical resistivity along the strain gauge was measured by a strain indicator, and recorded in a computer. Fig. 2.8 shows the magnetostriction, λ, (a) and piezomagnetic coefficient, $d\lambda/dH$, (b) for the X=3 composition, both curves for the as-quenched state ribbon.

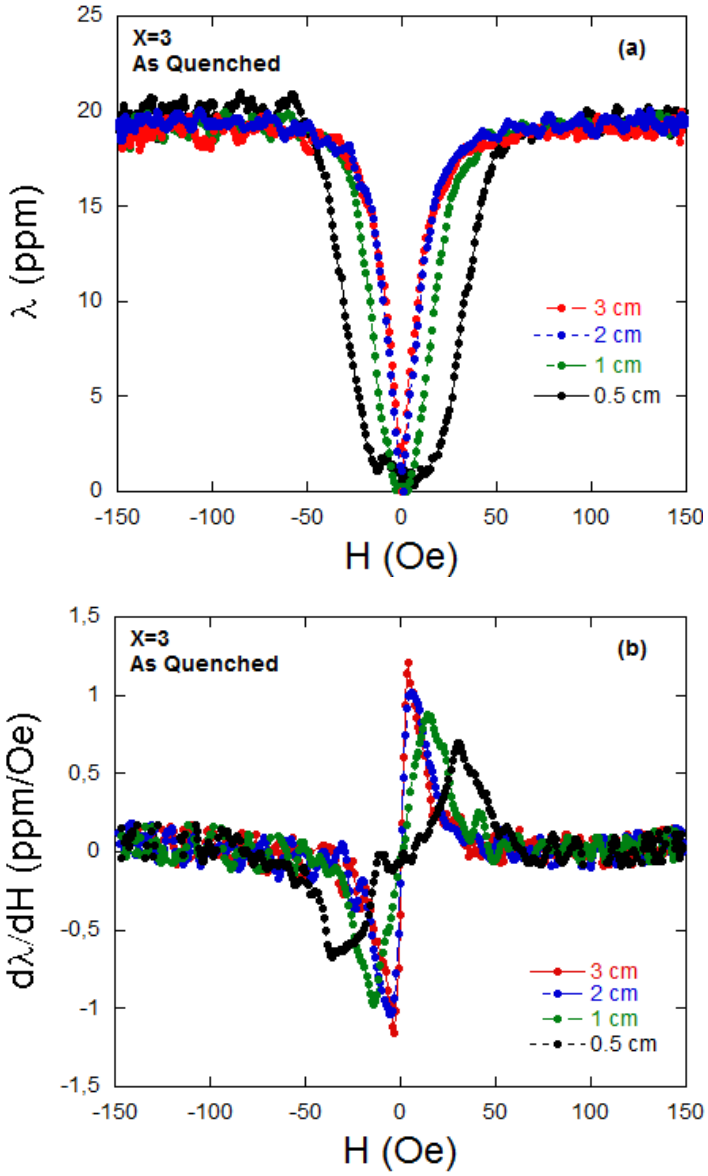

Figure 2.8. Magnetostriction (a) and piezomagnetic coefficient (b) curves for different lengths of the as-quenched X=3 composition.

As it can be observed, the magnetostriction curve gets wide and the piezomagnetic coefficient decreases its value as the length of the magnetostrictive ribbon shortens. Both behaviors are consequence of the demagnetizing field, which influence is higher as reducing the length of the ribbons.

2.1.3.3. Magnetoelastic resonance and ΔE effect

The magnetoelastic resonance (MER) curves and derived ΔE effect were measured using an experimental set up consisting of three coaxial solenoids. The external solenoid applies a static magnetic field (or bias) of 138.2 Oe/A (see Fig. 2.9, right). The so called primary coil is located within this solenoid and applies an AC magnetic field of 36.9 Oe/A. A secondary coil placed within this primary one picks the induced signal up, which is then visualized in a HP 3589A spectrum analyzer (see Fig. 2.9, left) and recorded in a computer.

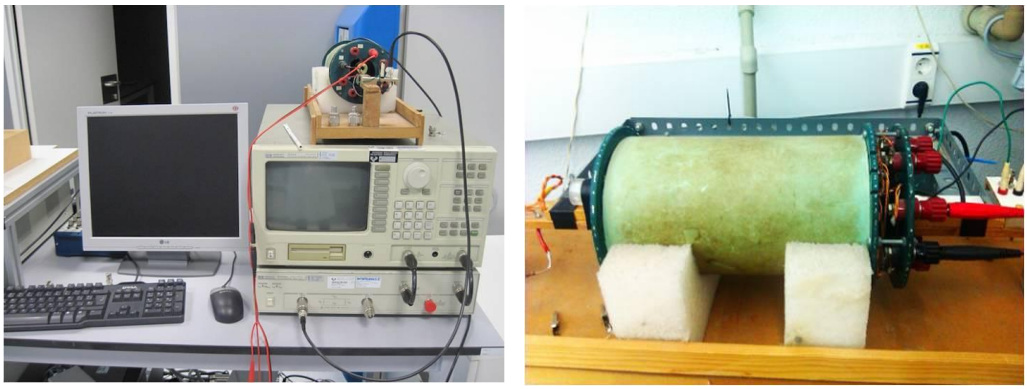

Figure 2.9. General view of the set up used to measure the Magnetoelastic Resonance frequency and ΔE effect (left). Picture of the solenoid where the sample is located (rigth).

The spectrum analyzer not only allows us to observe the MER curve in a wide frequency range between 10 Hz and 150 MHz, but also provides the AC voltage to excite magnetically (via the primary coil) the ferromagnetic ribbons. The DC magnetic field is applied by a HP 6653A power supplier. The MER frequency was determined by switching the frequency from 10 kHz to 500 kHz, keeping both the excitation field and the DC magnetic field constant.

Fig 2.10 shows the resonance curve for the 3 cm long ribbon of the X=0 composition in annealed state, which was obtained at a DC magnetic field of 4.4 Oe, the field for the maximum resonance amplitude. The MER frequency of the ribbon shows high resonance amplitude of 1.6 mV at a resonance frequency of 75.8 kHz. This resonance frequency evidently increases as reducing the length of the magnetostrictive ribbons, as it will be better analysed in chapter 3.

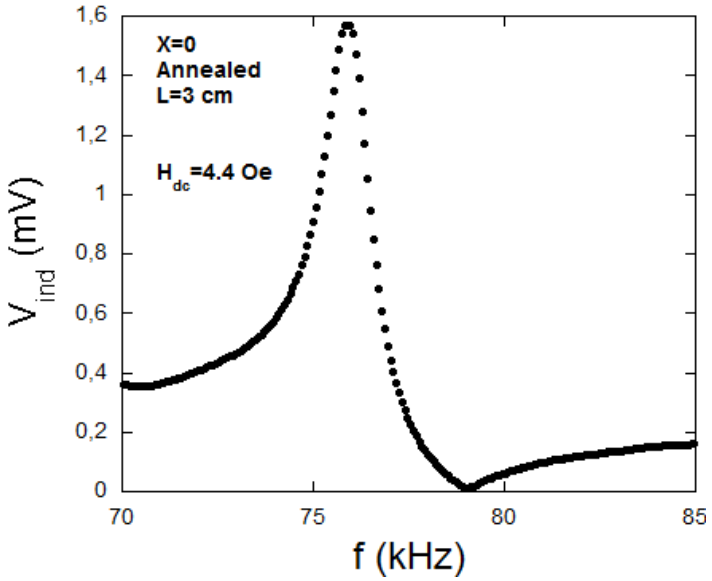

Figure 2.10. Magnetoelastic resonance curve for the annealed 3 cm long X=0 ribbon.

From the MER curve of the ribbon, the main magnetoelastic parameters can be derived. Using equations 1.12, 1.15 and 1.17, the magnetoelastic coupling coefficient, the Young modulus and the quality factor, respectively, were obtained. In the case of the quality factor, it is usually represented its inverse, Q^{-1}, which quantifies the damping or internal friction. Fig. 2.11 shows these magnetoelastic parameters in a function of the applied magnetic field.

The maximum magnetoelastic coupling parameter is 0.33, which means that the 33 % of the magnetic energy has been transformed into elastic. Concerning the inverse of the quality factor, the maximum damping of the resonance happens at the same anisotropy field.

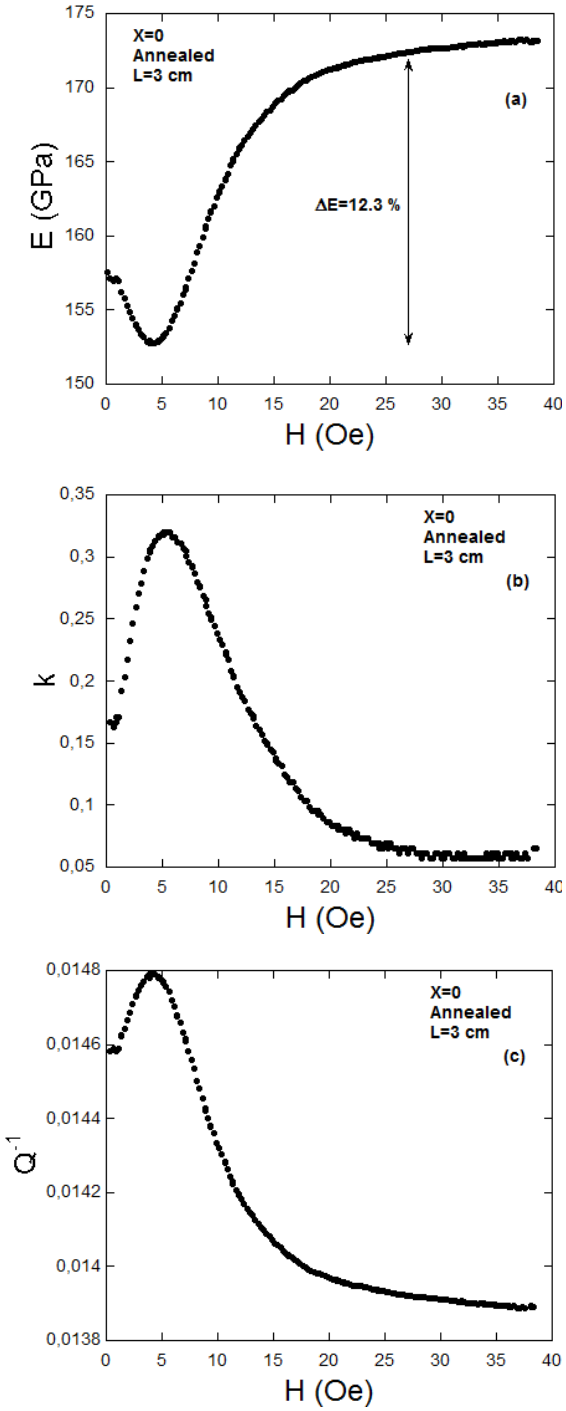

Figure 2.11. ΔE effect (a), magnetoelastic coupling coefficient (b) and inverse of quality factor (c) as a function of the applied magnetic field for the 3 cm long annealed X=0 composition.

2.2. Piezoelectric constituent

A commercial metallized film sheet of polyvinylidene fluoride (PVDF) was purchased from Quality by Measurement (QBM), with a thickness of 52 μm. As it was already mentioned in the introduction, the PVDF was chosen as the piezoelectric element due to the good mechanical properties, as well as the high piezoelectric response that shows at room temperature [9]. The longitudinal and perpendicular piezoelectric coefficients of the purchased PVDF are d_{33}=33 pC/N and d_{31}=23 pC/N, respectively. The dielectric constant is about 100 x 10^{-12} F/m, with a Young modulus of 2 GPa and an elastic compliance of 5 x 10^{-10} m^2/N. In order to test the thermal stability of the PVDF, the remnant polarization of the PVDF was measured as a function of temperature (see Fig. 2.12) by using the thermally stimulated depolarizing current method.

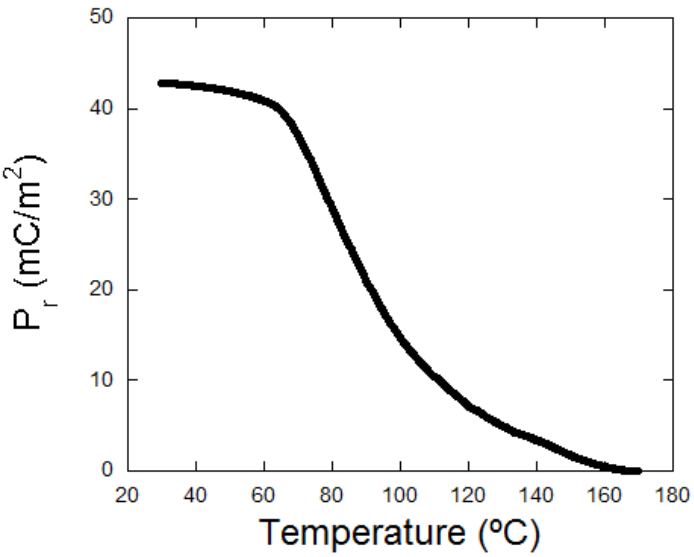

Figure 2.12. Remnant polarization of the PVDF in a function of temperature.

The results show a remnant polarization of 43 mC/m^2, which keeps constant up to 60 ºC, where the α-relaxation of the PVDF starts, resulting in an initial linear decrease of this polarization [10]. When temperature reaches 80 ºC, the PVDF undergoes a contraction, which softens the drop of the remnant polarization.

2.3. Selection and characterization of the epoxy

When fabricating the ME laminates, the magnetostrictive and piezoelectric constituents must be bonded by using an appropriate epoxy. Three different epoxies were deeply analysed for their use in the fabrication of ME laminated composites [11]. The epoxies were the Devcon 5 minute epoxy, the M-Bond and the Stycast 2850. The results obtained in [11] show a better transmission of the strain from the magnetostrictive constituents to the piezoelectric one for those epoxies with lower Young modulus. Actually, a higher Young modulus leads to a loss in the ability to transmit the deformation from the magnetostrictive layer to the piezoelectric one, due to the increased rigidity. Thus, whereas the Young modulus of the Stycast 2850 is 9 GPa, the Devcon 5 minute epoxy and the M-bond have a Young modulus of 0.7 GPa and 0.3 GPa, respectively. Between the Devcon 5 minute epoxy and the M-bond, the Devcon 5 minute was selected due to its better thermal stability (see Fig. 2.13) showed in the Thermogravimetric analysis (TGA).

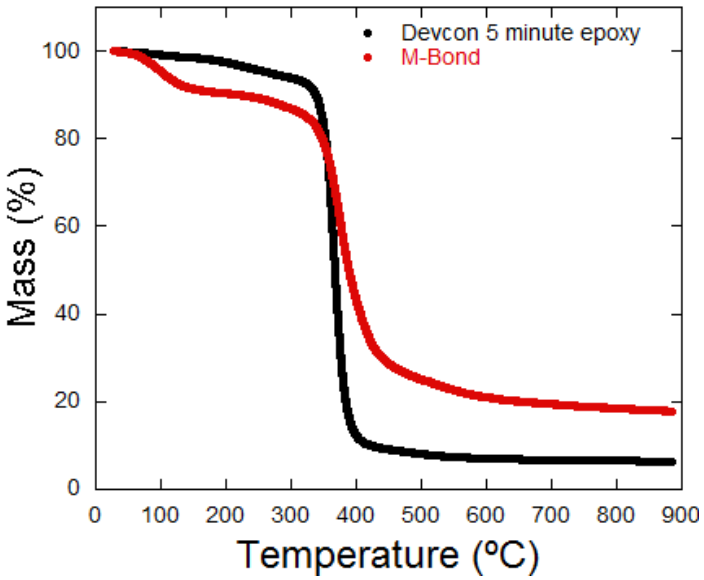

Figure 2.13. Thermogravimetric analysis (TGA) of the Devcon 5 minute and M-Bond epoxies.

Particularly, the TGA shows a better behaviour of the Devcon 5 minute epoxy at temperatures close to 100 ºC, where the M-Bond undergoes a higher mass loss

than the Devcon. The thermal stability for the Devcon 5 minute epoxy is maintained up to 300 ºC. At that temperature, the epoxy starts degrading progressively and it is almost decomposed at 400 ºC.

Once it is selected the epoxy to be used in the fabrication of the laminated composites, the curing process was studied. The Differential Scanning Calorimetry (DSC) technique was used for that purpose. Four scanning processes at different times were carried out in order to determine the right cure time. These periods were chosen according to the technical specifications of the datasheet.

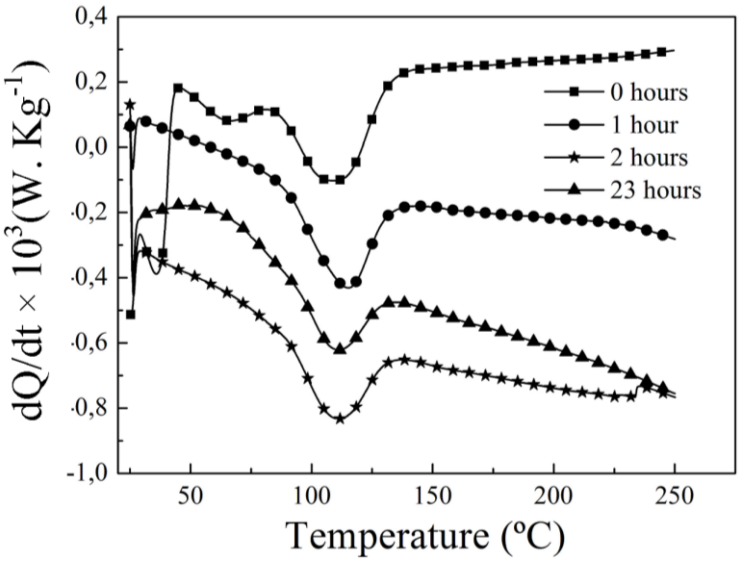

Figure 2.14. Differential Scanning Calorimetry (DSC) of the Devcon 5 minute epoxy at different times.

The results displayed in Fig. 2.14 show that at 0 hours (after mixing), the epoxy undergoes an increase in the heat flow up to 50 ºC, which is probably attributed to the evaporation of the solvent, since it disappears in the rest of time periods. At 1, 2 and 23 hours the behaviour of the epoxy is very similar, with an exothermic pick at 115 ºC that corresponds to the melting of the epoxy. Therefore, it can be concluded that the epoxy is completely cured at room temperature after one hour.

2.4. Magnetoelectric laminated composites

2.4.1. Fabrication process

Three-layer L-T type ME laminated composites were fabricated by cutting separately pieces of PVDF and magnetostrictive alloys in lengths of 3, 2, 1 and 0.5 cm. The width of the piezoelectric element was chosen to be 2 mm wider than the magnetostrictive elements (see Fig. 2.15), wide enough to deposit the electric contacts to the piezoelectric element and narrow enough to reduce damping effects as much as possible [12]. Actually, with increasing PVDF surface area not directly bonded to the magnetostrictive constituent, damping effects arise, since the not bonded area attenuates the strain variations of the effective one. In this way, stress damping of the not bonded PVDF area hinders polarization switching on the effective one, reducing the piezoelectric response [13] and, as a consequence, decreasing the ME response.

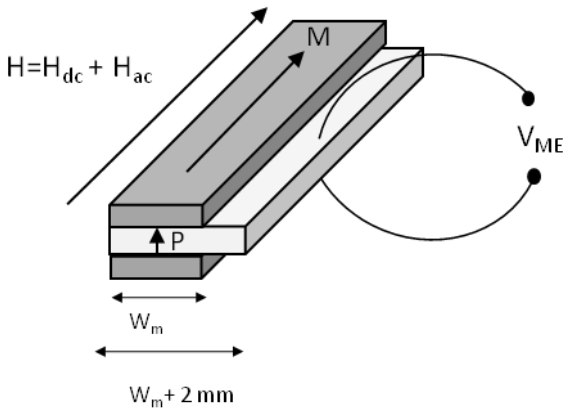

Figure 2.15. Diagram of the fabricated L-T type ME laminated composite.

Before fabricating the composites, all the magnetostrictive ribbons were carefully cleaned with acetone and ethanol, in order to ensure a good coupling between layers. The ME laminated composites were fabricated by gluing two equal magnetostrictive ribbons to both sides of a PVDF layer. Afterwards, the

laminated composites were cured at room temperature using the vacuum bagging technique [14].

This technique consists in placing the ME laminated composite into a plastic bag, which includes a small valve and a pump to extract the air from inside (Fig 2.16, left). After closing the bag, the air is removed until bag conforms tightly around the laminate, obtaining a uniform ambient pressure of approximately 1 atm. The laminates were cured for 1 hour, according to the curing time of the Devcon 5 minute epoxy.

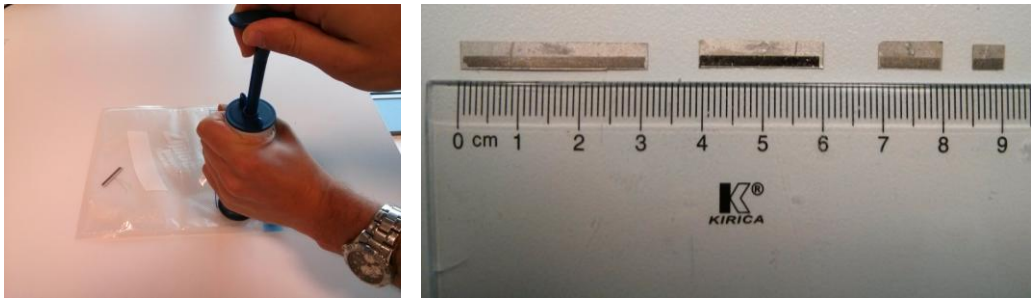

Figure 2.16. Picture of the vacuum bagging technique (left). ME laminated composites of different lengths with the electric contacts (right).

The vacuum bagging technique has many advantages over the use masses or presses. Actually, it not only guarantees a homogeneous pressure along the laminate, but also avoids the appearance of bubbles that may worsen the coupling between magnetostrictive and piezoelectric layers.

After their fabrication (Fig. 2.16, right), the total thicknesses of the ME laminates were measured using a digital micrometer, in order to estimate de thickness of the epoxy layer. Epoxy thicknesses between 16 and 19 microns were obtained for all the laminates, confirming the good homogeneity achieved for the epoxy after applying the vacuum bagging technique.

Once the ME composite was cured, a silver paint was used to place the electric contacts to both sides of the piezoelectric film.

2.4.2. Experimental set-up for the magnetoelectric effect determination

The ME effect measurement set-up is shown in Fig. 2.17. A static magnetic field is applied along the ME composites longitudinal axis by a pair of Helmholtz coils with a calibration constant of 19 Oe/A. An AC field is superimposed in the same direction by small split coils of 9.9 Oe/A driven by a function generator (HP 33120A), giving a net magnetic field of $H = H_{dc} + H_{ac}$, being $H_{dc} >> H_{ac}$.

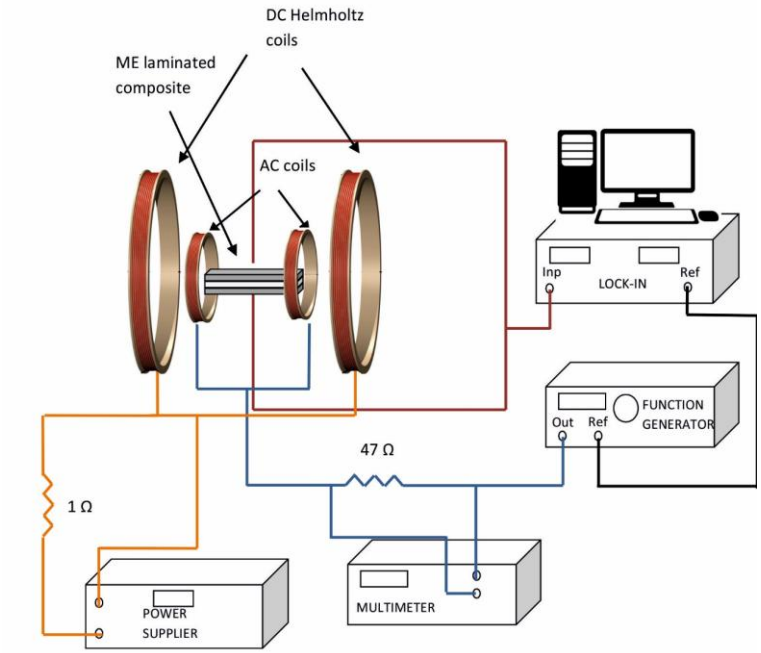

Figure 2.17. Diagram of the experimental set up used to measure the ME response of the laminates.

The AC field makes the magnetostrictive ribbons elongate and shrink in the longitudinal axis. That strain is then transmitted to the PVDF layer, inducing an output voltage, V_{ME}, which is continuously recorded by a Lock-In amplifier with a frequency range up to 2 MHz (Signal Recovery 7280). From this V_{ME} value, the ME coefficient α_{31} is obtained through equation 1.9.

The value of the static magnetic field is obtained by measuring the voltage drop in 1 Ohm resistance, while the voltage drop in a non-inductive 47 Ohm standard resistor gives the measurement of the AC magnetic field.

All the ME measurements were carried out at the MER frequency, where the induced ME voltage is maximum [4, 15]. The MER frequency was fixed after changing the frequency from 10 kHz to 400 kHz, depending on the length of the laminate, and keeping both the AC and DC magnetic fields constant. The AC magnetic field was set at 0.12 Oe and the DC (bias) field was tuned according to the anisotropy field, previously determined from the hysteresis loops of each laminate.

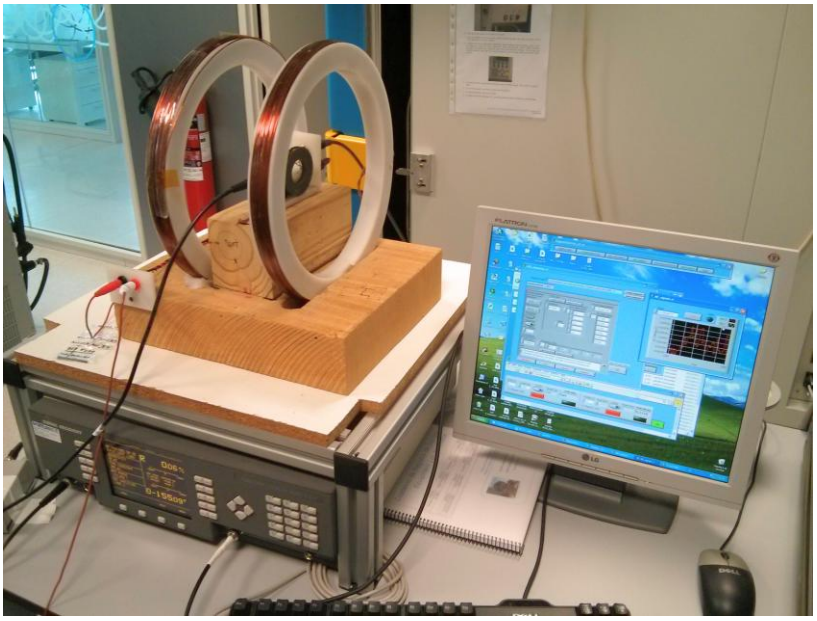

Figure 2.18. Picture of the ME measurement set-up.

This experimental set-up (see Fig. 2.18) allows us not only to measure the ME effect value as a function of the applied H_{dc}, but also to determine the sensitivity of the laminates to the applied H_{ac} and H_{dc} magnetic fields. That is, the experimental set-up will be also used to test their performance as magnetic field sensors.

2.5. Results

This section summarizes the main magnetic and magnetoelectric properties of the magnetostrictive alloys and ME laminated composites, respectively, as starting point of the next chapters of the Thesis.

Table 2.2. Saturation magnetization, magnetostriction and intrinsic magnetic susceptibility of the each magnetostrictive alloy. All parameters, except the saturation magnetization, are showed for as-quenched and annealed states.

Magnetostrictive alloys		$\mu_o M_s$ (T)	As-quenched		Annealed	
			λ (x 10^{-6})	χ	λ (x 10^{-6})	χ
$(Fe_{0.79}Co_{0.21})_{75+x}Si_{15-1.4x}B_{10+0.4x}$	X=0	1.3	18	55000	22	45000
	X=3	1.4	20	36000	25	32000
	X=6	1.7	23	50000	26	27000
$Fe_{85-x}Co_xB_{15}$	X=0	1.9	25	70000	27	55000

Table 2.3. Anisotropy field, ΔE effect value, magnetoelastic anisotropy constant and quality factor of the as-quenched and annealed magnetostrictive alloys, measured for the 3, 2, 1 and 0.5 cm long ribbons.

Magnetostrictive alloys		L (cm)	As-quenched				Annealed			
			H_k (Oe)	**ΔE (%)**	**k**	**Q**	**H_k (Oe)**	**ΔE (%)**	**k**	**Q**
$(Fe_{0.79}Co_{0.21})_{75+x}Si_{15-1.4x}B_{10+0.4x}$	X=0 $Fe_{59.2}Co_{15.8}Si_{15}B_{10}$	**3**	3.3	10.0	0.24	42	2.3	12.3	0.32	25
		2	5.2	8.0	0.21	55	3.9	7.0	0.22	47
		1	14.2	8.1	0.19	70	13.2	6.9	0.18	72
		0.5	30.8	8.3	0.18	71	29.8	5.0	0.16	83
	X=3 $Fe_{61.6}Co_{16.4}Si_{10.8}B_{11.2}$	**3**	4.5	18.5	0.38	16	5.1	15.1	0.4	15
		2	7.2	21.5	0.37	17	9.0	16.0	0.39	15
		1	15.3	19.2	0.28	30	17.7	14.5	0.25	38
		0.5	35.4	15.6	0.17	84	36.0	6.6	0.15	109
	X=6 $Fe_{64}Co_{17}Si_{6.6}B_{12.4}$	**3**	2.7	27.5	0.46	11	2.8	16.5	0.42	14
		2	3.6	20.7	0.37	17	4.3	17.2	0.39	15
		1	10.4	24.2	0.31	24	14.8	16.0	0.28	31
		0.5	25.5	13.0	0.13	140	28.2	7.2	0.14	121
$Fe_{85-x}Co_xB_{15}$	X=21 $Fe_{64}Co_{21}B_{15}$	**3**	3.4	18.8	0.34	20	3.0	13.0	0.37	18
		2	5.5	21.4	0.32	23	7.3	11.1	0.28	30
		1	13.0	20.5	0.21	53	12.8	10.7	0.24	41
		0.5	30.0	17.5	0.15	107	29.0	7.5	0.22	44

Table 2.4. Maximum piezomagnetic coefficient and elastic compliances of the as-quenched and annealed magnetostrictive compositions, measured for the 3, 2, 1 and 0.5 cm long ribbons.

Magnetostrictive alloys		L (cm)	As-quenched		Annealed	
			$d_{11,m}$ (10^{-6}/Oe)	s_{11}^{H} (x10^{-12}m^2/N)	$d_{11,m}$ (10^{-6}/Oe)	s_{11}^{H} (x10^{-12}m^2/N)
$(Fe_{0.79}Co_{0.21})_{75+x}Si_{15-1.4x}B_{10+0.4x}$	X=0 $Fe_{59.2}Co_{15.8}Si_{15}B_{10}$	**3**	1.4	6.3	2.0	6.5
		2	1.0	6.4	1.6	6.3
		1	0.8	6.0	1.3	5.6
		0.5	0.5	6.3	1.0	6.1
	X=3 $Fe_{61.6}Co_{16.4}Si_{10.8}B_{11.2}$	**3**	1.5	7.0	2.4	6.8
		2	1.2	7.0	1.6	7.0
		1	1.0	6.4	1.2	6.3
		0.5	0.9	7.9	0.9	7.7
	X=6 $Fe_{64}Co_{17}Si_{6.6}B_{12.4}$	**3**	2.0	7.7	1.7	7.2
		2	1.8	7.4	1.5	7.1
		1	1.4	6.4	1.3	6.4
		0.5	1.0	7.1	1.0	6.4
$Fe_{85-x}Co_xB_{15}$	X=21 $Fe_{64}Co_{21}B_{15}$	**3**	2.8	7.3	1.7	6.9
		2	1.5	7.1	1.2	6.8
		1	1.2	7.0	1.0	7.0
		0.5	0.9	6.5	0.9	6.4

Table 2.5. Maximum magnetoelectric voltages obtained for each laminate. Note that the values showed in this table were obtained at the MER frequency of each laminate, at the DC magnetic field that corresponds to the maximum ME coupling and under an excitation field of 0.12 Oe.

Magnetoelectric laminates		L (cm)	$V_{ME,AQ}$ (mV)	$V_{ME,ANN}$ (mV)
$(Fe_{0.79}Co_{0.21})_{75+x}Si_{15-1.4x}B_{10+0.4x}$/PVDF	X=0	**3**	68.5	86.0
		2	23.8	17.0
		1	6.0	8.3
		0.5	1.7	1.54
	X=3	**3**	28.3	164.0
		2	12.7	48.9
		1	4.6	9.5
		0.5	1.5	4.3
	X=6	**3**	75.4	116.7
		2	35.5	26.3
		1	2.9	3.8
		0.5	2.1	2.4
$Fe_{85-x}Co_xB_{15}$/PVDF	X=21	**3**	118.9	105.0
		2	58.8	34.3
		1	9.1	5.9
		0.5	3.2	5.0

The results obtained for the magnetoelastic parameters in Table 2.3 do not show in general a clear change between the as-quenched and annealed magnetostrictive ribbons. However, they do show a trend as the length of the ribbon is reduced. Whereas the magnetoelastic coupling coefficient decreases as the length of the magnetostrictive ribbon does, the quality factor shows the opposite behaviour.

The magnetostrictive parameters, on the contrary, show different behaviours between the as-quenched and annealed ribbons depending on the composition. Whereas the piezomagnetic coefficient, for example, increases after annealing for the X=0 and X=3 compositions, the values for the X=6 and X=21 compositions are lower. These results directly affect the induced ME voltage in the laminate, as it can be observed in Table 2.5.

The maximum ME voltages measured for the laminates show pretty high values, especially, for the longest ones. A maximum induced voltage of 164 mV has been measured for the 3 cm long X=3/PVDF laminate, with annealed magnetostrictive ribbons. The induced ME voltage decreases as the length of the laminate does, due to the demagnetizing filed. These effects will be better explained in Chapter 3.

2.6. References

[1] J. G. Etxebarria, "Propiedades magnéticas y magnetoelásticas de nuevas aleaciones amorfas de interés tecnológico " PhD dissertation, Universidad del País Vasco/Euskal Herriko Unibertsitatea (UPV/EHU), 1992.

[2] J. Gutierrez, J. M. Barandiaran, and O. V. Nielsen, "Magnetoelastic properties of some Fe-rich Fe-Co-Si-B metallic glasses," *Physica Status Solidi (A) Applied Research,* vol. 111, pp. 279-283, 1989.

[3] J. Gutiérrez, V. Muto, and P. T. Squire, "Induced anisotropy and magnetoelastic properties in Fe-rich metallic glasses," *Journal of Non-Crystalline Solids,* vol. 287, pp. 417-420, 2001.

[4] J. Zhai, Z. Xing, S. Dong, J. Li, and D. Viehland, "Magnetoelectric laminate composites: An overview," *Journal of the American Ceramic Society,* vol. 91, pp. 351-358, 2008.

[5] F. E. Luborsky, "Chapter 6 Amorphous ferromagnets," in *Handbook of Ferromagnetic Materials*. vol. Volume 1, E. P. Wohlfarth, Ed., ed: Elsevier, 1980, pp. 451-529.

[6] K. Mandal, "The role of stress in amorphous magnetic materials," *Japanese Journal of Applied Physics, Part 1: Regular Papers and Short Notes and Review Papers,* vol. 35, pp. 93-96, 1996.

[7] H. Kronmueller and W. Fernengel, "Role of internal stresses in amorphous ferromagnetic alloys," *Physica Status Solidi (A) Applied Research,* vol. 64, pp. 593-602, 1981.

[8] J. M. Barandiarán, J. Gutiérrez, Z. Kaczkowski, and D. De Cos, "Influence of annealing temperature on the magnetic and magnetoelastic properties in Fe-Co-B metallic glasses," *Journal of Non-Crystalline Solids,* vol. 329, pp. 43-47, 2003.

[9] P. Martins, A. C. Lopes, and S. Lanceros-Mendez, "Electroactive phases of poly(vinylidene fluoride): Determination, processing and applications," *Progress in Polymer Science,* vol. 39, pp. 683-706, 4// 2014.

[10] V. Sencadas, S. Lanceros-Méndez, R. Sabater i Serra, A. Andrio Balado, and J. L. Gómez Ribelles, "Relaxation dynamics of poly(vinylidene fluoride) studied by dynamical mechanical measurements and dielectric spectroscopy," *The European Physical Journal E,* vol. 35, pp. 1-11, 2012/05/30 2012.

[11] M. Silva, S. Reis, C. S. Lehmann, P. Martins, S. Lanceros-Mendez, A. Lasheras*, et al.*, "Optimization of the magnetoelectric response of poly(vinylidene fluoride)/epoxy/vitrovac laminates," *ACS Applied Materials and Interfaces,* vol. 5, pp. 10912-10919, 2013.

[12] M. P. Silva, P. Martins, A. Lasheras, J. Gutiérrez, J. M. Barandiarán, and S. Lanceros-Mendez, "Size effects on the magnetoelectric response on PVDF/Vitrovac 4040 laminate composites," *Journal of Magnetism and Magnetic Materials,* vol. 377, pp. 29-33, 2015.

[13] T. A. Berfield, R. J. Ong, D. A. Payne, and N. R. Sottos, "Residual stress effects on piezoelectric response of sol-gel derived lead zirconate titanate thin films," *Journal of Applied Physics,* vol. 101, p. 024102, 2007.

[14] Y. Shen, J. Gao, Y. Wang, J. Li, and D. Viehland, "High non-linear magnetoelectric coefficient in Metglas/PMN-PT laminate composites under zero direct current magnetic bias," *Journal of Applied Physics,* vol. 115, pp. -, 2014.

[15] J. Y. Zhai, S. Dong, Z. P. Xing, J. Gao, J. F. Li, and D. Viehland, "Tunable magnetoelectric resonance devices," *Journal of Physics D: Applied Physics,* vol. 42, 2009.

3. Shape effects in the magnetoelectric response of laminated composites

This chapter deals with the effect of the size of the laminated composites in the ME response. The first part of the Chapter deeply analyzes this ME effect, as well as the influence in the ME response of metallic glass/PVDF laminates with the annealing of the magnetostrictive constituents. First, the expected behaviour of the ME laminates are analysed through the introduction of a figure of merit. Afterwards, the correlation of the ME coefficient of the laminates with parameters such as the piezomagnetic coefficient of the metallic glasses and quality factor of the laminates is analysed. The calculation of theoretical ME coefficient of the laminates will allow us to quantify the effective coupling between the piezoelectric and magnetostrictive constituents of each ME laminate. The second part of the Chapter deals with the quantification of losses arisen from size effects in these laminated composites. The losses in the ME response are caused mainly by the increase of the operating frequency and by the reduction of the length of the magnetostrictive ribbons. Values of all of these losses in laminates with lengths of 3, 2, 1 and 0.5 cm will be given. Finally, the reduction factor of the laminates will be defined and used to estimate the intrinsic ME coefficient of each laminate.

3.1. Influence of the size in the magnetoelectric response of the laminates

The ME laminates to be studied in this chapter will be L-T type (see Fig. 1.3) three-layer structures fabricated with different metallic glasses (X=0, X=3, X=6, and X=21), in as-quenched state and after annealing, and with the piezoelectric polymer PVDF (in the following, labelled as X=0/PVDF, X=3/PVDF, X=6/PVDF and X=21/PVDF). Laminates of 3, 2, 1 and 0.5 cm length were prepared. This will allow us to study the size effects in identical laminates but with different magnetostrictive/magnetoelastic properties.

Before measuring the ME response, we measured the hysteresis loops of each whole laminate. In fact, since the laminates are fabricated with an epoxy, some stresses can be induced in the magnetostrictive ribbons, which lead to a change in the shape of the hysteresis loops and so in the anisotropy field. Fig. 3.1 show the hysteresis loops measured for all the X=6/PVDF laminates, when using as-quenched magnetostrictive ribbons.

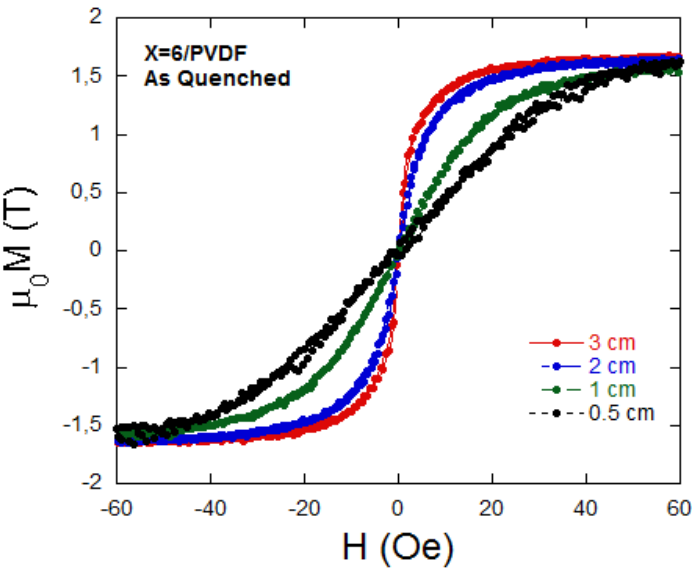

Figure 3.1. Hysteresis loops for different lengths of the X=6/PVDF laminate, with as-quenched magnetostrictive ribbons.

If we compare these hysteresis loops with the ones obtained for the single magnetostrictive ribbons (see Fig. 2.6), we appreciate significant changes in the anisotropy field. Actually, in all the cases the magnetic field required to reach the saturation is higher than for the single magnetostrictive ribbons.

In order to have a first idea about how well each ME laminate (with different magnetostriction constituent and different lengths, but the same PVDF piezoelectric constituent) will work, we can use the so called *figure of merit*, *FM,* that characterize the magnetic performance of the magnetostrictive material in such ME devices. This figure of merit can be defined as follows [1]:

$$FM = \lambda_s \chi \tag{3.1}$$

Thus, taking into account our previous values of the measured susceptibilities and magnetostrictions, we can estimate the FM value for each used magnetostrictive ribbon, calculated values that appear in Table 3.1.

Table 3.1. Values of figure of merit of each magnetostrictive composition, both in as-quenched and annealed states.

	$(Fe_{0.79}Co_{0.21})_{75+x}Si_{15-1.4x}B_{10+0.4x}$			$Fe_{85-x}Co_xB_{15}$
X	0	3	6	21
$FM_{,AQ}$	0.99	0.72	1.15	1.75
$FM_{,ANN}$	0.99	0.80	0.70	1.35

Therefore, from all these values we can expect to get better results for ME measurements for the laminates corresponding to the X=0/PVDF system (ribbons in as-quenched state) than for the X=3/PVDF, despite the higher value of the magnetostriction of this last one. To confirm this, we can represent the obtained maximum ME voltages for the laminates with as-quenched magnetostrictive ribbons, versus their corresponding (calculated) FM values (see Fig. 3.2, left).

As it is appreciated, a good linear dependence is obtained, which also supports the reliability of the definition given for the FM parameter. Only the 1 cm long X=6/PVDF laminate fails from this behavior. This disagreement can be

attributed to a bad fabrication of the laminate, most probably due to a bad bonding between magnetostrictive and piezoelectric layers.

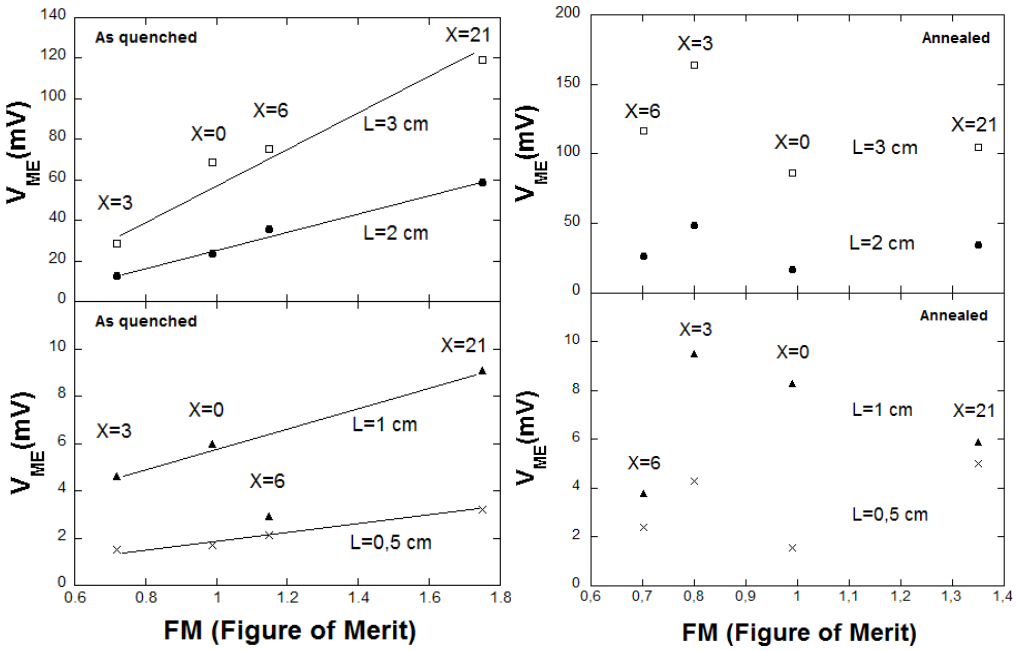

Figure 3.2. Maximum ME voltages of the laminates as a function of the figure of merit of each magnetostrictive ribbon, both in as-quenched and annealed states.

However, the behavior for the laminates with annealed magnetostrictive ribbons seems to be completely different. Actually, there is no a linear correlation between the maximum magnetoelectric voltages and the FM (see Fig. 3.2, right). The reason for such behavior can be attributed to the fact that the susceptibilities for the annealed compositions were extrapolated, since our annealing set up does not allow us to introduce a very long ribbon in order to determine its true intrinsic magnetic susceptibility (see Fig. 2.4).

Prior to measure the ME response of the laminates, we have to determine the MER frequency of the each laminate by sweeping the frequency from 10 kHz to 400 kHz, knowing that typical values of MER frequencies range from some tenths of kHz in 2-3 cm long samples to frequencies close to 400 kHz for 0.5 cm long samples. The AC magnetic field was set at 10 A/m and the DC one was tuned according to the anisotropy field of each laminated composite, where the

amplitude of the MER is maximum [2]. This procedure establishes the optimum working point of the ME laminates. Table 3.2 shows the measured MER frequencies of all the laminates, as well as the DC fields at which those resonance were observed:

Table 3.2. MER frequencies, f_r, and DC magnetic fields at those resonance frequencies, H^*, of all the laminates with the magnetostrictive ribbons in as-quenched state and after annealing.

Magnetoelectric laminates		L (cm)	As-quenched		Annealed	
			f_r (kHz)	H* (Oe)	f_r (kHz)	H* (Oe)
$(Fe_{0.79}Co_{0.21})_{75+x}Si_{15-1.4x}B_{10+0.4x}$/PVDF	X=0	**3**	49.5	4.5	51.4	5.4
		2	68.4	6.7	69.8	7.0
		1	193.5	21.0	192.2	21.8
		0.5	336.7	51.0	361.9	56.1
	X=3	**3**	49.1	6.7	50.0	7.0
		2	70.8	9.0	74.2	9.5
		1	165.5	23.5	167.3	21.8
		0.5	303.7	50.5	305.7	51.0
	X=6	**3**	41.7	3.7	41.6	4.7
		2	63.3	5.7	66.0	7.0
		1	185.1	15.0	148.6	16.7
		0.5	312.9	29.4	322.7	43.0
$Fe_{85-x}Co_xB_{15}$/PVDF	X=21	**3**	42.7	5.0	47.3	6.5
		2	65.7	7.4	67.2	10.0
		1	171.3	19.0	170.1	20.9
		0.5	291.9	40.5	323.4	52.0

Some differences in the MER frequencies can be appreciated when ribbons are used in the as-quenched or after annealing states, even being the magnetostrictive constituents and the length of the laminates the same.

This is attributed to slight differences in their geometry, mainly to small differences in the lengths of magnetostrictive and/or piezoelectric constituents that may lead to a change in the MER frequency of the whole laminate. Anyway, this will not affect the ME response of the laminates.

It is also useful to compare the MER frequencies obtained for single magnetostrictive ribbons and for the whole laminates. Fig. 3.3 shows this comparison for the single as-quenched X=21 magnetostrictive ribbons (left) and the corresponding X=21/PVDF laminated composites (right) for lengths ranging from 3 cm down to 0.5 cm.

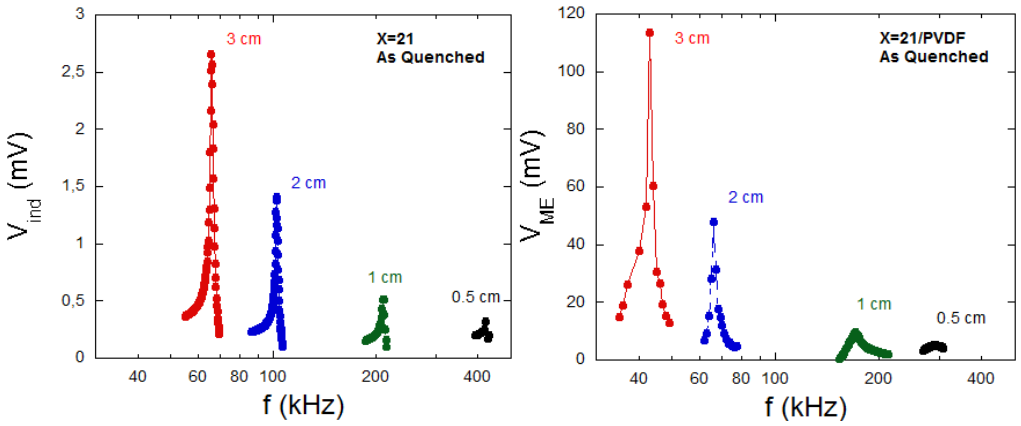

Figure 3.3. Comparison between MER frequencies of the single as quenched X=21 magnetostrictive ribbons and the corresponding X=21/PVDF laminates for lengths ranging from 3 cm down to 0.5 cm. These curves were measured under the anisotropy magnetic field of each magnetostrictive ribbon and each laminate.

As can be observed, the MER frequencies are lower for the laminates than for the single ribbons, due to the increase in the effective mass when the PVDF layer is bonded. It is also appreciated that the width of the MER frequency curve in the laminates increases as the length of the laminate is reduced, which leads to a lower quality factor.

Once we determined the MER frequency for all the laminates, we proceeded to measure the ME response. From the induced magnetoelectric voltage, the ME coefficient was obtained using equation 1.9 for laminates with lengths ranging from 3 cm down to 0.5 cm, and using both as-quenched and annealed magnetostrictive ribbons. Fig. 3.4 shows the behavior of the ME coefficient as a function of the applied magnetic field for the X=0/PVDF (up) and X=21/PVDF (down) laminates, with as-quenched (left) magnetostrictive ribbons and after annealing (right).

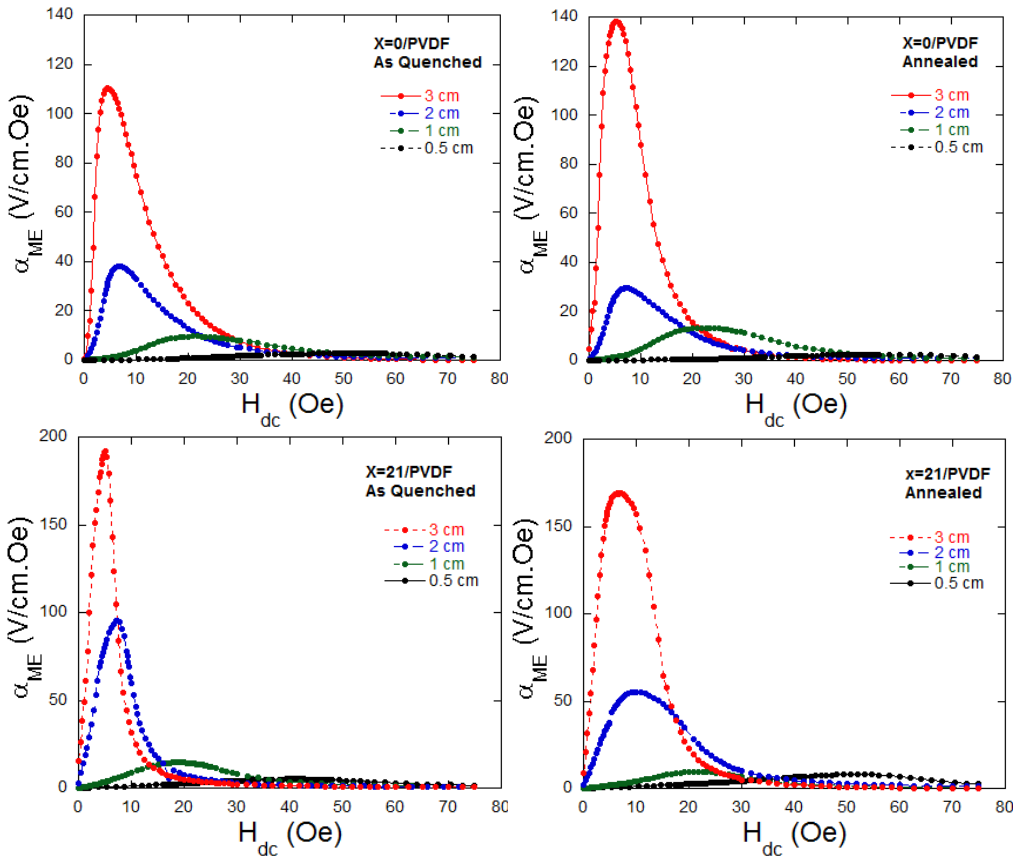

Figure 3.4. ME response in a function of the applied magnetic field, both with as-quenched and annealed magnetostrictive ribbons, of the X=0/PVDF (up) and X=21/PVDF (down) laminates.

Table 3.3 shows the obtained maximum ME coefficient for all the laminates. As it is observed, the maximum ME coefficient among all the laminates was

obtained for the 3 cm long X=3/PVDF laminate, with annealed magnetostrictive ribbons (267 V/cm.Oe).

Table 3.3. ME coefficients of all the laminates with the magnetostrictive ribbons in as-quenched state, $\alpha_{ME,AQ}$, and after annealing, $\alpha_{ME,,ANN}$.

Magnetoelectric laminates		L (cm)	$\alpha_{ME,AQ}$ (V/cm.Oe)	$\alpha_{ME,ANN}$ (V/cm.Oe)
$(Fe_{0.79}Co_{0.21})_{75+x}Si_{15-1.4x}B_{10+0.4x}$/PVDF	X=0	**3**	110.2	138.2
		2	38.1	29.5
		1	9.7	13.3
		0.5	2.8	2.5
	X=3	**3**	46.0	267.0
		2	20.5	78.8
		1	7.3	15.2
		0.5	2.3	6.9
	X=6	**3**	120.8	189.5
		2	56.9	44.3
		1	4.7	6.1
		0.5	3.3	3.8
$Fe_{85-x}Co_xB_{15}$/PVDF	X=21	**3**	191.7	169.2
		2	95.5	55.3
		1	14.6	9.5
		0.5	5.1	8.0

As expected, the ME coefficient decreases as the length of the laminate does, due to the effect of the demagnetizing field and also due to the less effective deformation, ΔL, that the magnetostrictive ribbons undergoes, according to equation 1.10. It is also observed that the obtained ME coefficients for laminates with as- quenched magnetostrictive ribbons agree with the predicted behaviour of the figure of merit, being the highest ME coefficients for the X=21/PVDF

laminates and the lowest for the X=3/PVDF ones. Nevertheless, and as it was expected according to the obtained values of the FM, this trend is not followed for the laminates fabricated with annealed ribbons.

Another important observation is that the DC magnetic field necessary for the maximum ME coupling increases as the length of the composite decreases, due to the effect of the demagnetization field. Thus, the shorter the laminate, the higher is the required external field to reach the maximum ME coupling [3].

The measured curves show significant differences in the induced ME voltage between the used as-quenched and annealed magnetostrictive ribbons. In fact and as it was discussed in section 2.1.2, the influence of the annealing may vary from one composition to another. While for X=0/PVDF, X=3/PVDF and X=6/PVDF the induced ME voltage increases after annealing of the ribbons, in the case of the X=21/PVDF laminate this induced ME voltage undergoes a significant decrease after such annealing. Actually, according to table 2.4 in section 2.5, the piezomagnetic coefficient is higher for the annealed X=0 and X=3 magnetostrictive ribbons than for the as-quenched ones. However, the X=6 and X=21 magnetostrictive ribbons show the opposite behavior. In these cases, the as-quenched piezomagnetic coefficients show higher values than the annealed ones.

These different behaviors between some compositions after annealing are attributed to different anisotropies induced in the fabrication process. Although an appropriate heat treatment usually improves the magnetic and magnetoelastic properties of the ribbons, it is not proved that it happens in all the cases, especially due to the difficulty to reproduce the annealing process in the same conditions, which would hinder the expected relief of the stresses.

As it was explained in the Chapter 1 of this report, one of the main goals of this work is to show the theoretically expected correlations, according to equation 1.8, with parameters such as the piezomagnetic coefficient of the magnetostrictive ribbons or quality factor of the laminated composites. Therefore, in the following we will try to analyze the correlation of the measured ME coefficients with those parameters.

Thus, Fig. 3.5 shows the ME coefficients of the laminates as a function of the piezomagnetic coefficients of the magnetostrictive ribbons. Whereas the correlation is pretty good for the X=3/PVDF and X=21/PVDF, the X=0/PVDF and the X=6/PVDF show some disagreements in most of the laminates, with higher ME coefficients for lower piezomagnetic coefficients and vice versa.

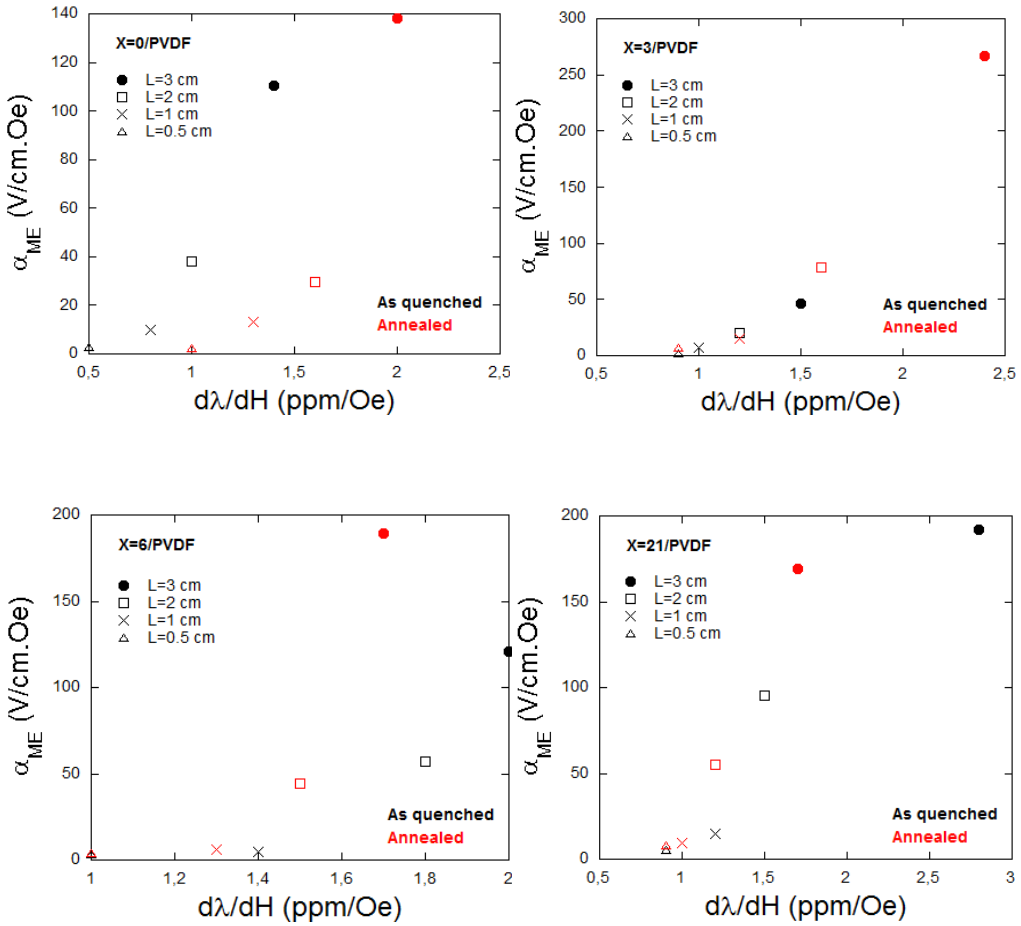

Figure 3.5. ME coefficient as a function of the piezomagnetic coefficients of the magnetostrictive ribbons for the X=0/PVDF (up, left), X=3/PVDF (up, right), X=6/PVDF (down, left) and X=21/PVDF (down, right) laminates, both with as-quenched and annealed ribbons.

Nevertheless, at the MER frequency the ME response not only depends on the piezomagnetic coefficient of the magnetostrictive constituent, but also on the

quality factor of the laminates, as it was commented in section 1.1.2. Therefore, it is necessary to determine these quality factors, *Q*, of the laminates.

It was already commented in section 1.2.4 that this *Q* factor can be easily obtained from the MER curve of the whole laminate. Consequently, its value depends, to a large extent, on the coupling between the magnetostrictive and piezoelectric layers. A bad coupling between both phases can lead to a low value of the quality factor, which would turn into a lower ME coefficient.

The obtained quality factors for all the laminates are shown in Table 3.4. These values were determined under the same conditions of applied DC and AC magnetic fields used to determine the working point of each laminate.

Table 3.4. Quality factors of the laminates with as-quenched magnetostrictive ribbons and after annealing.

Magnetoelectric laminates		L (cm)	Q_{AQ}	Q_{ANN}
$(Fe_{0.79}Co_{0.21})_{75+x}Si_{15-1.4x}B_{10+0.4x}$/PVDF	X=0	**3**	38	38
		2	44	18
		1	18	20
		0.5	6	4
	X=3	**3**	54	56
		2	33	29
		1	14	22
		0.5	8	8
	X=6	**3**	34	59
		2	30	15
		1	9	14
		0.5	6	6
$Fe_{85-x}Co_xB_{15}$ /PVDF	X=21	**3**	48	43
		2	39	33
		1	15	13
		0.5	10	8

As expected, the obtained quality factors are higher for the longest laminates, due to the sharpness of the curves (see Fig 3.3). When reducing the length of the laminate, the MER curve gets wider, which leads to a decrease in the quality factor and consequently, in the ME response [4].

If we analyze the ME coefficients of the laminates as a function of those *Q* factors (see Fig. 3.6), we can observe that there is a pretty good agreement between the behavior of the quality factors and the ME coefficients for the X=6/PVDF and X=21/PVDF laminates. Nevertheless, the ME coefficients of X=0/PVDF and X=3/PVDF do not match with the obtained quality factors, with higher ME coefficients for lower quality factors and vice versa.

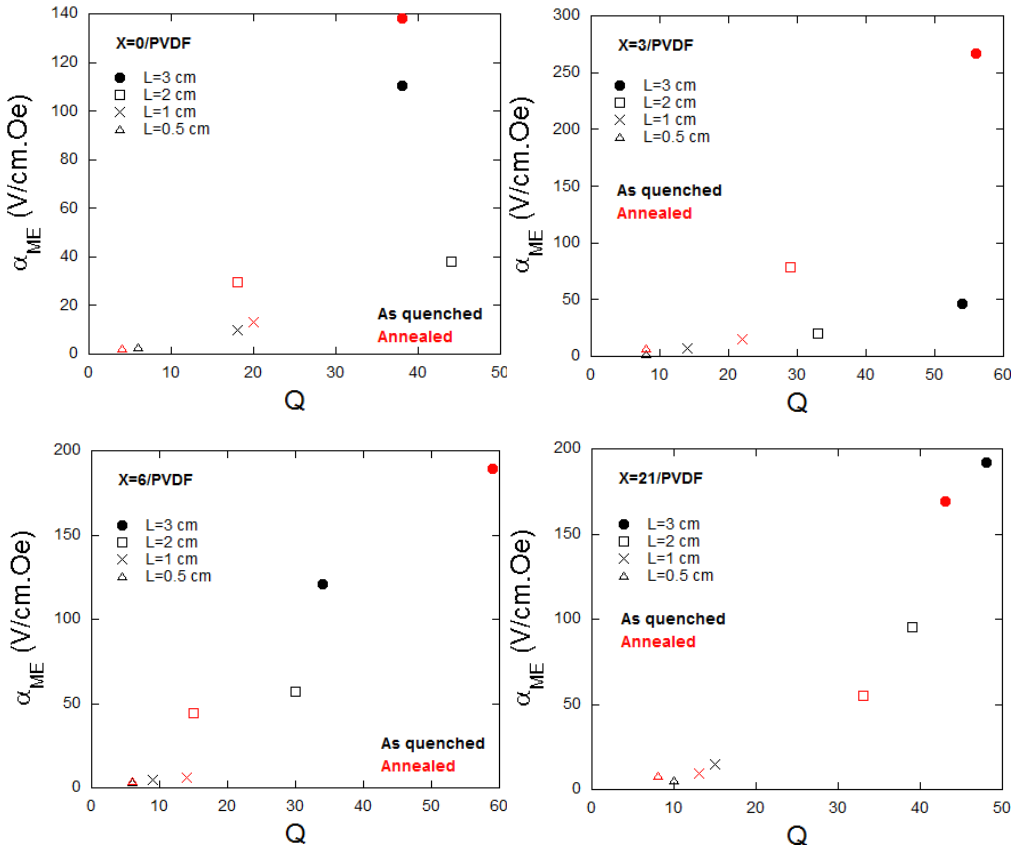

Figure 3.6. ME coefficient as a function of the quality factors for the X=0/PVDF (up, left), X=3/PVDF (up, right), X=6/PVDF (down, left) and X=21/PVDF (down, right) laminates, both with as-quenched and annealed ribbons.

Since we have observed such disagreements between the ME coefficients and piezomagnetic coefficients and quality factors values for some of the laminates, the next step was to analyze the correlation of the measured ME coefficients with the product of both parameters, a dependence that theory already predicts (see equation 1.8). Fig. 3.7 shows the ME coefficient as a function of the product of piezomagnetic coefficient and quality factor for all the studied laminates, using both as-quenched and annealed magnetostrictive ribbons.

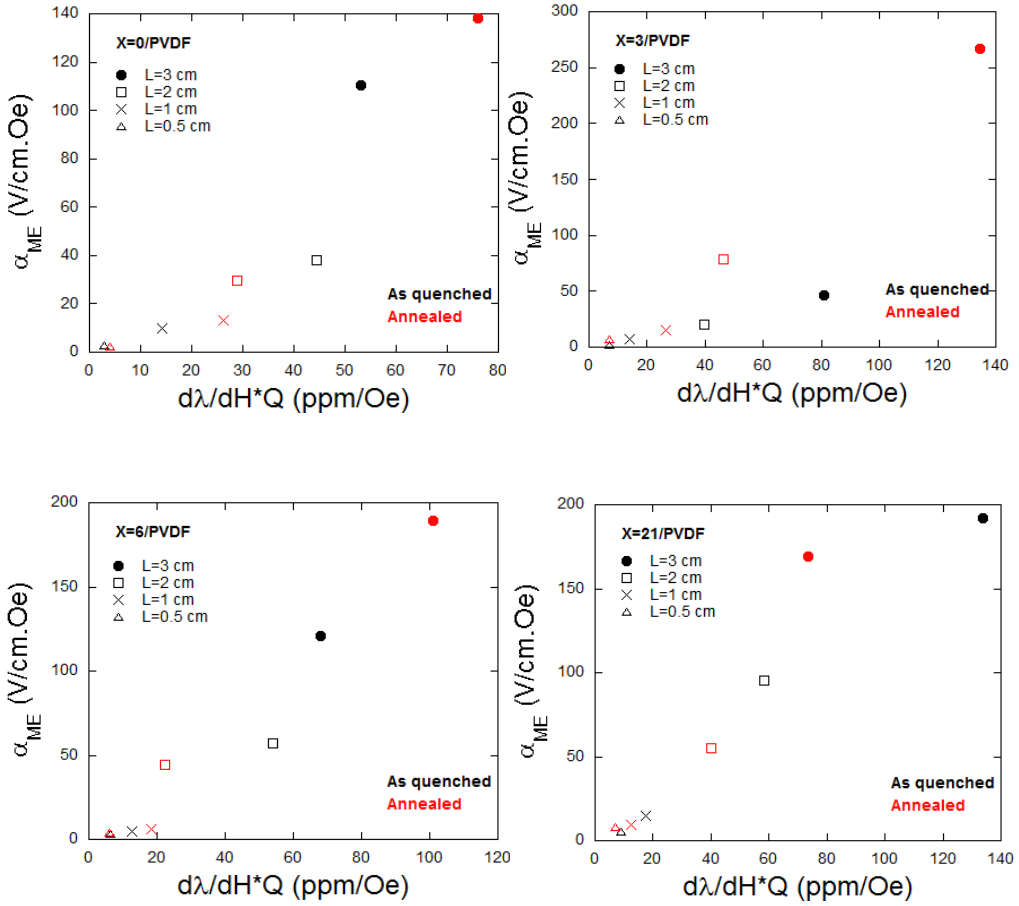

Figure 3.7. ME coefficient as a function of the product of piezomagnetic coefficient and quality factor for the X=0/PVDF (up, left), X=3/PVDF (up, right), X=6/PVDF (down, left) and X=21/PVDF (down, right) laminates, all of them represented considering as-quenched and annealed manetostrictive ribbons.

As it can be observed, the ME coefficients vary as the products of piezomagnetic coefficient and quality factor do, with the exception of the X=3/PVDF laminates fabricated with as-quenched magnetostrictive ribbons. However, if we have a look at Table 3.3, we can appreciate that the obtained ME coefficients for the 3 and 2 cm long X=3/PVDF laminates with as-quenched ribbons are particularly low, which lead us to think about a problem with the coupling between magnetostrictive and piezoelectric layers in those laminates.

If we represent in the same graphic the results obtained for all the different compositions (see Fig. 3.8), we see that the linearity is practically maintained for all the different cases. The greater the value of (dλ/dH)*Q, the higher the ME coefficient is. As previously mentioned, there are some exceptions in the X=3/PVDF laminates when using as-quenched ribbons. According to the obtained FM (see Fig. 3.2, left), the X=3/PVDF laminates are the ones with the lowest ME response for these laminates. In the case of the 3 cm long one, even being the one with the lowest induced ME voltage among the 3 cm long laminates, a bad ME coupling could have led to a slightly lower ME response than the one that should be, which would explain such disagreement.

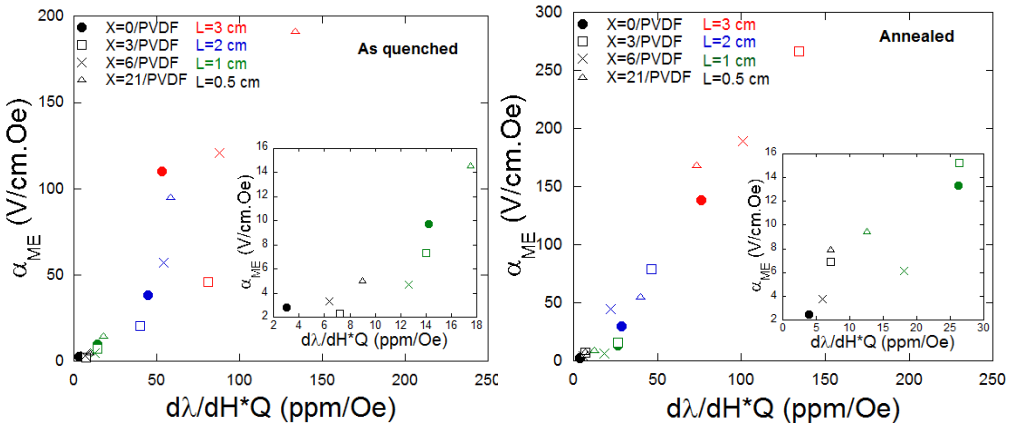

Figure 3.8. ME coefficient as a function of the product between piezomagnetic coefficient and quality factor represented for the different compositions, with as-quenched (left) and annealed (right) manetostrictive ribbons.

The influence of the ME coupling in the ME response of the laminates is discussed in the next section 3.2.

3.2. Determination of the effective magnetoelectric coupling in laminated composites

Let is now pay close attention to equations 1.7 and 1.8. Those equations not only consider a perfect bonding between the magnetostrictive and piezoelectric constituents, but they also neglect damping effects that may arise due to the PVDF surface area that is not directly bonded to the magnetostrictive constituents. This "not bonded" area is necessary to place the electric contacts in order to measure the induced ME voltage across the PVDF. Furthermore, they are other parameters such as the position of the sample within the coils, or the correct drying of the silver paint that must be taken into account when measuring the ME response.

All of these parameters, as well as the fabrication process of the laminates itself, may affect the induced ME voltage and they are not considered in equations 1.7 and 1.8. Therefore, it is necessary to evaluate the ME coupling coefficient of each laminate, k_c, which quantifies the ratio of the total ME response measured to the theoretically expected, considering all the mentioned parameters.

To do this, we have to calculate first, through equation 1.8, the theoretical expected ME coefficient value at the MER frequency. All the parameters involved in that equation have been already showed in previous sections, with the exception of the magnetic phase thickness ratio, n. This parameter is different for each composition, since the dimensions are different. Table 3.5 shows the magnetic phase thickness ratio for the laminates with different magnetostrictive constituents.

Table 3.5. Magnetic phase thickness ratios for the laminates with different magnetostrictive ribbons.

	$(Fe_{0.79}Co_{0.21})_{75+x}Si_{15-1.4x}B_{10+0.4x}$/PVDF			$Fe_{85-x}Co_xB_{15}$/PVDF
	X=0	X=3	X=6	X=21
n	0.36	0.28	0.23	0.24

As expected, the magnetic phase thickness ratio only varies according to the cross section of the magnetostrictive constituent, since we have used the same film of PVDF in all laminates.

Once we have all the parameters involved in equation 1.8, we proceeded to calculate the theoretical ME coefficients for all the laminates. Fig. 3.9 shows the theoretical and experimental ME coefficients (values showed in Table 3.3) as a function of the length of the laminates, when using both as-quenched and annealed magnetostrictive ribbons.

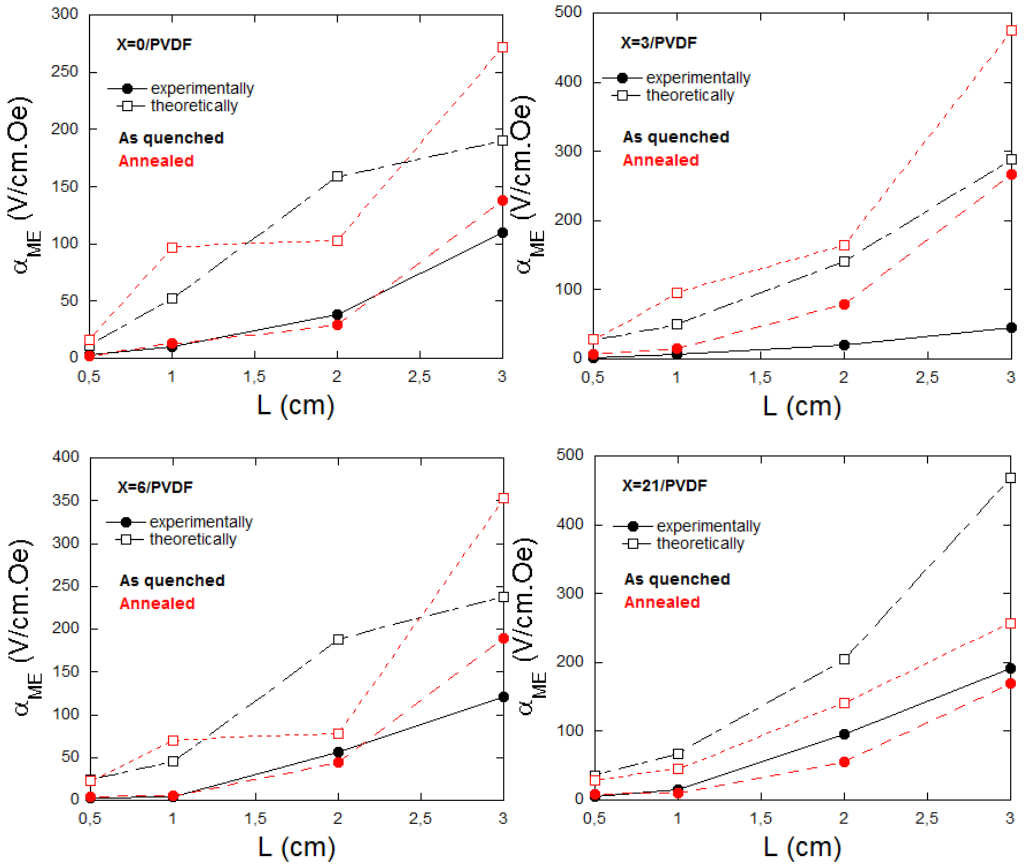

Figure 3.9. Theoretical and experimental ME coefficients as a function of the length of the laminate for the X=0/PVDF (up, left), X=3/PVDF (up, right), X=6/PVDF (down, left) and X=21/PVDF (down, right) laminates, all of them represented considering as-quenched and annealed manetostrictive ribbons.

Both theoretical and experimental ME coefficients decrease, as expected, as the length of the laminate does. Concerning the differences between theoretical and experimental ME coefficients, different behaviors are appreciated depending on the involved magnetostrictive constituent. Those differences are directly related to the ME coupling coefficient of the laminates.

Thus, this coefficient was obtained from the ratio between the experimental, α_{ME}, and theoretical, $\alpha_{ME,theo}$, ME coefficients:

$$k_c = \alpha_{ME} / \alpha_{ME,theo} \tag{3.2}$$

Table 3.6 shows the obtained ME coupling coefficients for all the laminates:

Table 3.6. ME coupling coefficients of all the laminates

Magnetoelectric laminates		L (cm)	$k_{c,AQ}$	$k_{c,ANN}$
$(Fe_{0.79}Co_{0.21})_{75+x}Si_{15-1.4x}B_{10+0.4x}$/PVDF	X=0	**3**	0.58	0.51
		2	0.24	0.29
		1	0.18	0.14
		0.5	0.24	0.16
	X=3	**3**	0.16	0.56
		2	0.14	0.48
		1	0.14	0.16
		0.5	0.08	0.24
	X=6	**3**	0.51	0.54
		2	0.30	0.57
		1	0.10	0.09
		0.5	0.13	0.16
$Fe_{85-x}Co_xB_{15}$ /PVDF	X=21	**3**	0.41	0.66
		2	0.47	0.39
		1	0.22	0.21
		0.5	0.15	0.28

As it can be observed, the ME coupling coefficient is, in general, higher for the longest laminated composites (3 cm and 2 cm long). To account for this, it must

be realized the lower deformation that the shortest (1 cm and 0.5 cm long) magnetostrictive ribbons transmit to the piezoelectric PVDF constituent. In fact, according to equation 1.10, the value of ΔL is smaller for the shortest ribbon, which in practice results in a lower induced ME voltage. Equation 1.8, however, does not take into account this effective deformation of the magnetostrictive ribbons, since the $d_{11,m}$ only accounts for the derivative of the λ. In some few cases, however, the ME coupling coefficient is higher for shorter laminates than for higher ones. This fact is just due to a worse bonding between layers in some laminates that make those laminates have a lower ME response.

The particularly low ME coupling coefficients observed mainly in the 3 and 2 cm long X=3/PVDF laminates when using as-quenched magnetostrictive ribbons can be attributed to a low ability of these ribbons to transmit the deformation from the magnetostrictive layers to the piezoelectric one and explain the disagreement observed in those laminates in Fig. 3.8. The rest of few disagreements observed in that figure are just attributed to slight differences in the coupling between magnetostrictive and piezoelectric layers of the different laminates.

3.3. Losses in magnetoelectric laminated composites

There are many parameters in the ME laminated composites apart from the ME response that have to be taken into account before incorporating into technological applications. Actually, the miniaturization of the devices is an important point in the implementation of the laminates. Therefore, it is essential to study the influence of the size in the ME response of the laminates, as well as to quantify the different losses arisen from the miniaturization of the devices.

Concerning the losses arising from the increase of the frequency, when a ME laminated composite operates at the MER frequency, there are losses arising both in magnetostrictive and piezoelectric constituents. These losses become very important when the size of the laminates is reduced, due to the increase in the

resonance frequency, and must be taken into account for a better understanding of the behavior of the ME response in miniaturized systems.

Several works have been reported so far concerning the effect of the size in the ME response in laminated composites [5-10]. However, few of them did a deep study about the influence of the demagnetizing effects in the ME response [3, 11, 12]. In those works, however, although they relate the effective ME coefficient with the intrinsic response, they do not obtain a direct correlation between them at the MER frequency.

3.3.1. Losses arising from the increase of the working frequency

The operating frequency is an important point to take into account, since with the increasing of frequency losses of the magnetic and piezoelectric constituents also increase.

The loss tangent of the whole composite includes contributions from the piezoelectric constituent and also from the magnetic one, and can be written as [10]:

$$tg\delta = n \cdot tg\delta_{mag} + (1-n) \cdot tg\delta_{PVDF} \tag{3.3}$$

where $tg\delta$ is the loss tangent of the whole composite, n is the magnetic thickness ratio of the laminate , $tg\delta_{mag}$ is the loss tangent of the magnetostrictive constituent and $tg\delta_{PVDF}$ is the loss tangent of the piezoelectric constituent.

In order to quantify the magnetic losses, we took into account the quality factors of the magnetostrictive constituents already showed in Table 2.3. From these values, we can obtain the loss tangent of the magnetostrictive constituents in the range of operating frequencies using the relationship $tg\delta_{mag}=1/Q_{mag}$.

Concerning the piezoelectric constituent, we measured the dependence of both permittivity and loss tangent of the PVDF with the frequency (see Fig. 3.10).

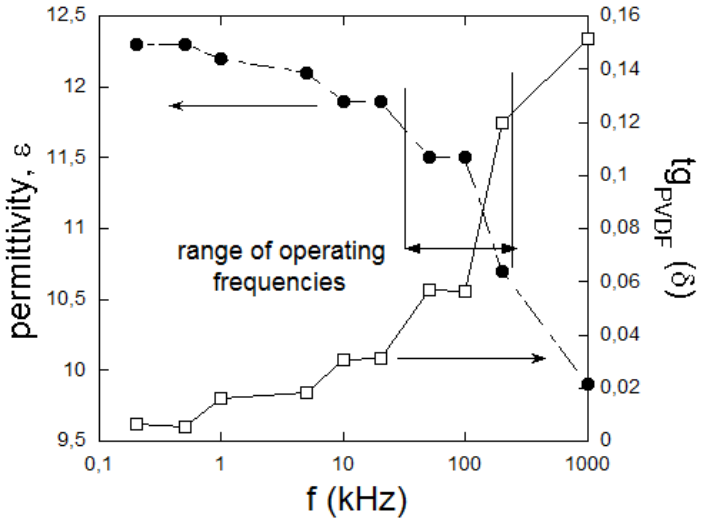

Figure 3.10. Dependence of the electric permittivity and tg (δ) of the PVDF with the frequency.

The results show a little change of the permittivity with frequency, from a value of 11.8 to 10.5 when the frequency is changed from 40 to 370 kHz ; the change in $tg\delta_{PVDF}$ for the same frequency range, from 0.04 to 0.12, turns out to be more pronounced.

Table 3.7 shows the loss tangent of the PVDF for 3, 2, 1 and 0.5 cm long pieces.

Table 3.7. Loss tangent of the PVDF, $tg\delta_{PVDF}$, for pieces of 3, 2, 1 and 0.5 cm long.

L (cm)	**3**	**2**	**1**	**0.5**
$tg\delta_{PVDF}$	0.057	0.057	0.10	0.12

With these values, and considering the values of the magnetic thickness ratio showed in Table 3.5, we can quantify the loss tangent of the whole composite in the range of operating frequencies. Table 3.8 summarizes the obtained loss tangents for each magnetostrictive constituent and for the whole laminate.

Table 3.8. Loss tangents of the magnetostrictive constituent, $tg\delta_{mag,}$ and the whole laminate, $tg\delta$, for lengths of 3, 2, 1 and 0.5 cm.

Magnetostrictive alloys		L (cm)	As-quenched		Annealed	
			$tg\delta_{mag}$	tgδ	$tg\delta_{mag}$	Tgδ
$(Fe_{0.79}Co_{0.21})_{75+x}Si_{15-1.4x}B_{10+0.4x}$	X=0	**3**	0.024	0.045	0.040	0.051
		2	0.018	0.043	0.021	0.044
		1	0.014	0.069	0.014	0.069
		0.5	0.014	0.081	0.012	0.081
	X=3	**3**	0.063	0.059	0.067	0.060
		2	0.059	0.057	0.067	0.060
		1	0.033	0.081	0.026	0.079
		0.5	0.011	0.089	0.009	0.089
	X=6	**3**	0.091	0.064	0.071	0.060
		2	0.059	0.057	0.067	0.059
		1	0.042	0.087	0.032	0.084
		0.5	0.007	0.094	0.008	0.094
$Fe_{85-x}Co_xB_{15}$	X=21	**3**	0.050	0.055	0.055	0.056
		2	0.043	0.054	0.033	0.051
		1	0.019	0.081	0.024	0.082
		0.5	0.009	0.093	0.023	0.097

All obtained values for the loss tangent of different origin merit a short explanation: while $tg\delta_{PVDF}$ continuously increases as operating frequency does, just the opposite behaviour has been measured for the magnetostrictive ribbons: as their length decreases (that is, the corresponding MER frequency increases), the $tg\delta_{mag}$ value continuously decreases. As a consequence, and since equation 3.3

gives the loss tangent of the whole composite as a weighted average taking into account both contributions, those final values range between (4-10) x 10^{-2} and increase as the working frequency does, independently if as-quenched or annealed magnetostrictive ribbons have been used in the laminate.

3.3.2. Losses arising from the decrease of the length of the laminate

As we already mentioned in previous Chapters, as the length of the magnetostrictive constituent reduces, the influence of the arising demagnetizing internal magnetic field increases significantly, through the so called demagnetizing factor. These demagnetizing factors are already well known for several shapes such as cylinders or ellipsoids [13, 14]. In our case, the demagnetizing factors for each laminate can be calculated just by considering the magnetostrictive ribbons as rectangular prisms, as Chang et al described in their work [15].

However, those works are limited to regular prism geometries. Since we are dealing with sandwiched laminated composites, a demagnetizing factor for a magnetostrictive/piezoelectric/magnetostrictive structure has to be defined. First of all, we calculated the demagnetizing factors for a single amorphous ribbon for each length. After that, we considered the thickness of two magnetostrictive ribbons and we calculated again the demagnetizing factors for each length. Since in practice we have a piezoelectric film between two magnetostrictive ribbons, the demagnetizing factor for the whole laminate will be an average between a single magnetostrictive ribbon and two ribbons put together:

$$N_{lam} \approx \frac{3}{2} N \tag{3.4}$$

It has to be pointed out that the obtained demagnetizing factors for the laminated composites have been estimated and they are just an approximation. Table 3.9 shows the demagnetizing factors for the single magnetostrictive ribbons, N, and for the laminated composite, N_{lam}.

As expected, the estimated values of the N_{lam} increase as reducing the length of the laminate, which means that the effect of the demagnetizing field becomes more important as decreasing the length of the laminates.

Table 3.9. Estimated demagnetizing factors for the single magnetostrictive ribbons, *N*, and for the laminated composites, $N_{lam.}$

Magnetostrictive alloys		L (cm)	N ($\times 10^{-5}$)	N_{lam} ($\times 10^{-5}$)
$(Fe_{0.79}Co_{0.21})_{75+x}Si_{15-1.4x}B_{10+0.4x}$	X=0	**3**	3.7	5.6
		2	7.9	11.9
		1	35.0	52.5
		0.5	120.0	180.0
	X=3	**3**	6.6	9.9
		2	16.5	24.8
		1	56.0	84.0
		0.5	160.0	240.0
	X=6	**3**	1.6	2.4
		2	3.5	5.3
		1	12.8	19.2
		0.5	53.0	79.5
$Fe_{85-x}Co_xB_{15}$	X=21	**3**	2.4	3.6
		2	5.4	8.1
		1	21.0	31.5
		0.5	75.0	112.5

Considering the estimated demagnetizing factors for the laminates, we will quantify the losses caused by the decrease of the length of the laminates, through the reduction factor (RF) of each laminate [16, 17]:

$$RF = \frac{1}{1 + N_{lam}\chi} = \frac{\alpha_{ME}(N)}{\alpha_{ME}(0)} \tag{3.5}$$

where N_{lam} is the demagnetizing factor of the laminate, χ is the intrinsic magnetic susceptibility of the magnetostrictive alloy, α_{ME} (0) is the intrinsic ME coefficient (N=0) and α_{ME} (N) is the measured ME coefficient. From the values of the RF,

we can also obtain the percentage of the induced ME voltage that has been lost due to that decrease of the length.

The values of the reduction factors depend, to a large extent, on length-to-width ratio (aspect ratio, AR) of the magnetostrictive ribbons. The lower the AR, the higher the effect of the demagnetizing field will be. Fig. 3.11 shows the reduction factor (represented as α_{ME} (N)/ α_{ME} (0)) as a function of the AR of the magnetostrictive ribbons.

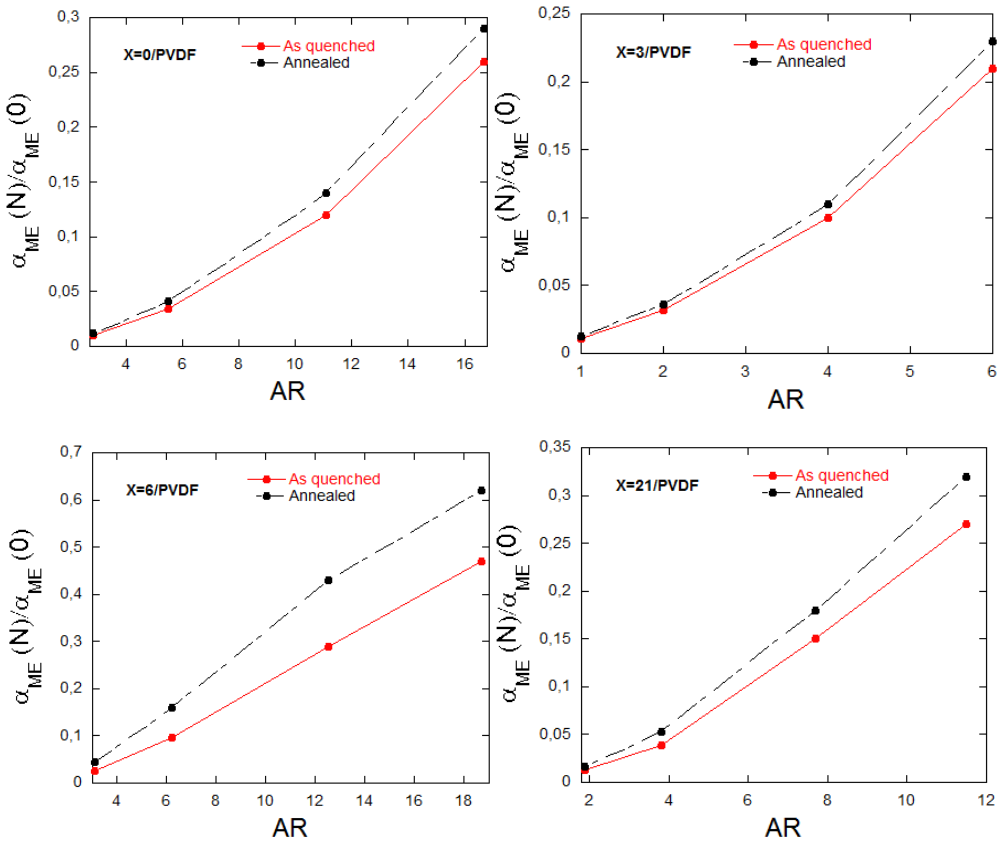

Figure 3.11. Dependence of the reduction factor (represented as α_{ME} (N)/ α_{ME} (0)) with the aspect ratio of the magnetostrictive ribbons, both when using as-quenched and annealed magnetostrictive ribbons.

As expected, the composition with the highest AR (X=6) is the one where the demagnetizing field has less influence, whereas the X=3 composition, with the lowest AR, is the most affected one. The longest 3 cm long X=6/PVDF

laminates show RF of 0.48 (with as-quenched magnetostrictive ribbons) and 0.62 (with annealed magnetostrictive ribbons), which means that the 52 % and 38 % of the total ME voltage has been lost due to the decrease of the length of the laminate, respectively. In the case of the 3 cm long X=3/PVDF laminates, the losses reach the 71 % and 77 %, with as-quenched and annealed magnetostrictive ribbons, respectively. Evidently, the losses increase as reducing the length of the laminates. As can be appreciated in Fig. 3.11, the losses of all 0.5 cm long laminates range between 95 % and 99 %.

So far, we only quantified the losses in the ME coefficient through the calculation of the RF. However, the calculation of the RF is only based on an estimation of the demagnetizing factors and on the intrinsic magnetic susceptibilities of the magnetostrictive ribbons, which in the case of the annealed ones are just an extrapolation. From equation 3.5, it is possible to obtain the intrinsic ME coefficient of the laminates, that is, the ME response of an ideal very large laminate that would not be affected by size effects. Fig. 3.12 shows the intrinsic ME coefficient of all the laminates when using as-quenched magnetostrictive ribbons as a function of the AR:

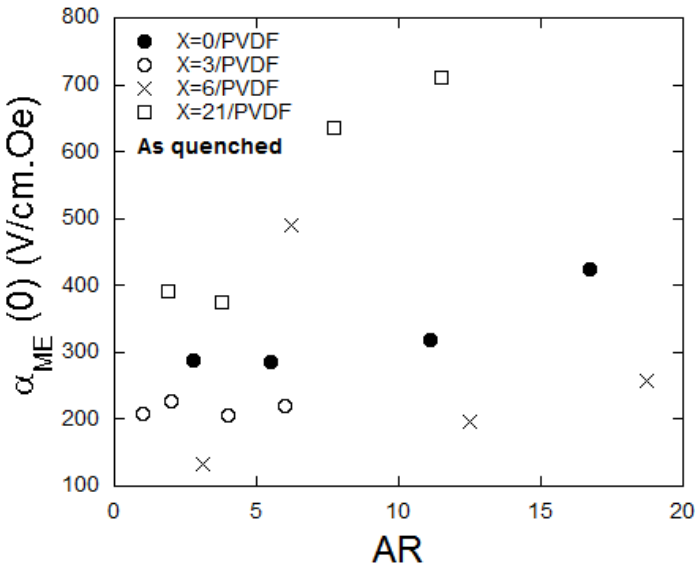

Figure 3.12. Intrinsic ME coefficient of the laminates with as-quenched magnetostrictive ribbons as a function of the aspect ratio.

The results displayed in Fig. 3.12 shows a good correction for the laminates with the shortest AR. For laminates with an AR higher than 6, the correction is worse. These disagreements for the longest laminates can be attributed to the worse homogeneity of the epoxy in the fabrication process of those laminates, which leads to an inaccurate measurement of the ME voltage. Therefore, laminates where the corrections work better are X=3/PVDF ones, since the X=3 is the composition with the lowest AR. Fig. 3.13 shows the intrinsic ME coefficient for the X=3/PVDF laminates, when using as-quenched magnetostrictive ribbons.

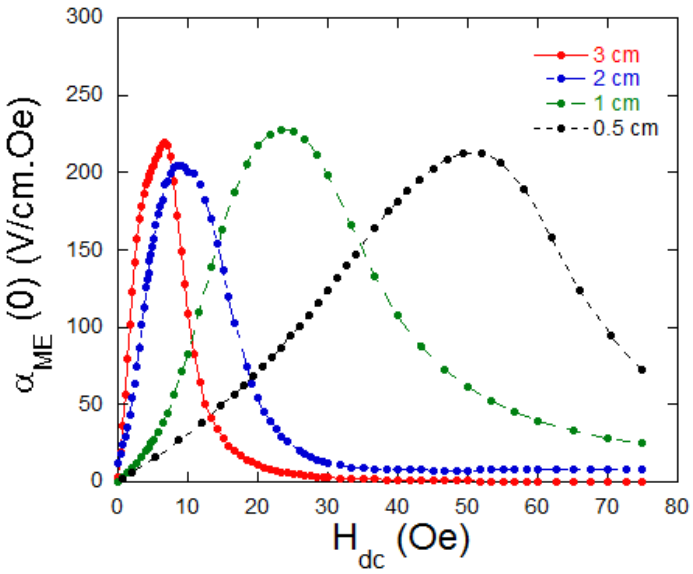

Figure 3.13. Intrinsic ME coefficient of the laminates with as-quenched magnetostrictive ribbons as a function of the applied magnetic field for the X=3/PVDF laminates, when using as-quenched magnetostrictive ribbons.

As can be observed, a ME coefficient about 225 V/cm.Oe was obtained for all the laminates. These results confirm the good approximation of the demagnetizing factors of the laminates and also support the obtained RF values.

Nevertheless, and as it was discussed when analyzing the information extracted from the FM, the inaccurate determination of the intrinsic magnetic susceptibility of the annealed ferromagnetic compositions makes difficult a good correlation between the induced ME response and the parameters were this susceptibility is involved (see Fig. 3.2, right). Fig. 3.14 shows the intrinsic ME coefficient of the

all the laminates when using annealed magnetostrictive ribbons in a function of the AR:

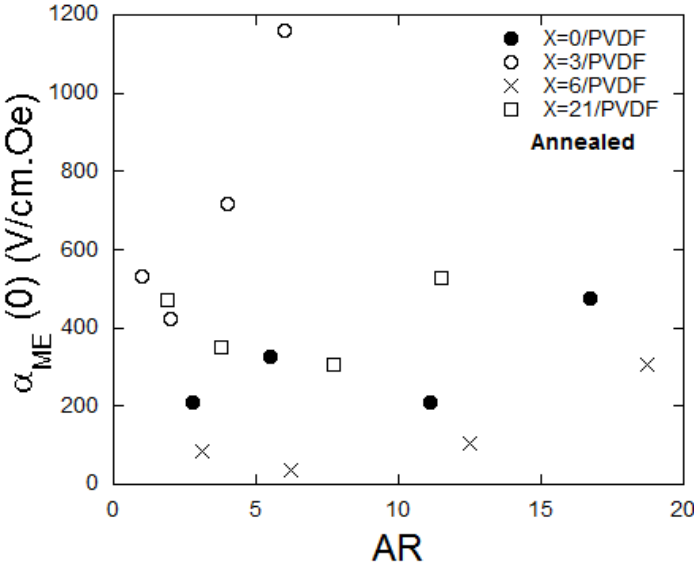

Figure 3.14. Intrinsic ME coefficient of the laminates with annealed magnetostrictive ribbons as a function of the aspect ratio.

As it is observed, the corrections for the laminates with annealed magnetostrictive ribbons are quite fuzzy. Even the corrections of the laminates with magnetostrictive compositions of low AR are inaccurate, which confirms the difficulties of correlating the ME response with the intrinsic susceptibility of the annealed magnetostrictive ribbons.

3.4. Discussion and conclusions

The effect of the size in the ME response has been studied for three-layer L-T type ME laminates composites fabricated with different metallic glasses as magnetostrictive constituents and PVDF as the piezoelectric one. The expected behavior of the ME responses has been discussed through a figure of merit. The results show a pretty good agreement between the ME voltages and the figure of merit for laminates with as-quenched magnetostrictive ribbons. The ME responses of the laminates with annealed magnetostrictive ribbons, however, do

not show a correlation with this figure of merit. This behavior is due to the fact that the intrinsic magnetic susceptibility has been extrapolated, and apparently, that extrapolation does not work as it should.

It has been observed that the ME coefficient decreases in all the cases as the length of the laminate does, effect that was mainly attributed to the demagnetizing fields and also to the less effective deformation of the magnetostrictive ribbons.

The correlation between the ME coefficient and different parameters that affect the ME response has been also studied. Whereas the correlation of the measured ME coefficients with the piezomagnetic coefficient and quality factor shows separately some disagreements, the correlation with the product of both quantities shows a much better agreement. The X=3/PVDF laminates with as-quenched magnetostrictive ribbons, however, show very low ME coefficient in comparison with the other laminates. In this case, those low responses arise from the low ME coupling coefficients obtained mainly for the 3 and 2 cm long laminates.

Concerning this ME coupling between the constituents of the laminates, we have observed that the longest laminates show, in general, higher ME couplings than the shortest ones, which is attributed to the lower deformation that the short magnetostrictive ribbons transmit to the piezoelectric constituent. The different coupling values obtained for all the studied laminates allows to understand the results obtained for the measured ME maximum coefficients in all cases.

Finally, the losses in the ME response arising from size effects have been quantified. The losses arisen from the increase of the frequency show loss tangents below 0.1 in all the laminates, a low enough value to have big influence in the ME response of the laminates.

The losses in the ME coefficient arisen from the reduction of the length have been quantified by calculating the corresponding reduction factors, RF. The shortest ME laminates show losses ranging between 95 % and 99 %, being the lowest value of 38 % for the 3 cm long X=6/PVDF laminate with annealed magnetostrictive ribbons.

Using the obtained RF values, the ME coefficients of the laminates have been corrected. The laminates with as-quenched magnetostrictive ribbons show good corrections for aspect ratios up to 6. Above that value the corrections is not so good, due to the worse homogeneity of the epoxy in the fabrication process of the longer laminates. Since the values of the intrinsic magnetic susceptibility of the annealed magnetostrictive are not accurate, the corrections do not work for laminates that use annealed ribbons.

3.5. References

[1] Y. Jia, W. Zhou, K. Ma, and Y. Liu, "Enhanced Magnetoelectric Effect in Permendur/Pb($Zr_{0.52}$ $Ti_{0.48}$)O_3 Laminated Magnetostrictive/Piezoelectric Composite," *Applied Sciences,* vol. 5, p. 587, 2015.

[2] J. Gutiérrez and J. M. Barandiarán, "High Magnetostriction Metallic Glasses Used as Magnetoelastic Labels," *IEEE Transactions on Magnetics,* vol. 31, pp. 3146-3148, 1995.

[3] Z. Fang, S. G. Lu, F. Li, S. Datta, Q. M. Zhang, and M. El Tahchi, "Enhancing the magnetoelectric response of Metglas/polyvinylidene fluoride laminates by exploiting the flux concentration effect," *Applied Physics Letters,* vol. 95, p. 112903, 2009.

[4] S. Dong, J.-F. Li, and D. Viehland, "Magnetoelectric coupling, efficiency, and voltage gain effect in piezoelectric-piezomagnetic laminate composites," *Journal of Materials Science,* vol. 41, pp. 97-106, 2006/01/01 2006.

[5] D. A. Pan, J. J. Tian, S. G. Zhang, J. S. Sun, A. A. Volinsky, and L. J. Qiao, "Geometry effects on magnetoelectric performance of layered Ni/PZT composites," *Materials Science and Engineering: B,* vol. 163, pp. 114-119, 7/15/ 2009.

[6] F. Fang, C. Zhao, and W. Yang, "Thickness effects on magnetoelectric coupling for Metglas/PZT/Metglas laminates," *Science China Physics, Mechanics and Astronomy,* vol. 54, pp. 581-585, 2011/04/01 2011.

[7] Y. Wang, M. Li, D. Hasanyan, J. Gao, J. Li, and D. Viehland, "Geometry-induced magnetoelectric effect enhancement and noise floor reduction in Metglas/piezofiber sensors," *Applied Physics Letters,* vol. 101, p. 092905, 2012.

[8] A. Lasheras, J. Gutiérrez, A. Balza, J. M. Barandiarán, and A. Rodríguez Pierna, "Radiofrequency magnetoelastic resonators for magnetoelectric applications," *Journal of Physics D: Applied Physics,* vol. 47, 2014.

[9] M. P. Silva, P. Martins, A. Lasheras, J. Gutiérrez, J. M. Barandiarán, and S. Lanceros-Mendez, "Size effects on the magnetoelectric response on PVDF/Vitrovac 4040 laminate composites," *Journal of Magnetism and Magnetic Materials,* vol. 377, pp. 29-33, 2015.

[10] F. Yang, Y. M. Wen, P. Li, M. Zheng, and L. X. Bian, "Resonant magnetoelectric response of magnetostrictive/piezoelectric laminate composite in consideration of losses," *Sensors and Actuators A: Physical,* vol. 141, pp. 129-135, 1/15/ 2008.

[11] X. Cui and S. Dong, "Theoretical analyses on effective magnetoelectric coupling coefficients in piezoelectric/piezomagnetic laminates," *Journal of Applied Physics,* vol. 109, p. 083903, 2011.

[12] D. Pan, J. Lu, Y. Bai, W. Chu, and L. Qiao, "Shape demagnetization effect on layered magnetoelectric composites," *Chinese Science Bulletin,* vol. 53, pp. 2124-2128, 2008/07/01 2008.

[13] D. X. Chen, E. Pardo, and A. Sanchez, "Fluxmetric and magnetometric demagnetizing factors for cylinders," *Journal of Magnetism and Magnetic Materials,* vol. 306, pp. 135-146, 2006.

[14] J. A. Osborn, "Demagnetizing Factors of the General Ellipsoid," *Physical Review,* vol. 67, pp. 351-357, 06/01/ 1945.

[15] D.-X. Chen, E. Pardo, and A. Sanchez, "Demagnetizing factors of rectangular prisms and ellipsoids," *Magnetics, IEEE Transactions on,* vol. 38, pp. 1742-1752, 2002.

[16] D. T. Huong Giang, P. A. Duc, N. T. Ngoc, N. T. Hien, and N. H. Duc, "Enhancement of the magnetic flux in Metglas/PZT-Magnetoelectric integrated 2D geomagnetic device," *Journal of Magnetics,* vol. 17, pp. 308-315, 2012.

[17] A. E. Clark and M. Wun-Fogle, "A new method of magnetostrictivity and magnetostriction measurement," *Magnetics, IEEE Transactions on,* vol. 25, pp. 3611-3613, 1989.

4. Analysis and performance of some applications based on magnetoelectric laminates

This Chapter deals with some potential applications of the magnetoelectric laminated composites that have been previously studied. In particular, it will be focused on the use of laminates as energy harvesting devices and magnetic field sensors. The laminates used for those applications are the 3 cm long X=3/PVDF and X=6/PVDF laminates, both laminates using annealed magnetostrictive ribbons. These laminates were chosen due to their high ME response, according to the results showed in Chapter 3. The first part of the chapter studies the different energy harvesting circuits that are used to convert the AC voltage into a DC one. The output electric power is measured for all of them in order to find out the most suitable one. The second part of the chapter is focused on the development of the laminates as magnetic field sensors. The sensitivity of the laminates to the applied AC and DC magnetic fields, as well as the hysteresis of the devices has been measured. Finally, first tests of equivalent magnetic noise in the X=6/PVDF laminate have been performed.

4.1. Magnetoelectric laminates as energy harvesting devices

4.1.1. Energy harvesting from environmental sources

Polymer based ME composites have recently been evaluated for their use in energy harvesting applications [1]. These devices harvest energy from sources already present in the environment (such as wind, solar, electromagnetic, etc). One of the technologies that has suffered one of the most rapid development in the last years is the harvesting of energy from vibrations, being those mainly of electromagnetic, electrostatic, magnetoelastic or piezoelectric origin [2]. Thus, any vibration arising from ground or machines shaking, ambient sound or human movements enables to extract energy from it.

It is expected that ME energy harvesters will enhance energy collection and conversion efficiency by taking advantage of combining the direct piezoelectric effect stimulated by both vibration and electromagnetic signal, the later through the ME coupling (see Fig. 4.1).

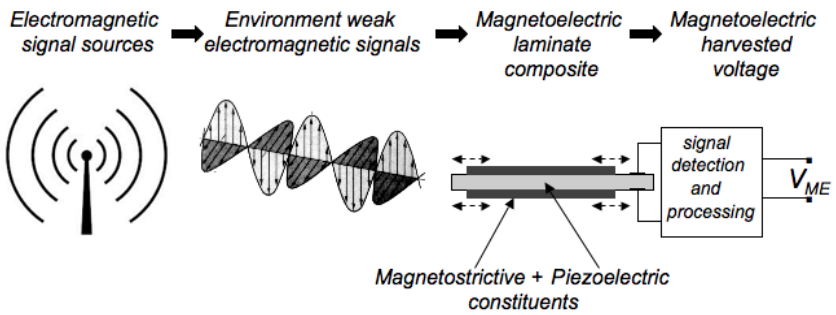

Figure 4.1. Schematic representation of the energy harvesting process for a magnetoelectric device (MED): even a weak electromagnetic signal is able to deform the magnetostrictive constituent of the MED, driving so an alternating deformation on its piezoelectric constituent and generating an alternating output voltage.

If we have a look at the energy sources that are present in the environment, we realize that many of them can be used as energy supplier for different purposes. At the end of section 4.1.4 will be showed some of sources that could act as energy suppliers for our laminates.

Several ME energy harvesters designs have been proposed with Fe-Ni rich alloy and PZT [3], Terfenol-D and PZT [4] or PMNT [5], Ni-Mn-Ga and PZT [6] as magnetostrictive and piezoelectric constituent, respectively. Values of the harvested energy range typically between few μW and some mW.

The next generation of energy-harvesting applications in areas such as wearable energy-harvesting systems will require the system to be flexible, lightweight and even biocompatible [1]. Thus, ME materials based on piezoelectric polymers such as PVDF appear as the most suitable approach to meet these requirements due to their flexibility, versatility of production and low cost [7].

Some of the highest reported ME coefficients on polymer-based ME laminates are already of the same order of magnitude of the best ME materials being used/investigated as energy harvesters, encouraging the use of polymer-based ME materials in such applications [8, 9].

In the following, it is demonstrated the feasibility of the 3 cm long X=6/PVDF and X=3/PVDF laminates as energy harvesting devices, both using annealed magnetostrictive ribbons. The output power is evaluated as a function of the load resistance of the circuitry used to rectify the output electric signal, working at the MER frequency and DC magnetic field for the maximum ME response of each laminate.

4.1.2. Energy harvesting circuits

The output electric power of the laminates was optimized by testing four different energy harvesting circuits: a full-wave bridge voltage rectifier, two Cockcroft-Walton voltage multipliers with one and two stages and a three stages Dickson voltage multiplier. Schottky diodes (BAT15-03W) and Polyphenylene Sulfide film capacitors with a surface-mounted device (SMD) package were used in the development of the circuits. These diodes were specially chosen due to their low forward voltage of approximately 100 mV for a forward current of 10 μA. The capacitors were selected due to their charge discharge rate speed and their low equivalent series resistance [10, 11]. The values for the capacitors were

calculated for a maximum ripple value of 1 mV, low enough to obtain an almost continuous signal. The ripple is the residual periodic variation of the rectified signal derived from the output AC voltage (see Fig. 4.2) and it has to be as low as possible in order to get a clear DC signal.

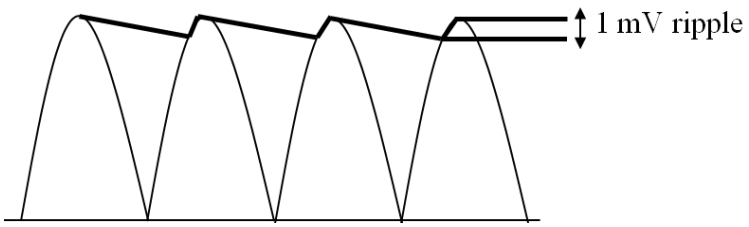

Figure 4.2. Scheme of the sinusoidal and rectified signal with the ripple.

The full-wave bridge voltage rectifier circuit is widely used in energy harvesting systems that converts AC voltage to DC voltage [4, 12]. The main advantages of this circuit are its low energy loss, low complexity and high efficiency. This circuit consists of four Schottky diodes (see Fig. 4.3, (a)) which convert the AC output voltage of the ME laminate into a DC one [13] through the two half cycles (positive and negative). The value of the capacitors used for this circuit was 100 nF following equation 19 in Ref. [14].

The voltage multipliers are an efficient way to convert from AC to DC and simultaneously increase the output voltage [15]. The Cockcroft-Walton circuit is a half-wave rectifier constituted by *n* stages, each stage formed by two diodes and two capacitors (see Fig. 4.3, (b) and (c)). Whereas the one stage multiplier makes the output voltage increase twice the input one, the two stage multiplier increases it four times.

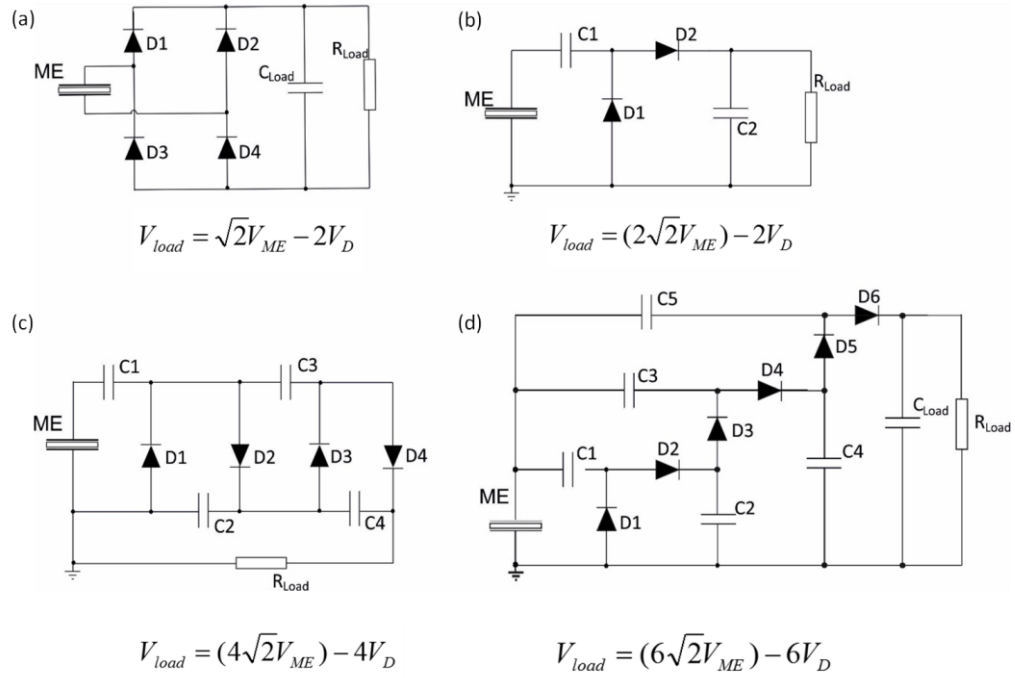

Figure 4.3. Schematic representation of a Full-wave bridge voltage rectifier (a), Cockcroft-Walton voltage multiplier with one stage (b), Cockcroft-Walton voltage multiplier with two stages (c) and Dickson voltage multiplier with three stages (d). V_{ME} represents the induced voltage in the ME laminate, V_D represents forward voltage drop across each diode and V_{Load} measured voltage at the load resistance.

The one-stage Cockcroft-Walton voltage multiplier (see Fig. 4.3 (b)) consists on a clamper constituted by the capacitor C1 and the diode D1 and a peak detector constituted by the capacitor C2 and the diode D2. The clamper signal is measured in the diode D1 and corresponds to the wave input shifted from the negative peak to zero. The peak detector assigns a DC voltage with approximately twice the input peak voltage value. The two-stage Cockcroft-Walton voltage multiplier (see Fig. 4.3 (c)) has a similar behavior than the previous one but the input signal is increased four times by adding another multiplier level. The values of the capacitors were 220 nF and 680 nF, for the one-stage and two-stage circuits, respectively, following equation 3 in Ref. [16].

The Dickson voltage multiplier circuit is also a half-wave rectifier, which can be constructed with *n* stages, wherein each one is formed by two diodes and two

capacitors. The Dickson multiplier showed in Fig. 4.3 (d) is a three-stage circuit based on the original Dickson charge pump, a DC-DC converter where the original DC input is shunted to the ground level and the logic control is replaced by the AC input signal to be harvested [17]. In this case, the values of the capacitors were 220 nF, following equation 1 in Ref. [18].

4.1.3. Measurement of the output electric power of the laminates

In order to measure the output electric power of the 3 cm long X=3/PVDF and X=6/PVDF laminates, the first step was to determine the working parameters to be used in the output power measurements. Fig. 4.4 shows the ME characterization of the laminates.

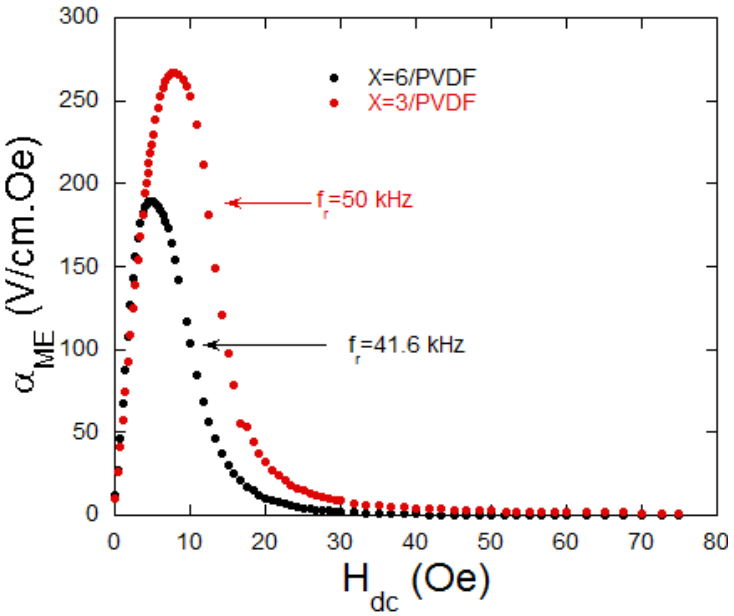

Figure 4.4. ME characterization of the 3 cm long X=6/PVDF and X=3/PVDF using annealed magnetostrictive ribbons.

The MER frequencies were the ones already showed in Table 3.2 in section 3.1. The DC magnetic field was set, in each case, at the field for the maximum ME response. In the case of the 3 cm long X=6/PVDF laminate, this field is about

4.7 Oe, whereas for the X=3/PVDF this field is slightly higher, about 7 Oe, due to the lower length-to width ratio. The AC magnetic field was in both cases 0.45 Oe.

Once we have the working parameters of each laminate, we proceeded to choose the most suitable circuit among the ones showed in Fig. 4.3. Thus, we selected the 3 cm long X=6/PVDF laminate to measure the output electric power in a function of the load resistance for all the energy harvesting circuits described in Fig. 4.3.

This measurement was performed varying the load resistance from 1 kΩ to 1 MΩ (see Fig. 4.5) and the obtained output voltage was continuously monitored by a Hewlett Packard 54603 oscilloscope.

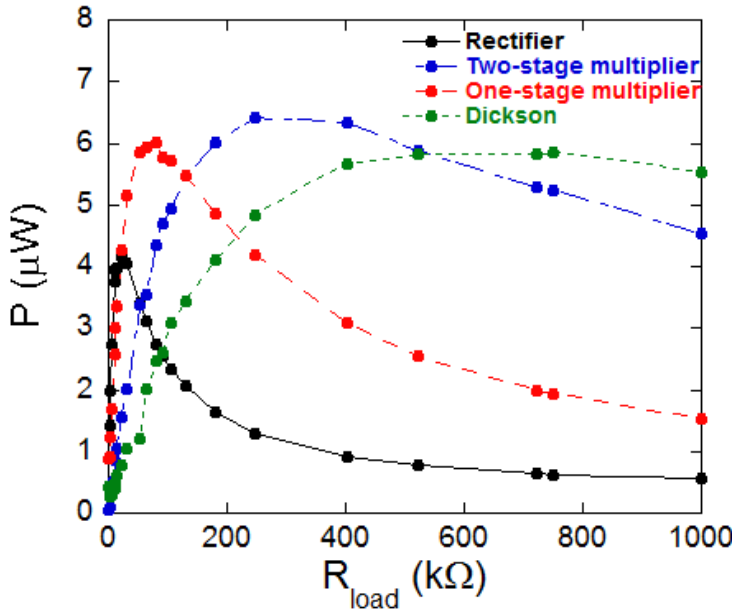

Figure 4.5. The output electric power as a function of the load resistance for all the studied energy harvesting circuits.

As can be observed, the two-stage multiplier is the circuit where the output electric power is maximum (6.4 μW), at a load resistance of 250 kΩ. An increase of the number of stages (three-stage Dickson multiplier) the optimal load resistance increases up to 500 kΩ, whereas a decrease in the stages leads to a

decrease down to 80 kΩ (one-stage multiplier), with a drop in both cases of the value of the output power.

Therefore, since the two-stage multiplier is the one that provides a higher output power, this circuit was used to measure the output electric power in a function of the load resistance for the 3 cm long X=3/PVDF laminate. Fig. 4.6 shows the output power as a function of the load resistance for both 3 cm long X=3/PVDF and X=6/PVDF laminates.

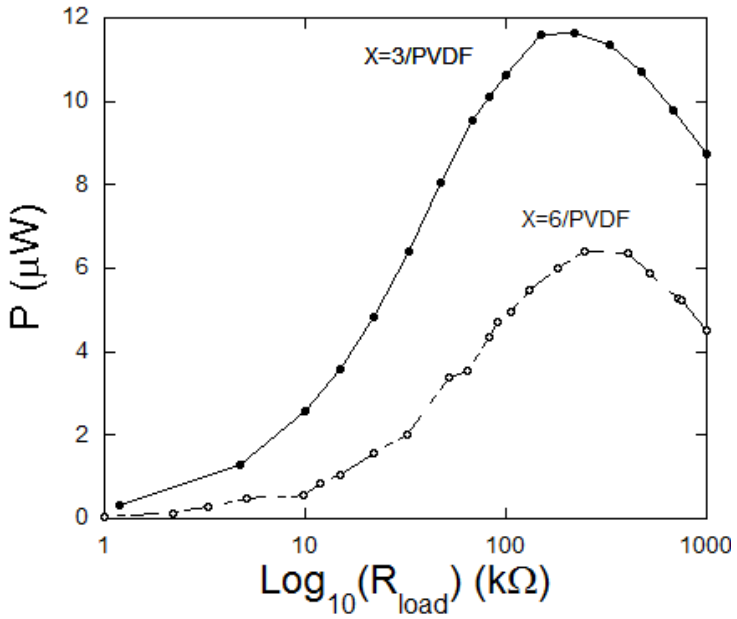

Figure 4.6. The output electric power as a function of the load resistance for the 3 cm long X=6/PVDF and X=3/PVDF laminates using annealed magnetostrictive ribbons, measured using the two-stage multiplier circuit.

Maximum output powers of 6.4 and 11.7 μW were obtained for the 3 cm long X=6/PVDF and X=3/PVDF laminates, respectively. As expected, the output power is higher for the 3 cm long laminate, since it has a higher ME coefficient (see Table 3.3 in section 3.1). The load resistances for the maximum power are very similar in both laminates, being 250 kΩ for the X=6/PVDF laminate and 180 kΩ for the X=3/PVDF one.

Table 4.1 summarizes the main parameters of each laminate involved in the measurement of the output power.

Table 4.1. Optimal load resistance (R_{load}), measured current across the load resistance (I_{DC}), measured rectified voltage (V_{DC}) and maximum power generated by the laminates (P_{max}).

Laminate	R_{load} (kΩ)	I_{DC} (μA)	V_{DC} (V)	P_{max} (μW)
X=6/PVDF	250	5.09	1.26	6.4
X=3/PVDF	180	8.04	1.45	11.7

As it is observed, the high value measured in the X=3/PVDF laminate arises mainly from the high current that circulates across the load resistance in comparison with the X=6/PVDF laminate.

With these measured maximum power outputs and considering the total volume of the laminates, the corresponding power densities can be easily calculated. For the 3 cm long X=6/PVDF, a value of 1.2 mW/cm^3 was obtained, whereas the 3 cm long X=3/PVDF shows a value of 0.55 mW/cm^3. Therefore, although the X=3/PVDF laminate shows a higher output power, the corresponding power density is lower than one obtained for the X=6/PVDF laminate. This is obviously attributed to the differences in the geometry between both laminates. Actually, the effective volume (without considering the not directly bonded PVDF) of the 3 cm long X=3/PVDF laminate is significantly higher than the 3 cm long X=6/PVDF one, which directly leads to a lower power density.

4.1.4. Discussion and conclusions

It has to be noticed that the obtained maximum (magnetoelectric) power generated values are comparable to some previously reported power densities for laminates containing PZT and PVDF (see Table 4.2) as piezoelectric constituents.

The low DC magnetic field required greatly simplifies the implementation of our ME laminated composites, in comparison with the other ME energy harvesting devices. Since the performance the energy harvesting device is proportional to the induced ME voltage (see Fig. 4.3, (c)), the dependence of the energy harvesting performance follows the same behavior as the ME coefficient does,

being the best performance achieved at the DC magnetic field needed for the maximum ME coupling.

Table 4.2. Comparison of some power output and power densities reported so far for both ME laminates and renewable source energy harvesting devices

L(cm)	H_{ac}(Oe)	H*(Oe)	f_r (kHz)	P (μW)	P/V (mW/cm^3)	Materials involved
3	0.45	4.7	41.6	6.4	1.2 (our work)	X=6 and PVDF
3	0.45	7.0	50.0	11.7	0.55 (our work)	X=3 and PVDF
0.1	1	66.1	66.1	0.065	0.7 Ref.[19]	$Fe_{0.7}Ga_{0.3}$ and PZT
8	0.3	50	26.9	917.7	0.956 Ref.[3]	FeNi and PZT
12	1	800	27.0	20	0.12 Ref.[4]	Terfenol-D and PZT
4	———	———	———	93.6	0.1579 Ref.[20]	PVDF and PZT
6	———	———	———	75000	0.0051 Ref.[21]	APC 855 (piezoelec.)

Therefore, the used two-stage multiplier circuit working with high performance ME devices could act as simple and low cost ME effect based energy harvesters with good output electric power responses. It has to highlight that the obtained output values are within the ultra low-power consumption devices suitable for biomedical wireless communications systems [22], among others.

Concerning the environmental radiation spectrum in which this device is expected to work, Table 4.3 summarizes some of the potential energy suppliers that could be used for the laminates.

Table 4.3. Some of the potential energy sources to be used as energy supplier for ME laminates.

Energy source	Frequency range (kHz)	AC magnetic field (Oe)
Induction plates	20-100 [23]	0.015 [24]
Laptops	0.1-20	0.002-0.015 [25]
Compact fluorescent lamps	0.05-100	0.0002-0.0015 [26]
Smart board	5-15	0.0005 [26]
Touchscreen	44	0.002 [26]

Among all the potential sources, the induction plates seem to be the most suitable ones, due to their working frequencies (in the range of our laminates) and also due to the used AC magnetic field magnitudes.

Other sources coming from electromagnetic fields such as vacuum cleaners or microwave ovens work at frequencies in the range of 50-60 Hz and with magnetic fields between 0.5 Oe–0.7 Oe. The power density for a WLAN short-range standard wireless device in the GHz range can reach 23 mW/m^2 [27, 28].

The major part the RF public exposure comes from mobile and wireless portable devices, and this exposure level in the living areas is continuously increasing. The general results of European site measurements surveys (year 2010 [29]) showed that more than 60% of the total measured electromagnetic exposure is about 3 mW/m^2. It is clear that in electromagnetic energy harvesting, due to the low magnetic field amplitude and input power, the obtained response voltage is up to date quite weak [4].

Nevertheless, in this first section it has been demonstrated that a useful ME signal can be achieved by choosing proper constituents of the energy transduction material or device, in our case, ME laminated composites made of home-made metallic glasses and PVDF. So, future work in this field points directly to the improvement of the performance of the magnetostrictive and piezoelectric materials of these ME devices, as well as the development of adequate power management circuits in order to produce appropriate energy supply performance.

4.2. Magnetoelectric laminates as magnetic field sensors

4.2.1. Sensitivity of the magnetoelectric laminates to the applied magnetic field

The high ME responses showed by these laminates, as well as the low magnetic fields at which they work, allow them to be used as magnetic field sensors and/or actuators [30, 31]. The performance of a magnetic field sensor is mainly determined by its sensitivity to the magnetic field [32, 33], although they are other parameters such as hysteresis that have to be also taken into account. Among the ME effect based magnetic field sensors that use a piezoelectric polymer, the

obtained sensitivities are in general in the order of nT at out of resonance frequencies and about 10 pT at the MER [34, 35].

The ME set-up used to measure the sensitivity of the devices was the one previously showed in Fig. 2.18. The sensitivity was measured both to the applied AC and DC magnetic fields. In the case of the DC magnetic field, the maximum sensitivity can be easily obtained from the maximum slope of the ME characterization curves of the laminates (see Fig. 4.7).

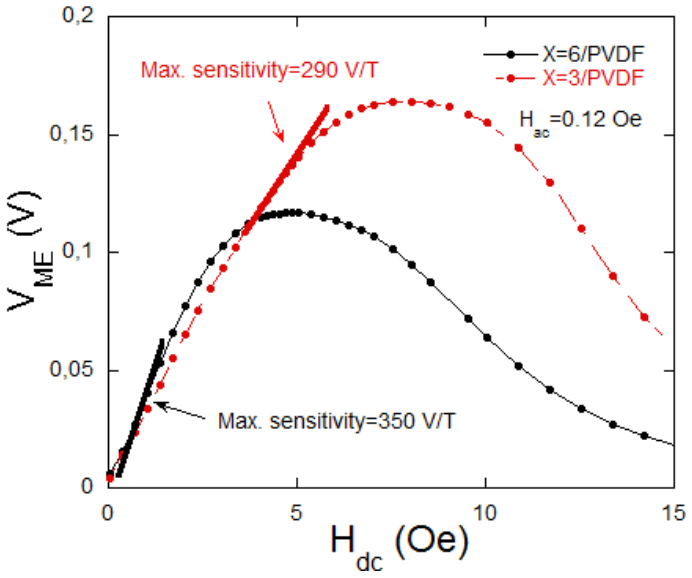

Figure 4.7. Induced ME voltage as a function of the DC magnetic field for the 3 cm long X=3/PVDF and X=6/PVDF laminates.

As it can be observed, the obtained maximum sensitivities are 290 and 350 V/T for the X=3/PVDF and X=6/PVDF laminates at DC magnetic fields of 5 and 1 Oe, respectively.

Measurements were also performed by monitoring several times the induced ME voltage as a function of increasing and decreasing applied magnetic field, observing some hysteresis in these measurements.

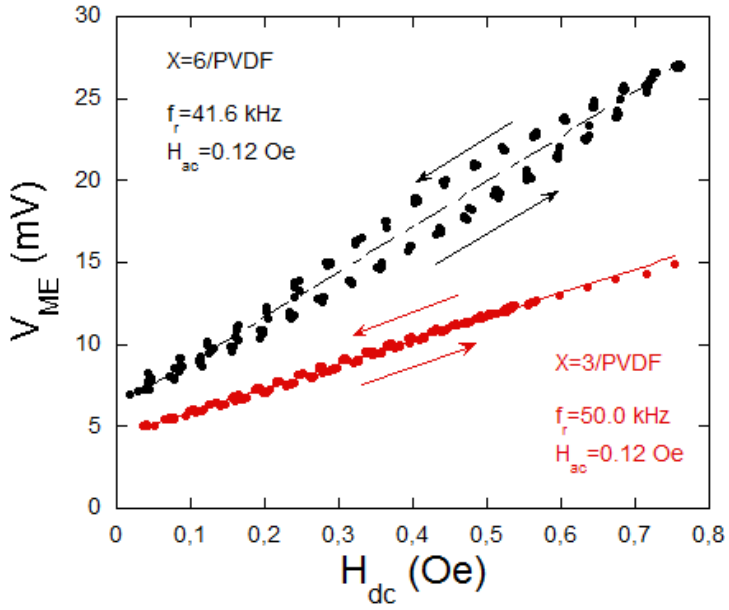

Figure 4.8. Measurements of the induced ME voltage as a function of the increasing and decreasing applied DC magnetic field, for the X=3/PVDF and X=6/PVDF laminates.

Fig. 4.8 shows this hysteresis measurement of the induced ME voltage as a function of the applied DC magnetic field, with magnetic fields ranging from 0.01 up to 0.8 Oe. In the case of the X=3/PVDF laminate, a hysteresis about ±0.2 mV was measured, whereas for the X=6/PVDF one this hysteresis is significantly higher, about ±1.3 mV.

The determination of the sensitivity to the applied AC magnetic field is slightly different, since the maximum sensitivity is located at the DC magnetic field that corresponds to the maximum ME coupling [36-38]. The measurement of this sensitivity was carried out by measuring the induced ME voltage as a function of the applied AC magnetic field, keeping the frequency at the MER and at a DC magnetic field of the maximum ME coupling. Fig. 4.9 shows the induced ME voltage as a function of the applied AC magnetic field for the X=3/PVDF and X=6/PVDF laminates.

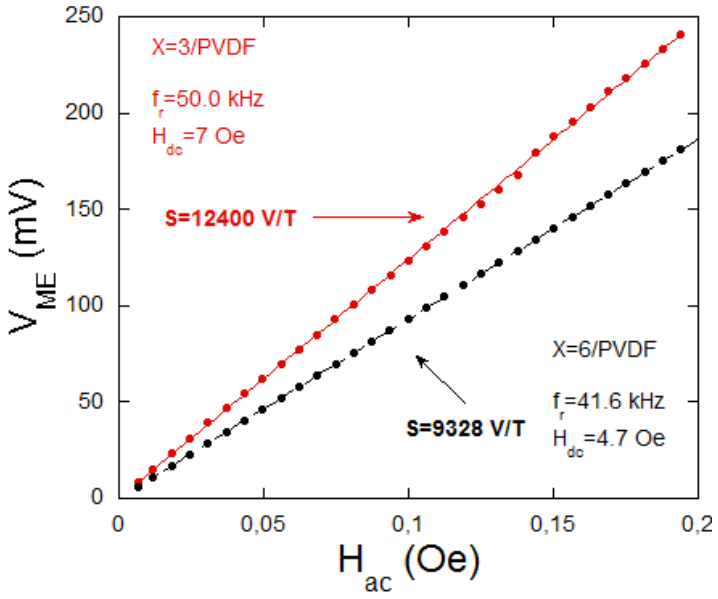

Figure 4.9. Measurement of the induced ME voltage as a function of the applied AC magnetic field for the X=3/PVDF and X=6/PVDF laminates, measured at the MER frequency of each laminate and at the DC magnetic field of the maximum ME coupling.

Unlike the sensitivity to the DC magnetic field, the X=3/PVDF laminate is now more sensitive (12400 V/T) to the AC magnetic field than the X=6/PVDF one (9328 V/T).

Aiming to find some hysteresis, measurements were also performed in a range between 5 and 80 mOe, again increasing and decreasing the field amplitude. Fig. 4.10 shows the obtained results for the induced ME voltage as a function of the AC magnetic field.

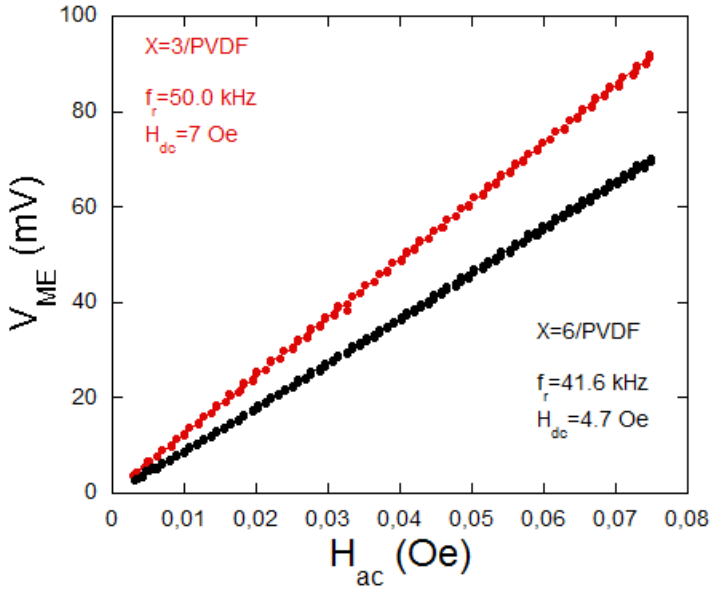

Figure 4.10. Measurements of the induced ME voltage as a function of the increasing and decreasing applied AC magnetic field, for the X=3/PVDF and X=6/PVDF laminates.

As it can be seen, in contrast to the results as a function of the applied DC magnetic field, there is no appreciable hysteresis in the measurement of the induced ME voltage as a function of the applied AC magnetic field.

4.2.2. Noise level measurements

The suitability of a magnetic field sensor is not only determined by the output voltage obtained at the optimal working parameters, but also by its equivalent magnetic noise [39, 40]. Few works have been reported so far concerning noise measurements in polymer based ME laminates, obtaining an equivalent magnetic noise in the order of $nT/Hz^{1/2}$ [35].

In order to evaluate the noise level of our ME devices, we performed noise measurements in one of our ME field sensors.

The set-up used to measure the noise of the ME laminated composites was very similar to the one showed in Fig. 2.17. However, in this case the Helmholtz coils that apply the static magnetic field were replaced by two permanent magnets

located at a certain distance to the laminates, ensuring a uniform magnetic field along the laminate. This magnetic field value was chosen according to the best working point of the ME device. The sensor was then placed into a high mu-metal magnetic shielding chamber, in order to avoid any electromagnetic noise presented in the environment (see Fig. 4.11). The output ME voltage of the laminates was fed to a low noise amplifier (SR560 by Stanford Research Systems), and then directed to a HP35670A dynamic signal analyzer, which performs a Fast Fourier Transform of the signal and measures the frequency spectrum. The amplifier was also used as electronic filter in order to avoid the appearance of noise arising from instrumentation, and therefore, assuring an equivalent noise originated mainly from the ME device [32].

Figure 4.11. Experimental set-up used for noise measurements.

The noise measurements were carried out both at low frequencies and at frequencies around the MER. In the case of the low frequency measurements, since we are close to the DC region, the maximum field sensitivity is located at the maximum slope of the ME voltage curve (see Fig. 4.7), whereas at frequencies around the MER, the maximum sensitivity is at the DC magnetic field of the maximum ME voltage (see Fig. 4.9).

This noise is usually quantify by the corresponding spectral density, ***S(f)***, defined as follows:

$$S(f)=\frac{\langle v_n^2\rangle}{\Delta f} \tag{4.1}$$

where $\langle v_n^2\rangle$ is the squared rms value of the noise voltage V_n ***(f)*** and Δf is the frequency bandwidth. Alternatively, the noise is quantified by the root squared value of ***S(f)***, also known as equivalent noise e_n and measured in $V/Hz^{1/2}$:

$$e_n=\sqrt{S(f)} \tag{4.2}$$

The amplification gain used to obtain the equivalent noise spectrum was 100 at low resonance frequencies and 20 at frequencies around the MER. Once we obtained the spectrum, the equivalent noise values were divided by these gains to obtain the real values. Fig. 4.12 shows the equivalent noise of the X=6/PVDF laminate both at low and around the MER frequencies.

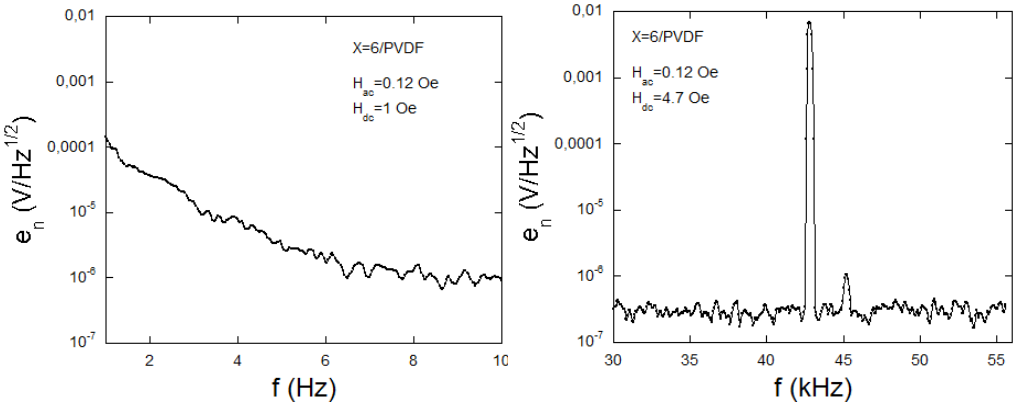

Figure 4.12. Equivalent noise as a function of the frequency for the X=6/PVDF laminate, both at low (left) and around the MER (right) frequencies.

The conversion to equivalent magnetic noise, b_n, is performed through the transfer function of the sensor, T_r, that is, the ratio between the induced ME voltage of the sensor and the applied magnetic field for different frequencies:

$$b_n = \frac{e_n}{T_r} \tag{4.3}$$

At low frequencies, this transfer function can be considered constant and it is directly extracted from the maximum slope of the ME voltage response showed in Fig. 4.7, since the maximum sensitivity is located at that point. At frequencies around the MER, however, a frequency dependence of the T_r must be obtained. This T_r is obtained by measuring the induced ME voltage of the sensor as a function of the frequency, keeping the DC magnetic field at the one of the maximum ME coupling, where the sensitivity to the AC magnetic field is maximum. Fig. 4.13 shows the transfer function as a function of the frequency for the X=6/PVDF laminate:

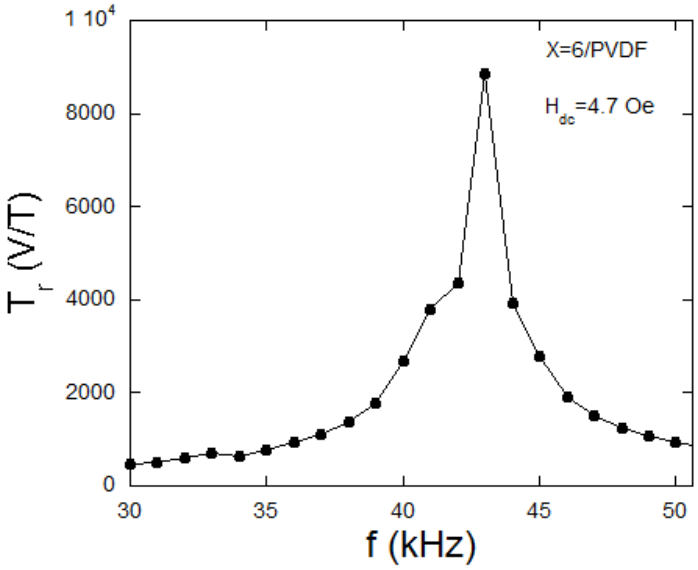

Figure 4.13. Transfer function as a function of the frequency for the X=6/PVDF laminate, at a H_{dc}=4.7 Oe.

If we vary the DC magnetic field, we observe that the maximum value of the transfer value decreases (see Table 4.4), since the sensitivity of the device to the applied AC magnetic field is lower:

Table 4.4. Maximum transfer function values for different applied DC magnetic fields for the X=6/PVDF laminate, obtained at the MER frequency of 41.6 kHz.

H_{dc} (Oe)	2	4.7	10	70
Max. T_r (V/T)	5940	9328	5350	51.3

With the transfer functions measured in Fig. 4.7 and 4.13, we can easily obtain the equivalent magnetic noise of the X=6/PVDF laminate (see Fig. 4.14):

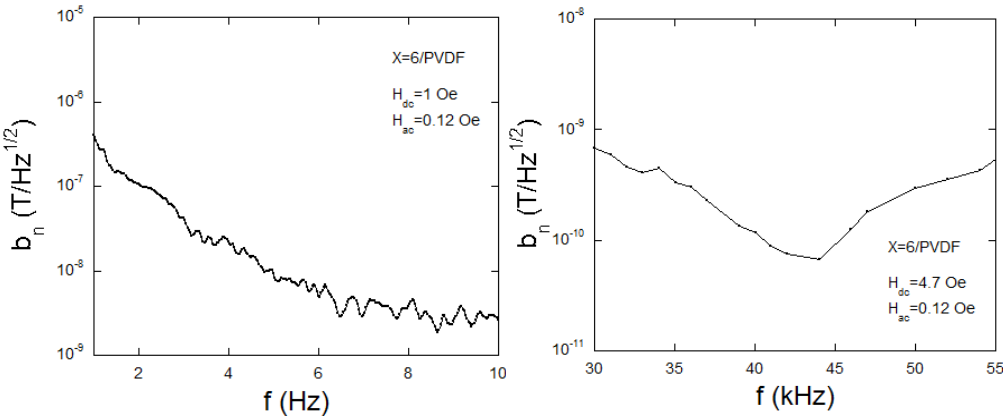

Figure 4.14. Equivalent magnetic noise as a function of the frequency for the X=6/PVDF laminate, both at low (left) and around the MER (right) frequencies.

As can be appreciated, the equivalent magnetic noise at low frequencies decreases from 0.5 $\mu T/Hz^{1/2}$ at 1 Hz to 3 $nT/Hz^{1/2}$ at 10 Hz. As expected, the equivalent magnetic noise reaches its minimum around the MER, where it shows a value of 67 $pT/Hz^{1/2}$.

4.2.3. Discussion and conclusions

The results obtained in section 4.2 show high sensitivities of the X=3/PVDF and X=6 laminates to both DC and AC magnetic fields. Particularly high are the sensitivities to the AC magnetic fields, which in the case of the X=3/PVDF laminates reaches the value of 12400 V/T. The maximum sensitivities to the applied AC magnetic field have been obtained at the fields that correspond to the maximum ME coupling.

The maximum sensitivity to the DC magnetic field was obtained for the X=6/PVDF laminate (350 V/T). In this case, however, this sensitivity is achieved at the magnetic field that correspond to the maximum slope of the ME voltage curve. These high values of sensitivities measured both for AC and DC magnetic fields confirm the suitability of these ME laminates as magnetic field sensors.

Low hysteresis have been observe in the sensitivity measurements to the DC magnetic field, with a maximum value ±1.3 mV for the X=6/PVDF laminate. The sensitivity measurement to the AC magnetic field does not show any hysteresis.

In order to explain the higher sensitivities obtained to the AC magnetic field than to the DC one, it is necessary to have a look at the transfer functions obtained for both cases. As it was shown in Fig. 4.7 and 4.13, the transfer function is highly dependent on the frequency. This T_r increases progressively as approaching the MER frequency, where the sensitivity is maximum. In the case of the X=3/PVDF laminate, the sensitivity to the AC magnetic field increases by a factor of 43 respect to the DC one, whereas for the X=6/PVDF laminate, this factor is about 27.

With the obtained sensitivities, we performed some equivalent magnetic noise measurements in the X=6/PVDF laminate, with the aim to determine the behavior of this noise at different frequencies. The results show a minimum equivalent magnetic noise at frequencies around the MER, with a minimum value of 67 $pT/Hz^{1/2}$. This values is in the same order of magnitude of the minimum equivalent magnetic noise of 10 $pT/Hz^{1/2}$ reported in Ref. [35] at a frequency of 165 Hz for a Metglas/P(VDF-TrFE) laminate. However, at low frequencies, the minimum equivalent magnetic noise was measured at 10 Hz, obtaining a value of 3 $nT/Hz^{1/2}$. This last value is very close to the one reported in Ref [35] at 1 Hz, where they obtained a minimum magnetic equivalent noise of 1 $nT/Hz^{1/2}$.

The higher values of the equivalent magnetic noise observed at low frequencies are due to smaller sensitivity of the devices at those frequencies, combined with the increased 1/f noise level (flicker noise) [41].

4.3. References

[1] P. Martins and S. Lanceros-Méndez, "Polymer-Based Magnetoelectric Materials," *Adv. Funct. Mater.,* vol. 23, pp. 3371-3385, 2013.

[2] S. P. Beeby, M. J. Tudor, and N. M. White, "Energy harvesting vibration sources for microsystems applications," *Measurement Science and Technology,* vol. 17, pp. R175-R195, 2006.

[3] L. Bian, Y. Wen, P. Li, Q. Gao, and M. Zheng, "Magnetoelectric transducer with high quality factor for wireless power receiving," *Sensors and Actuators, A: Physical,* vol. 150, pp. 207-211, 2009.

[4] P. Li, Y. Wen, P. Liu, X. Li, and C. Jia, "A magnetoelectric energy harvester and management circuit for wireless sensor network," *Sensors and Actuators, A: Physical,* vol. 157, pp. 100-106, 2010.

[5] J. Yang, Y. Wen, P. Li, X. Dai, and M. Li, "A new vibration energy harvester using magnetoelectric transducer," *Journal of Magnetics,* vol. 16, pp. 150-156, 2011.

[6] S. Ju, S. H. Chae, Y. Choi, S. Lee, H. W. Lee, and C. H. Ji, "A low frequency vibration energy harvester using magnetoelectric laminate composite," *Smart Materials and Structures,* vol. 22, 2013.

[7] Y. Qi, N. T. Jafferis, K. Lyons, C. M. Lee, H. Ahmad, and M. C. McAlpine, "Piezoelectric Ribbons Printed onto Rubber for Flexible Energy Conversion," *Nano Letters,* vol. 10, pp. 524-528, 2010/02/10 2010.

[8] P. Martins, A. C. Lopes, and S. Lanceros-Mendez, "Electroactive Phases of Poly(vinylidene fluoride): Determination, Processing and Applications," *Prog. Polym. Sci.,* vol. 39, pp. 683-706, 2013.

[9] M. Silva, S. Reis, C. S. Lehmann, P. Martins, S. Lanceros-Mendez, A. Lasheras*, et al.*, "Optimization of the Magnetoelectric Response of Poly(vinylidene fluoride)/Epoxy/Vitrovac Laminates.," *ACS Appl. Mater. Interfaces,* vol. 5, pp. 10912-9, 2013.

[10] J. Liu, P. Fei, J. Song, X. Wang, C. Lao, R. Tummala*, et al.*, "Carrier density and schottky barrier on the performance of DC nanogenerator," *Nano Letters,* vol. 8, pp. 328-332, 2008.

[11] A. Lasheras, J. Gutiérrez, S. Reis, D. Sousa, M. Silva, P. Martins*, et al.*, "Energy harvesting device based on a metallic glass/PVDF magnetoelectric laminated composite," *Smart Materials and Structures,* vol. 24, 2015.

[12] A. Tabesh and L. G. Fréchette, "A low-power stand-alone adaptive circuit for harvesting energy from a piezoelectric micropower generator," *IEEE Transactions on Industrial Electronics,* vol. 57, pp. 840-849, 2010.

[13] L. Karthikeyan and B. Amrutur, "Signal-powered low-drop-diode equivalent circuit for full-wave bridge rectifier," *IEEE Transactions on Power Electronics,* vol. 27, pp. 4192-4201, 2012.

[14] C. M. Young, M. H. Chen, S. H. Yeh, and K. H. Yuo, "A Single-phase single-stage high step-Up AC-DC matrix converter based on cockcroft-walton voltage multiplier with PFC," *IEEE Transactions on Power Electronics,* vol. 27, pp. 4894-4905, 2012.

[15] N. M. Roscoe and M. D. Judd, "Harvesting energy from magnetic fields to power condition monitoring sensors," *IEEE Sensors Journal,* vol. 13, pp. 2263-2270, 2013.

[16] C. G. H. Maennel, "Improvement in the modelling of a half-wave Cockroft-Walton voltage multiplier," *Review of Scientific Instruments,* vol. 84, p. 064701, 2013.

[17] R. E. Barnett, J. Liu, and S. Lazar, "A RF to DC voltage conversion model for multi-stage rectifiers in UHF RFID transponders," *IEEE Journal of Solid-State Circuits,* vol. 44, pp. 354-370, 2009.

[18] C. Yoo and K. L. Lee, "A low-ripple poly-Si TFT charge pump for driver-integrated LCD panel," *IEEE Transactions on Consumer Electronics,* vol. 51, pp. 606-610, 2005.

[19] T. D. Onuta, Y. Wang, C. J. Long, and I. Takeuchi, "Energy harvesting properties of all-thin-film multiferroic cantilevers," *Applied Physics Letters,* vol. 99, 2011.

[20] D. Vatansever, R. L. Hadimani, T. Shah, and E. Siores, "An investigation of energy harvesting from renewable sources with PVDF and PZT," *Smart Materials and Structures,* vol. 20, 2011.

[21] S. Priya, "Modeling of electric energy harvesting using piezoelectric windmill," *Applied Physics Letters,* vol. 87, 184101, 2005.

[22] Y. C. Shih, T. Shen, and B. P. Otis, "A 2.3 μ W wireless intraocular pressure/temperature monitor," *IEEE Journal of Solid-State Circuits,* vol. 46, pp. 2592-2601, 2011.

[23] S. Llorente, F. Monterde, J. M. Burdío, and J. Acero, "A comparative study of resonant inverter topologies used in induction cookers," in *Conference Proceedings - IEEE Applied Power Electronics Conference and Exposition - APEC*, 2002, pp. 1168-1174.

[24] B. Kos, B. Valič, D. Miklačvič, T. Kotnik, and P. Gajšek, "Pre- and post-natal exposure of children to EMF generated by domestic induction cookers," *Physics in Medicine and Biology,* vol. 56, pp. 6149-6160, 2011.

[25] D. Brodić and A. Amelio, "Classification of the Extremely Low Frequency Magnetic Field Radiation Measurement from the Laptop Computers," *Measurement Science Review,* vol. 15, pp. 202-209, 2015.

[26] M. Van Den Bossche, L. Verloock, S. Aerts, W. Joseph, and L. Martens, "In Situ exposure assessmentof intermediate frequency fields of diverse devices," *Radiation Protection Dosimetry,* vol. 164, pp. 252-264, 2015.

[27] "Electric and Magnetic Fields associated with the use of electric power," National Institute of Environmental Health Sciences and the National Insitute of HealthJune 2012.

[28] "Health and Electromagnetic Fields," European Commission - Research Directorate-General - European Communities2005.

[29] "Report on the level of exposure (frequency, patterns and modulation) in the European Union Part 1: Radiofrequency (RF) radiation," European Health Risk Assessment Network on Electromagnetic Fields ExposureAugust 2010.

[30] P. Martins and S. Lanceros-Méndez, "Polymer-Based Magnetoelectric Materials," *Advanced Functional Materials,* vol. 23, pp. 3371-3385, 2013.

[31] M. Alnassar, A. Alfadhel, Y. P. Ivanov, and J. Kosel, "Magnetoelectric polymer nanocomposite for flexible electronics," *Journal of Applied Physics,* vol. 117, 2015.

[32] G. Sreenivasulu, U. Laletin, V. M. Petrov, V. V. Petrov, and G. Srinivasan, "A permendur-piezoelectric multiferroic composite for low-noise ultrasensitive magnetic field sensors," *Applied Physics Letters,* vol. 100, p. 173506, 2012.

[33] J. Gao, D. Gray, Y. Shen, J. Li, and D. Viehland, "Enhanced dc magnetic field sensitivity by improved flux concentration in magnetoelectric laminates," *Applied Physics Letters,* vol. 99, p. 153502, 2011.

[34] J. Zhai, S. Dong, Z. Xing, J. Li, and D. Viehland, "Giant magnetoelectric effect in Metglas/polyvinylidene-fluoride laminates," *Applied Physics Letters,* vol. 89, 2006.

[35] A. Kulkarni, K. Meurisch, I. Teliban, R. Jahns, T. Strunskus, A. Piorra*, et al.*, "Giant magnetoelectric effect at low frequencies in polymer-based thin film composites," *Applied Physics Letters,* vol. 104, 2014.

[36] S. Dong, J. Zhai, F. Bai, J. F. Li, and D. Viehland, "Push-pull mode magnetostrictive/piezoelectric laminate composite with an enhanced magnetoelectric voltage coefficient," *Applied Physics Letters,* vol. 87, 2005.

[37] C.-W. Nan, M. I. Bichurin, S. Dong, D. Viehland, and G. Srinivasan, "Multiferroic magnetoelectric composites: Historical perspective, status, and future directions," *Journal of Applied Physics,* vol. 103, p. 031101, 2008.

[38] J. Gutiérrez, A. Lasheras, J. M. Barandiarán, J. L. Vilas, M. S. Sebastián, and L. M. León, "Temperature response of magnetostrictive/piezoelectric polymer magnetoelectric laminates," in *Key Engineering Materials* vol. 495, ed, 2012, pp. 351-354.

[39] X. Zhuang, M. L. C. Sing, C. Cordier, S. Saez, C. Dolabdjian, J. Das*, et al.*, "Analysis of noise in magnetoelectric thin-layer composites used as magnetic sensors," *IEEE Sensors Journal,* vol. 11, pp. 2183-2188, 2011.

[40] E. Fernandez, A. Garcia-Arribas, J. M. Barandiaran, A. V. Svalov, G. V. Kurlyandskaya, and C. P. Dolabdjian, "Equivalent Magnetic Noise of Micro-Patterned Multilayer Thin Films Based GMI Microsensor," *Sensors Journal, IEEE,* vol. 15, pp. 6707-6714, 2015.

[41] E. Fernandez, "Thin-film Magnetoimpedance micro-structure for sensing applications," University of the Basque Country, 2013.

5. Temperature response of the magnetoelectric laminated composites

This Chapter deals with one of the main problem that all the up-to-now studied PVDF based ME laminates show, which is the limited range of the temperature in which the ME device will work properly. Actually and as it was already commented in section 1.2, the main limitation of this polymer is that at temperatures higher than 60 ºC, the PVDF starts to lose its piezoelectric response. As a first consequence, a decrease in the ME response of the laminates working at such temperatures is observed. This Chapter introduces new high temperature piezoelectric poly and copolyimides in order to overcome that temperature limitation of the PVDF. The remnant polarization of those poly and copolyimides is also analyzed and compared with the one obtained for the pure PVDF. Finally, the temperature dependence of the ME coefficient for laminates containing PVDF and also some of the new polyimides are showed and compared.

5.1. High temperature piezoelectric polyimides

Few works have been reported so far concerning the ME effect at high temperatures (see for example [1, 2]), using in most of the cases ceramic materials such as PZT as piezoelectric constituent. As it was previously discussed, although the PZT shows a high piezoelectric response, some problems such as high mass density or brittleness limit its applicability. Nevertheless, these studies are important in order to develop new magnetoelectric laminates able to bear aggressive environments. If we want to add also other properties such as flexibility (to bond our ME device to any shaped material, for example), the use of polymeric piezoelectric materials in such ME devices turns out to be a much more interesting solution. Following this line of reasoning, nowadays there is a great interest in synthesizing new piezoelectric polymers for high-temperature applications. In order to reach this goal, several formulations of amorphous piezoelectric polymers with high dipolar moment in the repetitive units have been studied [3-6], all of them showing good pyro- and piezoelectric properties. Therefore, the next study will be focused on fabricating laminates using those new high temperature piezoelectric polymers and testing them at temperatures about 100 ºC.

Among these new classes of piezopolymers, polyimides have received a lot of interest lately due to their excellent thermal, mechanical and dielectric properties. Additionally, their piezoelectric properties can be improved by adding pendant highly polar groups in the main chain (–CN, –CF3, –SO2…) [7, 8]. Particularly, the polar cyano group (–CN) has been chosen as a pendant group in the main chain, and the N-phenylphthalyimide as a group to be incorporated in the chain. Aromatic polyimides have been extensively used in the aeronautic and microelectronic industries in applications such as high temperature insulators, dielectrics, coatings [9], adhesives [10], membranes and matrices for high-performance composites [11]. Although investigations in piezoelectric polyimides have only begun recently [12], piezoelectric polyimides have a promising future due to their interesting properties, which are suitable for many applications. As it can be expected, there is a much interest in the industry regarding the

development of new piezoelectric polymers with a much better thermal stability for applications at temperatures higher than 100 °C.

Seeking to combine the best mechanical and piezoelectric response in the same polymer, different polyimides and copolyimides have been synthesized.

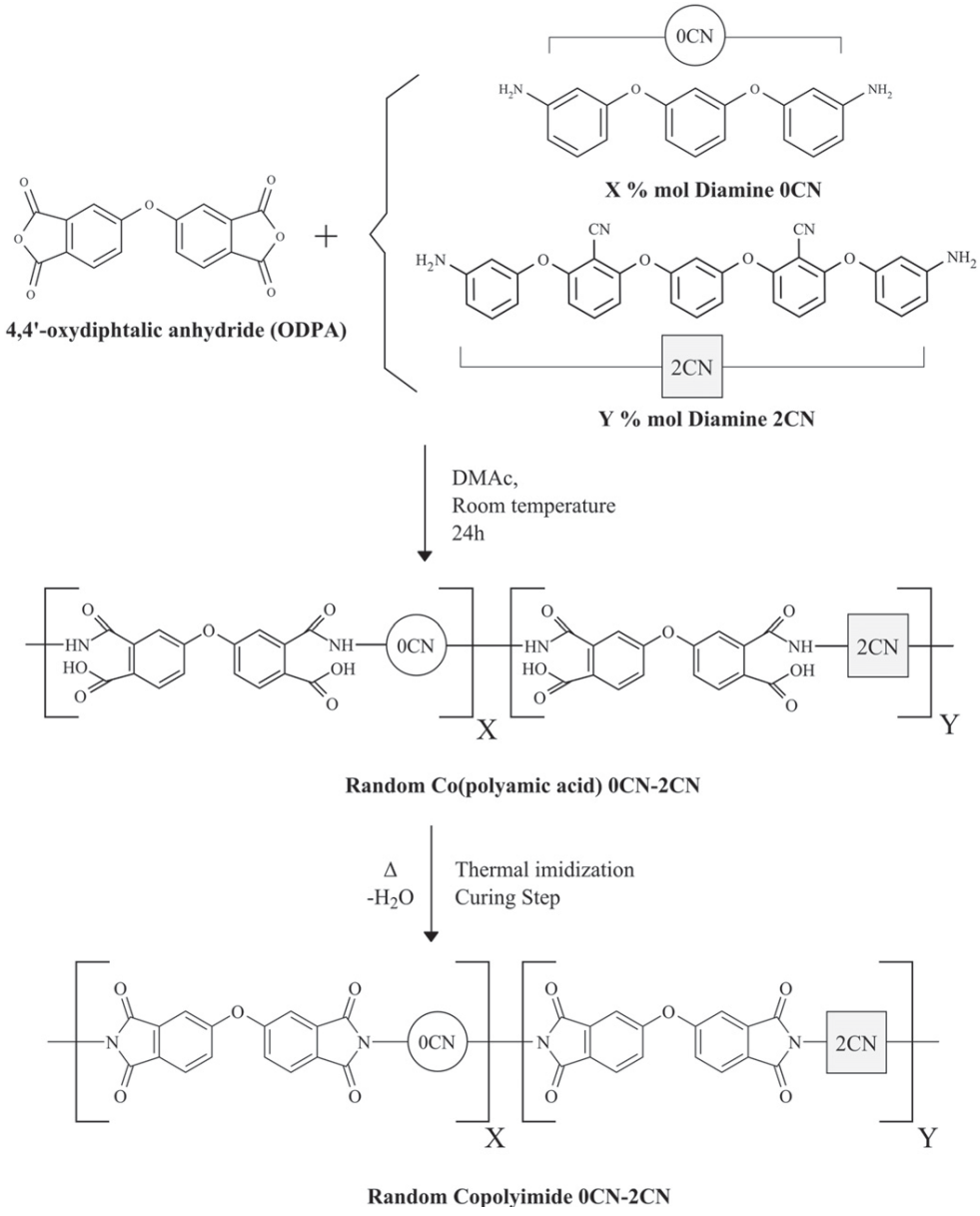

Figure 5.1. Scheme of the two-step reaction to synthesize the copolyimides.

Copolyimides were obtained by reaction between the dianhydride ODPA and a 50 % mol mixture of two aromatic diamines, namely 1,3-Bis-2-cyano-3-(3-aminophenoxy) phenoxybenzene (diamine 2CN) and 1,3-Bis(3-aminophenoxy)benzene (diamine 0CN) in a two-step reaction. In the first step, a nucleophilic attack of amine groups toward carbonyl groups in the dianhydride produces the copoly(amic acid); in the second step, the cyclodehydration reaction caused by thermal treatment gives rise to the copolyimide. The general scheme of the synthesis of polyimide is shown in Fig. 5.1.

After synthesis, each poly(amic acid) or copoly(amic acid) is converted into the corresponding polyimide by thermal imidization. Polyimide films were prepared in a Teflon mould with a rectangular centered cavity of dimensions 50 mm x 20 mm.

These polyimides are not piezoelectric materials yet, so they must be polarized before their use. They were polarized following the contact method: a silver layer was evaporated on both sides of the films and polarized by a DC electric field (7,2 MV/m) at an elevated temperature of approximately T_g + 10 ºC. After that, the system is cooled down keeping the electric field. The remnant polarization is then measured using the thermally stimulated depolarization current technique (see Fig. 5.2).

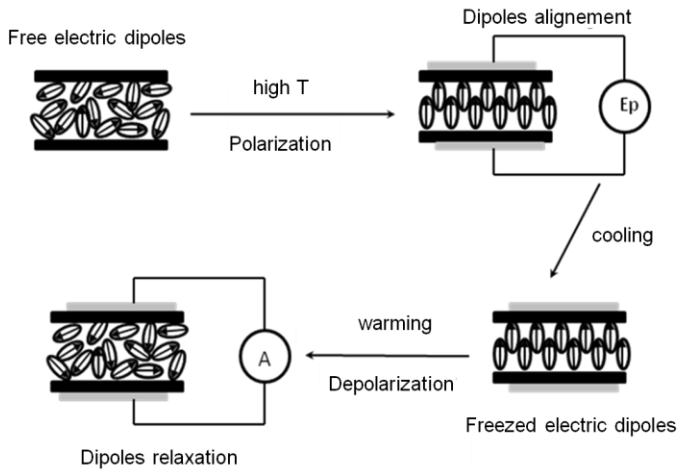

Figure 5.2. Scheme of the polarization and depolarization of the poly and copolymides

In amorphous polyimides the piezoelectric contribution can be written as the following [13]:

$$d(T) = -\left(\frac{\varphi}{3}\right)\varepsilon_0 P_r \propto P_r(T) \tag{5.1}$$

where φ is the volumetric compressibility, ε_0 is the vacuum permittivity and P_r is the remnant polarization.

From this equation, we infer that the piezoelectric contribution only depends on the remnant polarization of the amorphous polyimide and therefore the effective piezoelectricity of these polyimides will be dominated by the temperature dependence of the remnant polarization showed by the amorphous films.

Fig. 5.3 shows the remnant polarization as a function of temperature for the polyimides poly 2,6, poly 2CN (left) and the copolyimides 0CN/2CN (50/50), 0CN/2CN (40/60) and 0CN/2CN (30/70) (right). While the poly 0CN is responsible of the good mechanical properties, the poly 2CN accounts for the piezoelectric response of the copolyimide.

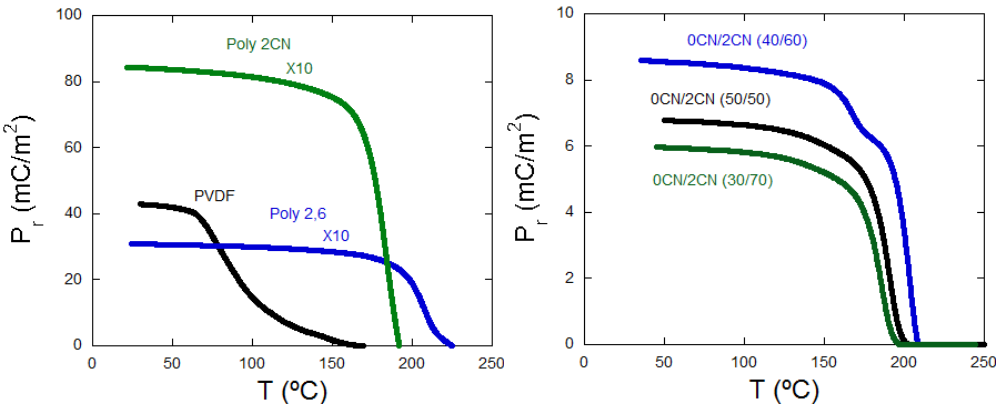

Figure 5.3. Dependence of the remnant polarizations of the PVDF, poly 2,6, and poly 2CN (left) and copolyimides 0CN/2CN (50/50), 0CN/2CN (40/60) and 0CN/2CN (30/70) with temperature. Note that the values for the poly 2,6 and poly 2CN are multiplied by 10 in order to scale them with the values of the PVDF.

In order to compare their properties with the ones of the PVDF, the curve of the remnant polarization as a function of the temperature for the PVDF (already showed in Fig. 2.12) has been also included.

As can be observed, although the remnant polarizations of the poly and copolyimides are significantly lower than the remnant polarization of the PVDF, the high temperatures poly and copolyimides keep the remnant polarization constant up to 160 ºC, which confirms the ability of these poly and copolyimides to work efficiently at high temperatures [14]. Table 5.1 shows the values of the remnant polarizations of the poly and colpoyimides and also the value for the PVDF.

Table 5.1. Values of the remnant polarization of the PVDF, poly 2,6, poly 2CN and copolyimides 0CN/2CN (50/50), 0CN/2CN (40/60) and 0CN/2CN (30/70) .

Polymer	**P_r (mC/m^2)**
Poly 2,6	3.1
Poly 2CN	8.4
Copo 0CN/2CN (50/50)	6.8
Copo 0CN/2CN (40/60)	8.6
Copo 0CN/2CN (30/70)	6.0
PVDF	42.8

5.2. Magnetoelectric effect at high temperature

There has been already analyzed in the different sections of this report the influence of temperature in the piezoelectric constituent (sections 2.2 and 5.1) and in the epoxy (section 2.3). To complete all the components that are involved in the ME laminated device, it is necessary to study the influence of temperature in the magnetostrictive constituents.

As it is well explained in Ref. [15], the temperature dependence of the magnetostriction and the uniaxial anisotropy constant with temperature in FeCoSiB magnetostrictive alloys (with exponent α=2, since the FeCoSiB alloys belong to the two-ion mechanism group due to the two different magnetic

elements in its composition) can be described as $\lambda_s(T) = k.M_s^{\alpha}(T)$ and $K_u(T) = k'.M_s^{\alpha}(T)$.

As $\partial M/\partial H \approx M_s^2/2K_u$, for the change of the magnetostriction with the applied magnetic field, we get:

$$\frac{\partial \lambda}{\partial H}(T) = \frac{\partial \lambda}{\partial M}\frac{\partial M}{\partial H} \propto M_s(T) \tag{5.2}$$

where M_s is the saturation magnetization. As an example, the dependence of this magnetization with temperature is showed in Fig. 5.4 for the X=3 as-quenched ribbon, measured at an applied magnetic field of 100 Oe.

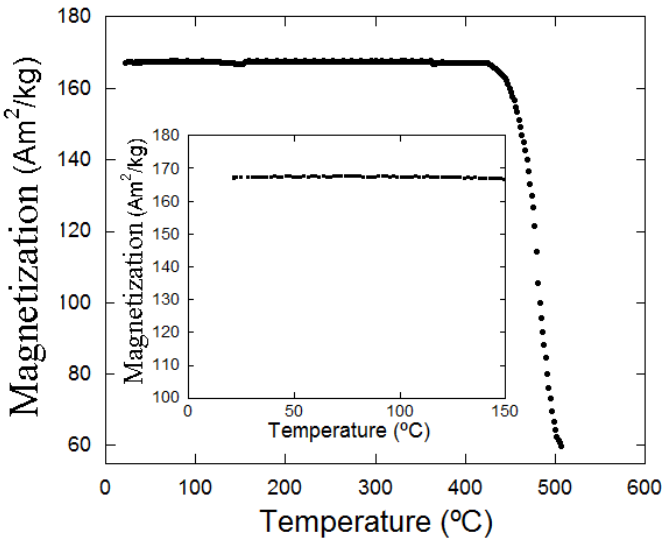

Figure 5.4. Dependence of the saturation magnetization of the as-quenched X=3 alloy with temperature.

As it can be noticed, the magnetization remains constant up to 400ºC, being the Curie temperature about 500 ºC. Although the values of the magnetic moment and Curie temperature can be slightly different from one composition to another, the behavior with temperature is expected to be similar for the rest of the ribbons studied in this work.

Since equation 5.2 predicts the proportionality between both the piezomagnetic coefficient and the magnetization dependencies with temperature, an example of this is showed in Fig. 5.5, where the magnetostriction and piezomagnetic coefficient of the commercial magnetostrictive alloy Vitrovac® 4040 ($Fe_{39}Ni_{39}Mo_4Si_6B_{12}$) have been measured for several increasing temperatures.

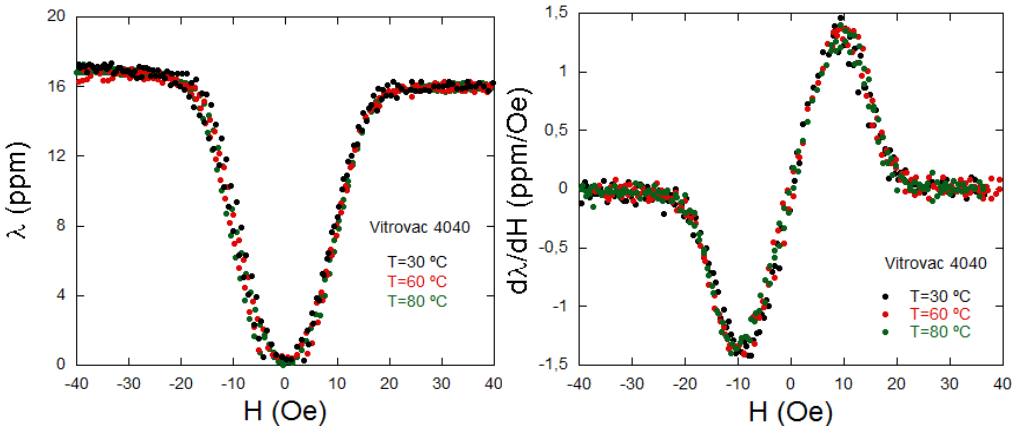

Figure 5.5. Dependence of the magnetostriction (left) and piezomagnetic coefficient (right) of the commercial Vitrovac® 4040 with temperature.

As expected, both magnetostriction and piezomagnetic coefficient keep their values constant at temperatures up to 80 ºC.

Considering the behavior of the magnetization and piezomagnetic coefficient with temperature, it is expected that the magnetostrictive constituent contribution to the ME effect will be not strongly affected at temperatures up to 100 ºC.

To probe this, we have performed some measurements of the ME effect at temperatures above the room one [16]. These measurements were carried out by introducing the ME characterization set-up within a climatic chamber (ACS, CH250), which controls de temperature from -40 ºC to 180 ºC (see Fig. 5.6). The temperature was changed from room temperature up to 90 ºC, measuring in each temperature the maximum induced ME voltage of the laminate.

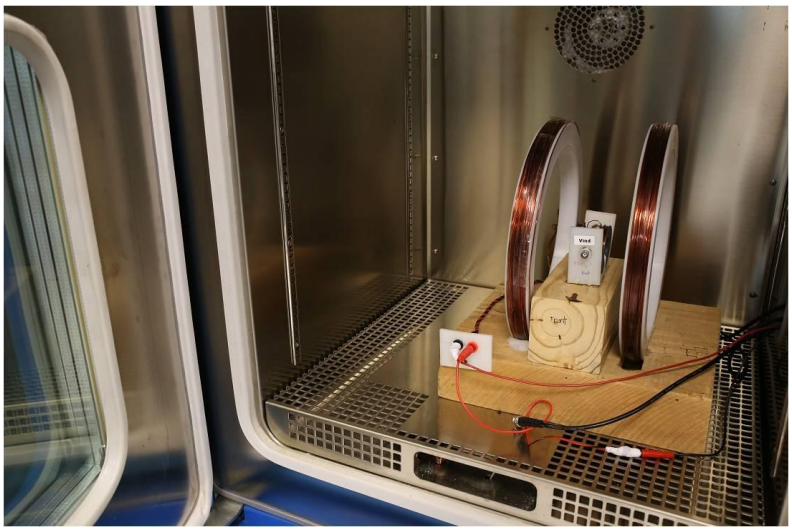

Figure 5.6. Set-up for the ME characterization under temperature.

Fig. 5.7 shows the dependence of the maximum ME coefficient with temperature for the 3 cm long X=3/PVDF laminated composite, when using as-quenched magnetostrictive ribbons. The results are also compared with the Vitrovac® 4040/poly 2,6 composite fabricated with a high temperature poly 2,6 polyimide.

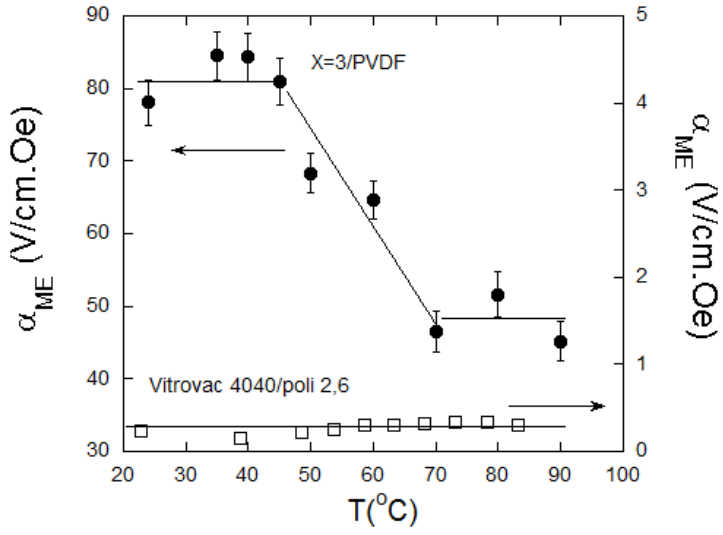

Figure 5.7. Dependence of the magnetoelectric coefficient with temperature for the X=3/PVDF and Vitrovac® 4040/poly 2,6 laminated L-T composites.

Fig. 5.7 clearly shows that the behavior of the laminates fabricated with PVDF agrees with the PVDF polarization value behavior with temperature. As it is already well established [17], at 60 ºC, the α-relaxation of the PVDF starts, resulting in a linear decrease of the ME response. When the temperature reaches 80 ºC, the PVDF undergoes a contraction (acting against magnetostriction), which is reflected in the ME coefficient as an almost constant behavior from that temperature up to 100 ºC. The relative change that the ME coefficient undergoes is about a 45%, decreasing from 82 V/cm.Oe at room temperature to 45 V/cm.Oe at 90 ºC. The laminate fabricated with Vitrovac® 4040 and poly 2,6, however, shows a much lower ME coefficient (about 0.35 V/cm.Oe), but with a good stability with temperature.

Note that the ME coefficient at room temperature for the 3 cm X=3/PVDF laminate is higher than the one showed in Table 3.3 for the same laminate (46.0 V/cm.Oe). This disagreement arises from the different widths of the magnetostrictive ribbons used in both cases. Actually, the 3 cm long X=3/PVDF laminate used in Fig. 5.7 was fabricated with 2.5 mm wide magnetostrictive ribbons, whereas the one used in Chapter 3 was 5 mm wide. Therefore, the laminate used to perform the temperature measurements is less affected by the demagnetizing field, which results in a higher ME response.

The reproducibility of our measurements is good, as we could check by repeating them and obtaining very similar results. Concerning error sources, we have done systematic measurements and confirmed an experimental error of about 3% at room temperature and about a 5% at high ones. So, we conclude that the main source in error when measuring by increasing temperature arises from the interference of electrical control (devices) of temperature within the climate chamber with our experimental detection system.

5.3. Discussion and conclusions

The results show in this Chapter demonstrated that high temperature poly and copolymides are a promising alternative to the PVDF piezoelectric polymer. Despite their remnant polarization is much more modest than the one of the PVDF, they show a good performance at temperatures up to 160 ºC, keeping their remnant polarization almost constant.

The results obtained for the maximum ME response as a function of temperature reveals that although the laminate fabricated with the commercial magnetostrictive alloy Vitrovac® 4040 and the high temperature poly 2,6 polyimide shows a much lower ME coefficient than the 3 cm long X=3/PVDF laminate, the ME coefficient remains constant up to 90 ºC, which confirms the great stability that these poly and copolyimides show at high temperatures.

Trends for future research points directly to the improvement of the piezoelectric response of the poly and copoyimides, in order to be competitive with that of the PVDF. This means either to perform a better adjustment of the composition of these copolyimides or to improve the mechanism (its parameters) for their polarization. Once this task is achieved, the first direct consequence will be the improvement of the ME response of these type of laminates while keeping that induced voltage constant up to high temperatures, above 100 ºC.

5.4. References

[1] D. A. Burdin, D. V. Chashin, N. A. Ekonomov, Y. K. Fetisov, and G. Srinivasan, "Multiferroic bending mode resonators and studies on temperature dependence of magnetoelectric interactions," *Applied Physics Letters,* vol. 100, p. 242902, 2012.

[2] Y. Shen, J. Gao, Y. Wang, J. Li, and D. Viehland, "Thermal stability of magnetoelectric sensors," *Applied Physics Letters,* vol. 100, p. 173505, 2012.

[3] A. Meskini, M. Raihane, B. Ameduri, C. Hakme, D. Sage, I. Stevenson*, et al.*, "Dielectric behaviour of copolymers based on 2,2,2-trifluoroethyl methacrylate and cyano co-monomers," *European Polymer Journal,* vol. 45, pp. 804-812, 3// 2009.

[4] S. Tasaka, N. Inagaki, T. Okutani, and S. Miyata, "Structure and properties of amorphous piezoelectric vinylidene cyanide copolymers," *Polymer,* vol. 30, pp. 1639-1642, 1989/09/01 1989.

[5] H. v. Berlepsch, M. Pinnow, and W. Stark, "Electrical conduction in acrylonitrile/methylacrylate copolymer films," *Journal of Physics D: Applied Physics,* vol. 22, p. 1143, 1989.

[6] J. I. Scheinbeim, "Piezoelectricity in γ-form Nylon 11," *Journal of Applied Physics,* vol. 52, pp. 5939-5942, 1981.

[7] E. Fukada, "History and recent progress in piezoelectric polymers," *Ultrasonics, Ferroelectrics, and Frequency Control, IEEE Transactions on,* vol. 47, pp. 1277-1290, 2000.

[8] E. Fukada, "Recent developments of polar piezoelectric polymers," *Dielectrics and Electrical Insulation, IEEE Transactions on,* vol. 13, pp. 1110-1119, 2006.

[9] H. Qi, F. Liu, N. Zhang, Y. Chen, H. Yang, and Z. Wang, "Studies on high performance nonvolatile polyimides coating: Gamma ray initiated bulk copolymerization of vinyl polar monomer and maleimide-terminated

polyimides with flexible backbone and the modifications," *Progress in Organic Coatings,* vol. 73, pp. 33-41, 1// 2012.

[10] Z. Huang, R. Lu, T. Huang, H. Wang, and T. Li, "An Investigation into the Migration of Segments in Crosslinked Fluorinated Polyimide Adhesive," *Journal of Macromolecular Science, Part B,* vol. 52, pp. 937-949, 2013/06/01 2013.

[11] J. Longun and J. O. Iroh, "Polyimide/substituted polyaniline–copolymer–nanoclay composite thin films with high damping abilities," *Journal of Applied Polymer Science,* vol. 128, pp. 1425-1435, 2013.

[12] C. Park, Z. Ounaies, K. E. Wise, and J. S. Harrison, "In situ poling and imidization of amorphous piezoelectric polyimides," *Polymer,* vol. 45, pp. 5417-5425, 7/21/ 2004.

[13] B. Gonzalo, "Nuevos materiales poliméricos con propiedades piezoeléctricas," Universidad del País Vasco, Leioa, 2009.

[14] J. Gutiérrez, A. Lasheras, J. M. Barandiarán, J. L. Vilas, A. Maceiras, and L. M. León, "Improving the performance of high temperature piezopolymers for magnetoelectric applications," in *Key Engineering Materials* vol. 543, ed, 2013, pp. 439-442.

[15] D. X. Chen, "Induced anisotropy and magnetostriction in metallic glasses," *Journal of Applied Physics,* vol. 61, pp. 3781-3783, 1987.

[16] A. Lasheras, J. Gutierrez Echevarria, A. Maceiras, M. San Sebastian, J. Barandiaran, J. Vilas*, et al.*, "Radio-Frequency Magnetoelectric Effect Measured at High Temperature," *Magnetics, IEEE Transactions on,* vol. PP, pp. 1-1, 2015.

[17] V. Sencadas, S. Lanceros-Méndez, R. Sabater i Serra, A. Andrio Balado, and J. L. Gómez Ribelles, "Relaxation dynamics of poly(vinylidene fluoride) studied by dynamical mechanical measurements and dielectric spectroscopy," *The European Physical Journal E,* vol. 35, pp. 1-11, 2012/05/30 2012.

6. General conclusions and open perspectives

6.1. General conclusions

Throughout the present Thesis, 32 L-T type three-layer ME laminated composites have been fabricated, 16 of them using as-quenched magnetostrictive ribbons, and the other 16 after annealing identically equal pieces of those ribbons. In all these laminates, the piezoelectric constituent was de same, piezoelectric PVDF. Prior to the fabrication of the laminates, each magnetostrictive constituent has been magnetically characterized by measuring the hysteresis loop and saturation magnetostriction, and by obtaining the main magnetoelastic parameters such as the magnetoelastic coupling coefficient, the elastic compliance and the quality factor. The commercial PVDF, as well as the piezoelectric poly and copolymides used in this work have been also characterized by measuring the main piezoelectric and thermal properties. All of the laminates have been fully characterized, measuring in each case the ME response as a function of the applied magnetic field. With the obtained results, we have answered the main questions presented in section 1.4:

1) By using magnetostrictive ribbons with different magnetic characteristics (mainly different magnetostriction value), we have demonstrated experimentally that there is a direct correlation between the induced ME response of the laminates and the product of the piezomagnetic coefficient and quality factor ($d\lambda/dH*Q$). We have also tested the validity of the product of saturation magnetostriction and magnetic susceptibility as figure of merit for the magnetostrictive constituent of ME laminates, inferring that only when those susceptibility and magnetostriction values (that its, the ribbon magnetic properties) are well controlled, the relationship between induced ME voltage or coefficient and figure of merit is absolutely direct. This has been the case of the used as-quenched

ribbons. For the annealed magnetostrictive ribbons, the difficulty to establish the value of the intrinsic susceptibility makes the relationship with that figure of merit much more inaccurate, being impossible to deduce which one of the fabricated devices will work the best.

2) We have obtained high ME voltages for 3 cm long laminates, obtaining a maximum value of 267 V/cm.Oe for the 3 cm long X=3/PVDF laminate, when using annealed magnetostrictive ribbons. We have also studied the behavior of these ME responses with the size of the laminate, for lengths ranging from 3 down to 0.5 cm. It has been observed a decrease in the ME response as reducing the length of the laminate, which can be attributed to the demagnetizing field effects and also to the less effective deformation of the magnetostrictive ribbons.

3) The losses arisen from the reduction of the size of the laminate have been quantified, obtaining values that reach the 95 % and 99 % of the expected signal for the shortest laminates. The minimum loss value is about 38 %, measured for the 3 cm long X=6/PVDF laminate when using annealed magnetostrictive ribbons.

4) The values of the ME coefficients can be properly corrected for aspect ratios values below 6, but only when using as-quenched magnetostrictive ribbons. Above this value, the corrections do not work, due to the worse homogeneity of the epoxy for the longest laminates. On the other hand, the inaccurate extrapolation of the intrinsic magnetic susceptibility of the annealed magnetostrictive ribbons hinders the corrections of the ME coefficients.

5) We have successfully studied the performance of the ME laminates as Energy Harvesting devices and as magnetic field sensors, using for this purpose the ME laminates with the highest ME response.

6) The energy harvesting measurements performed gave maximum output electric powers of 11.7 and 6.4 μW for the 3 cm long X=3/PVDF and X=6/PVDF laminates, respectively, when using annealed magnetostrictive ribbons. These values were obtained at the MER

frequency of each laminate, under an applied AC magnetic field of 0.45 Oe and at DC magnetic fields that correspond to the maximum ME coupling of each laminate. Considering the volume of each laminate, the power densities were calculated to be 0.55 and 1.2 mW/cm^3 for the X=3/PVDF and X=6/PVDF laminates, respectively. These values successfully compete with nowadays employed other energy harvesting devices fabricated with piezoelectric materials with better piezoelectric responses such as PZT or APC 855.

7) We have obtained maximum sensitivities to the applied DC magnetic field of 290 and 350 V/T for the X=3/PVDF and X=6/PVDF laminates, respectively, whereas the sensitivity to the AC magnetic field enhances significantly, obtaining maximum values of 12400 and 9328 V/T. The equivalent magnetic noise measurements performed in the X=6/laminate show a minimum value of 67 $pT/Hz^{1/2}$ at the MER frequency, whereas at lower frequency of 10 Hz this value is considerably higher, about 3 $nT/Hz^{1/2}$.

8) We have analyzed the effect of temperature in the 3 cm long X=3/PVDF laminate up to 90 ºC, when using as-quenched magnetostrictive ribbons. We have observed that the behaviour of the maximum ME coefficient under temperature varies in the same way as the remnant polarization of the piezoelectric constituent does, with a relative change of a 45 % respect to the maximum ME coefficient obtained at room temperature. We have also concluded that the high temperature poly and copolymides are a good alternative to the used PVDF, since they keep they remnant polarization (and therefore, the induced ME voltage and coefficient as well) constant up to 150 º C.

6.2. Open perspectives

1) The future research in the field of ME laminates will be devoted to the improvement of the properties of the high temperature poly and

copolymides, with the aim to be competitive with the PVDF. The main goal will be to obtain a ME coefficient as close as possible to the one obtained for the PVDF. This task will be performed by adjusting the composition of the poly and copolymides and to improve the polarization conditions for those polymers.

2) Concerning magnetic field sensitivity, we want to develop a ME laminate with higher ME response and so higher sensitivity than the ones the X=3/PVDF and X=6/PVDF laminates showed. This means most probably longer devices that the tested ones in this work. We also want to carry out more noise measurements, in order to see if we reduce also the measured noise level.

3) We will also focus on the miniaturization of the ME devices, which will lead to an increase in the operation frequency, and to test them in other type of applications such as near field communication systems.

4) Finally, it is a big challenge to try to fabricate the ME laminates without the epoxy constituent. This fact would significantly improve the bonding between the magnetostrictive and piezoelectric layers, increasing the ME response. The optimization of the piezoelectric properties of the high temperature poly and copolymides will play a key role in this task, since they can undergo high temperatures and therefore, magnetostrictive alloys could be deposited by a sputtering technique, for example.

Appendix A: List of publications

Publications directly arisen from this Thesis

1- P. Martins, A. Lasheras, J. Gutierrez, J. M. Barandiaran, I. Orue, and S. Lanceros-Mendez, "Optimizing piezoelectric and magnetoelectric responses on $CoFe_2O_4$/P(VDF-TrFE) nanocomposites," *Journal of Physics D: Applied Physics,* vol. 44, 495303, 2011.

2- J. Gutiérrez, J. M. Barandiarán, A. Lasheras, J. L. Vilas, M. S. Sebastián, and L. M. León, "Resonant response of magnetostrictive/new piezoelectric polymer magnetoelectric laminate," *Sensor Letters,* vol. 11, pp. 134-137, 2013.

3- M. Silva, S. Reis, C. S. Lehmann, P. Martins, S. Lanceros-Mendez, A. Lasheras*, et al.*, "Optimization of the magnetoelectric response of poly(vinylidene fluoride)/epoxy/vitrovac laminates," *ACS Applied Materials and Interfaces,* vol. 5, pp. 10912-10919, 2013.

4- A. García-Arribas, J. Gutiérrez, G. V. Kurlyandskaya, J. M. Barandiarán, A. Svalov, E. Fernández*, et al.*, "Sensor applications of soft magnetic materials based on magneto-impedance, magneto-elastic resonance and magneto-electricity," *Sensors (Switzerland),* vol. 14, pp. 7602-7624, 2014.

5- A. Lasheras, J. Gutiérrez, A. Balza, J. M. Barandiarán, and A. Rodríguez Pierna, "Radiofrequency magnetoelastic resonators for magnetoelectric applications," *Journal of Physics D: Applied Physics,* vol. 47, 315003, 2014.

6- A. Maceiras, P. Martins, M. San Sebastián, A. Lasheras, M. Silva, J. M. Laza*, et al.*, "Synthesis and characterization of novel piezoelectric nitrile copolyimide films for high temperature sensor applications,"*Smart Materials and Structures,* vol. 23, 105015, 2014.

7- M. P. Silva, P. Martins, A. Lasheras, J. Gutiérrez, J. M. Barandiarán, and S. Lanceros-Mendez, "Size effects on the magnetoelectric response on PVDF/Vitrovac 4040 laminate composites," *Journal of Magnetism and Magnetic Materials,* vol. 377, pp. 29-33, 2015.

8- A. Lasheras, J. Gutiérrez, S. Reis, D. Sousa, M. Silva, P. Martins*, et al.*, "Energy harvesting device based on a metallic glass/PVDF magnetoelectric laminated composite," *Smart Materials and Structures,* vol. 24, 065024, 2015.

9- A. Lasheras, J. Gutierrez, A. Maceiras, M. San Sebastian, J. Barandiaran, J. Vilas*, et al.*, "Radio-Frequency Magnetoelectric Effect Measured at High Temperature," *IEEE Transactions on Magnetics,* vol. PP, 7006700, 2015.

Publications derived from international conferences

1- J. Gutiérrez, A. Lasheras, J. M. Barandiarán, J. L. Vilas, M. S. Sebastián, and L. M. León, "Temperature response of magnetostrictive/piezoelectric polymer magnetoelectric laminates," in *Key Engineering Materials* vol. 495, ed, 2012, pp. 351-354.

2- J. Gutiérrez, A. Lasheras, J. M. Barandiarán, J. L. Vilas, A. Maceiras, and L. M. León, "Improving the performance of high temperature piezopolymers for magnetoelectric applications," in *Key Engineering Materials* vol. 543, ed, 2013, pp. 439-442.

3- J. Gutierrez, A. Lasheras, J. M. Barandiaran, J. L. Vilas, M. San Sebastian, and L. M. Leon, "Improving the magnetoelectric response of laminates containing high temperature piezopolymers," *IEEE Transactions on Magnetics,* vol. 49, pp. 42-45, 2013.

4- A. Lasheras, J. Gutiérrez, J. M. Barandiarán, D. A. Shishkin, and A. P. Potapov, "Parameters affecting the magnetoelectric response of magnetostrictive/piezoelectric polymer laminates," in *Key Engineering Materials* vol. 644, ed, 2015, pp. 40-44.

5- J. Guttierrez, A. Lasheras, J. M. Barandiaran, R. Goncalves, P. Martins, and S. Lanceros-Mendez, "Induced magnetoelectric effect driven by magnetization in $BaFe_{12}O_{19}$/P(VDF-TrFE) composites," *IEEE Transactions on Magnetics*, vol. 51, 2504004, 2015.

Publications from works developed in parallel to the Thesis

1- R. Gonçalves, P. M. Martins, C. Caparrós, P. Martins, M. Benelmekki, G. Botelho, S. Lanceros-Mendez, A. Lasheras, J. Gutiérrez, and J. M. Barandiarán, "Nucleation of the electroactive β-phase, dielectric and magnetic response of poly(vinylidene fluoride) composites with Fe_2O_3 nanoparticles," *Journal of Non-Crystalline Solids,* vol. 361, pp. 93-99, 2013.

2- Y. Le Bras, A. Lasheras, J. Gutierrez, F. Mazaleyrat, and J. M. Greneche, "A new magneto-elastic resonance based technique to determine magneto-mechanical parameters of amorphous ferromagnetic ribbons," *Review of Scientific Instruments,* vol. 84, 043904, 2013.

3- P. Martins, R. Gonçalves, S. Lanceros-Mendez, A. Lasheras, J. Gutiérrez, and J. M. Barandiarán, "Effect of filler dispersion and dispersion method on the piezoelectric and magnetoelectric response of $CoFe_2O_4$/P(VDF-TrFE) nanocomposites," *Applied Surface Science,* vol. 313, pp. 215-219, 2014.

4- J. Gutiérrez, P. Martins, R. Gonçalves, V. Sencadas, A. Lasheras, S. Lanceros-Mendez*, et al.*, "Synthesis, physical and magnetic properties of $BaFe_{12}O_{19}$/P(VDF-TrFE) multifunctional composites," *European Polymer Journal,* vol. 69, pp. 224-231, 2015.